Biomechanical Models and Stability Analysis of Bipedal Running

---

Biomechanische Modelle und Stabilitätsanalyse des zweibeinigen Rennens

Dissertation
zur Erlangung des Akademischen Grades

Doctor philosophiae (Dr. phil.)

vorgelegt dem Rat der Fakultät für Sozial- und Verhaltenswissenschaften
der Friedrich-Schiller-Universität Jena
von Dipl.-Phys. Yvonne Blum
geboren am 25. Januar 1980 in Delmenhorst

1. Gutachter: PD Dr. André Seyfarth, FSU Jena

2. Gutachter: Prof. Dr. Reinhard Blickhan, FSU Jena

Tag der Verteidigung: 20.12.2010

Zusammenfassung

Kapitel 1 bildet einen übergreifenden Rahmen für die folgenden, in internationalen wissenschaftlichen Zeitschriften publizierten Kapitel 2, 3 und 4. Zuerst wird ein allgemeiner Überblick über die verschiedenen Arten der terrestrischen Lokomotion gegeben. Danach werden die Gemeinsamkeiten und Unterschiede von menschlichem und vogelartigem Rennen beleuchtet. Zum Schluss folgt eine Betrachtung der Eigenschaften des Feder-Masse-Modells.

Kapitel 2* beschäftigt sich mit der Berechnung einer effektiven Beinsteifigkeit.

Ein gängiger Parameter, der häufig dazu genutzt wird Gangarten wie Rennen und Hüpfen zu beschreiben, ist die Beinsteifigkeit. Jedoch werden in der wissenschaftlichen Literatur viele unterschiedliche Methoden beschrieben die Beinsteifigkeit anhand von dynamischen und kinematischen Parametern abzuschätzen, wobei sich die Methoden hauptsächlich darin unterscheiden, wie die Beinkompression während des Kontaktes definiert ist. In dieser Arbeit werden fünf Methoden der Beinsteifigkeitsbestimmung beschrieben: Vier Methoden (Methode A-D) benötigen Bodenreaktionskräfte, während die fünfte Methode (Methode E) neben den Beinparametern ausschließlich temporale Parameter verlangt. Die nach diesen fünf Methoden berechneten Beinsteifigkeiten werden anschließend mit Rennmustern des Feder-Masse-Modells verglichen.

Die beste und gleichzeitig einfachste Abschätzung der Beinsteifigkeit liefert Methode E. Diese Methode benötigt nur leicht zugängliche Parameter (Kontaktzeit, Flugzeit, Beinlänge, Körpermasse und den Landewinkel des Beines). Methode D liefert zwar ähnlich gute Ergebnisse, benötigt jedoch zusätzlich den zeitlichen Verlauf der Bodenreaktionskräfte. Die übrigen drei Methoden zeigen, besonders bei geringen Geschwindigkeiten, deutliche Abweichungen von der Modellvorhersage und die ermittelten Beinsteifigkeiten fallen entweder zu hoch, oder zu gering aus.

Da es sich bei der Beinsteifigkeit um einen Parameter handelt, der von einem konzeptionellen Modell abgeleitet wird und daher ohne ein solches Modell nicht

*Blum Y., Lipfert S.W., Seyfarth A., *J. Biomech.,* 42: 2400-2405, 2009

existiert, muss für jede Aufgabenstellung geprüft werden, welche Methode am besten geeignet ist die Beinsteifigkeit abzuschätzen. Nur so können die Vorhersagen konzeptioneller Modelle (wie das Feder-Masse-Modell) mit experimentellen Daten verglichen werden.

In **Kapitel 3**[†] wird eine erweiterte Schwungbeinkontrolle hergeleitet und mit experimentellen Daten verglichen.

Menschen sind in der Lage mit beliebigen Geschwindigkeit zu rennen, ohne sich über die Stabilisierung dieser Rennbewegung Gedanken zu machen. Die Beinparameter scheinen auf ganz natürliche Art und Weise und ohne sensorische Rückkopplung eingestellt zu werden.

In dieser Arbeit wird die Dynamik des menschlichen Rennens durch das Feder-Masse-Modell beschrieben. Für dieses Modell ergeben sich für hinreichend hohe Geschwindigkeiten Rennmuster, die bereits ohne Kontrollmechanismen stabil sind. Wir stellen nun potentielle Kontrollstrategien vor, welche den Geschwindigkeitsbereich in dem stabiles Rennen möglich ist vergrößern, und vergleichen die theoretischen Vorhersagen mit experimentellen Renn-Daten.

Zunächst werden periodische Renn-Lösungen ausfindig gemacht und anschließend hinsichtlich ihrer Stabilität untersucht. Die hier angewandten Kontrollstrategien bestehen in der linearen Anpassung der Beinparameter - Beinwinkel, Beinsteifigkeit und Beinlänge - während der Schwungphase. Um diese Kontrollstrategien hinsichtlich ihres Einflusses auf die Landung zu beurteilen, werden zwei Parameter eingeführt: die Geschwindigkeit des Fußes relativ zum Boden (*ground speed matching*) und der Landewinkel des Fußes (*angle of approach*).

Die Ergebnisse zeigen, dass periodische Renn-Lösungen stabilisiert werden können und die Kontrollstrategien, welche die Rennbewegung stabilisieren, redundant sind. Daraus folgt, dass jede beliebige Schwungbeinkinematik (Anpassung des Beinwinkels und der Beinlänge) durch geeignete Anpassung der Beinsteifigkeit in Vorbereitung auf den Bodenkontakt stabilisiert werden kann.

Kapitel 4[‡] stellt eine Anwendung der zuvor in Kapitel 3 hergeleiteten Untersuchungsmethode vor, indem experimentelle Daten von menschlichem und Vogel-Rennen hinsichtlich ihrer vorhergesagten Beinsteifigkeitsanpassung, Stabilität und Robustheit untersucht werden.

Sowohl Menschen, als auch Vögel bewegen sich zweibeinig fort. Jedoch lassen

[†]Blum Y., Lipfert S.W., Rummel J., Seyfarth A., *Bioinspir. Biomim.,* 5: 026006, 2010
[‡]Blum Y., Birn-Jeffery A., Daley M.A., Seyfarth A., *J. Theor. Biol.,* (in press)

Beobachtungen der Gangmuster vermuten, dass die Unterschiede in der Beingeometrie zu spezifischen Kontrollstrategien führen. In der vorliegenden Arbeit werden Kontrollstrategien zur Stabilisierung des zweibeingen Rennens anhand eines konzeptionellen Modells hergeleitet und mit experimentellen Daten von Mensch und Fasan (*Phasianus colchicus*) verglichen.

Aus Modellperspektive betrachtet kann Rennen mit nachgiebigen Beinen durch ein zweidimensionale Masse-Feder-Modell beschrieben und durch Anwenden einer Schwungbeinkontrolle stabilisiert werden. In der vorliegenden Arbeit werden lineare Anpassungen der Schwungbeinparameter (Beinwinkel, Beinlänge und Beinsteifigkeit) angenommen. Experimentell ermittelte kinematische Kontrollparameter (Beinrotation und Beinlängenänderung) von Mensch und Vogel werden mit den Vorhersagen des Feder-Masse-Modells verglichen und in Hinblick auf Stabilität und Robustheit interpretiert.

Die Ergebnisse legen nahe, dass sich die Stabilität des Rennens und die angewandten Kontrollstrategien voneinander unterscheiden, was auf die Unterschiede in der Beinhaltung (gestreckte Beinhaltung bei Menschen, gebeugte Beinhaltung bei Vögeln) zurückzuführen sein könnte. Es wurde vermutet, dass eine gebeugte Beinhaltung die Stabilität des Rennens verbessere. Da das System von Kontrollstrategien jedoch überbestimmt ist, legen unsere Modellvorhersagen nahe, dass gebeugte Beinhaltungen nicht zwangsläufig die Stabilität erhöhen.

Das Modell sagt zudem unterschiedliche Beinsteifigkeitsanpassungen für Menschen und Vögel vorher und lässt vermuten, dass das gebeugte vogelartige Bein stabiles Rennen sogar ohne Beinsteifigkeitsanpassung ermöglicht, da es sowohl verkürzt, als auch verlängert werden kann. Beim menschlichen Rennen hingegen scheint die Vorbereitung auf den Bodenkontakt kritischer zu sein und nach einer Anpassung der Beinsteifigkeit zu verlangen.

Letztendlich legt die Berechnung eines einfachen Robustheitsmaßes, der normalisierten maximalen Stufe, die Vermutung nahe, dass ein gebeugtes Bein robuster auf Höhenunterschiede des Bodens reagiert.

In **Kapitel 5** werden die Kernaussagen der vorherigen Kapitel noch einmal zusammengefasst. Es wird ein kurzer Überblick über Erweiterungen des Feder-Masse-Modells gegeben, welche im Lauflabor etabliert und untersucht wurden. Diese erweiterten Modelle werden in den Kontext der vorliegenden Arbeit eingeordnet. Das Kapitel endet mit einem Ausblick auf künftige Arbeit bezüglich Modellen, Experimenten und Robotik.

Abstract

Chapter 1 provides an introductory framework for the following chapters 2, 3 and 4, which are published in international scientific journals. At first, I briefly summarize the various types of terrestrial legged locomotion. Then, we take a closer look at the commonalities and differences between human and avian running. At last, the characteristics of the spring mass model are elucidated.

Chapter 2[*] deals with the subject of estimating an effective leg stiffness.

Leg stiffness is a common parameter used to characterize leg function during bouncing gaits, like running and hopping. In the literature, different methods to approximate leg stiffness based on dynamic and kinematic parameters are described. A challenging point in estimating leg stiffness is the definition of leg compression during contact. In this paper four methods (methods A-D) based on ground reaction forces and one method (method E) relying on temporal parameters are described. Leg stiffness calculated by these five methods are compared with running patterns, predicted by the spring-mass model.

The best and simplest approximation of leg stiffness is method E. It requires only easily accessible parameters (contact time, flight time, resting leg length, body mass and the leg's touch down angle). Method D is of similar quality but additionally requires the time-dependent progression of the GRF. The other three methods show clear differences from the model predictions by over- or underestimating leg stiffness, especially at slow speeds.

Leg stiffness is derived from a conceptual model of legged locomotion and does not exist without this model. Therefore, it is important to prove which experimental method is suited best for approximating the stiffness in a specific task. This will help to interpret the predictions of the conceptual model in comparison with experimental data.

In **Chapter 3**[†] an extended swing leg control strategy is derived and compared with experimental data on human running.

[*]Blum Y., Lipfert S.W., Seyfarth A., *J. Biomech.,* 42: 2400-2405, 2009

[†]Blum Y., Lipfert S.W., Rummel J., Seyfarth A., *Bioinspir. Biomim.,* 5: 026006, 2010

Humans can run within a wide range of speeds without thinking about stabilizing strategies. The leg properties seem to be adjusted automatically without need of sensory feedback.

In this work, the dynamics of human running are represented by the planar spring mass model. Within this framework, for higher speeds, running patterns can be stable without control strategies. Here, potential strategies that provide stability over a broader range of running patterns are considered and these theoretical predictions are compared to human running data.

Periodic running solutions are identified and analyzed with respect to their stability. The control strategies are assumed as linear adaptations of the leg parameters - leg angle, leg stiffness and leg length - during swing phase. To evaluate the applied control strategies regarding their influence on landing behavior, two parameters are introduced: the velocity of the foot relative to the ground (*ground speed matching*) and the foot's *angle of approach*.

Results show that periodic running solutions can be stabilized and that control strategies, which guarantee running stability, are redundant. For any swing leg kinematics (adaptation of leg angle and leg length), running stability can be achieved by adapting the leg stiffness in anticipation of the ground contact.

Chapter 4[‡] presents one application of the method derived in chapter 3, namely the comparison of experimental data on human and avian running with respect to stiffness adaptation, stability and robustness.

Humans and birds both walk and run bipedally on compliant legs. However, differences in leg architecture may result in species-specific leg control strategies as indicated by the observed gait patterns. In this work, control strategies for stable running are derived based on a conceptual model and compared with experimental data on running humans and pheasants (*Phasianus colchicus*).

From a model perspective, running with compliant legs can be represented by the planar spring mass model and stabilized by applying swing leg control. Here, linear adaptations of the swing leg parameters, leg angle, leg length and leg stiffness, are assumed. Experimentally observed kinematic control parameters (leg rotation and leg length change) of human and avian running are compared, and interpreted within the context of this model, with specific focus on stability and robustness characteristics.

[‡]Blum Y., Birn-Jeffery A., Daley M.A., Seyfarth A., *J. Theor. Biol.,* (in press)

The results suggest differences in stability characteristics and applied control strategies of human and avian running, which may relate to differences in leg posture (straight leg posture in humans, and crouched leg posture in birds). It has been suggested that crouched leg postures may improve stability. However, as the system of control strategies is overdetermined, our model findings suggest that a crouched leg posture does not necessarily enhance running stability.

The model also predicts different leg stiffness adaptation rates for human and avian running, and suggests that a crouched avian leg posture, which is capable of both leg shortening and lengthening, allows for stable running without adjusting leg stiffness. In contrast, in straight-legged human running, the preparation of the ground contact seems to be more critical, requiring leg stiffness adjustment to remain stable.

Finally, the analysis of a simple robustness measure, the normalized maximum drop, suggests that a crouched leg posture may provide greater robustness to changes in terrain height.

In **Chapter 5**, the main findings of the previous chapters are summarized. Furthermore, a short overview on extensions to the spring mass model that were established and investigated at the Lauflabor Locomotion Laboratory is given and situated in the context of this work. The chapter ends with an outlook on future work, concerning models, experiments and robotics.

Contents

Zusammenfassung iii

Abstract vii

List of Symbols, Terms and Definitions xiv

1. General Introduction 1

1.1. Legged locomotion 1

1.1.1. Leg posture 1

1.1.2. Leg number and gaits 2

1.1.3. Leg structure 4

1.2. Human and avian locomotion 6

1.2.1. Dynamic similarity 7

1.2.2. Stride length and duty factor 7

1.2.3. Posture 8

1.2.4. Ground reaction force 8

1.3. Spring mass running 9

1.4. Thesis outline 12

2. Effective Leg Stiffness 13

2.1. Introduction 13

2.2. Methods 14

2.2.1. Sinusoidal force curve 14

2.2.2. Corrected force curve 16

2.2.3. Force - duty factor - relation 16

2.2.4. Experiments 17

2.2.5. Stiffness estimation 17

2.2.6. Modeling 18

2.3. Results 18

2.4. Discussion 20

3. Swing Leg Control **25**
3.1. Introduction . . . 25
3.2. Methods . . . 28
3.2.1. Model . . . 28
3.2.2. Stability analysis . . . 28
3.2.3. Periodic solutions . . . 29
3.2.4. Control strategy . . . 31
3.2.5. Landing strategy . . . 31
3.2.6. Simulation tools . . . 33
3.2.7. Experiments . . . 33
3.2.8. Leg stiffness . . . 35
3.3. Results . . . 35
3.3.1. Periodic solutions based on experimental data . . . 35
3.3.2. Stability of the model . . . 36
3.3.3. Comparison between model and experimental data . . . 37
3.4. Discussion . . . 39
3.4.1. Strategies to stabilize running . . . 40
3.4.2. Biological relevance . . . 41
3.4.3. Technical relevance . . . 42
3.4.4. Passive stability and energy control . . . 43

4. Crouched Leg Posture **45**
4.1. Introduction . . . 45
4.2. Methods . . . 47
4.2.1. Model . . . 47
4.2.2. Stability analysis . . . 48
4.2.3. Gait robustness . . . 49
4.2.4. Experiments . . . 49
4.2.5. Data analysis and simulation . . . 51
4.3. Results . . . 51
4.4. Discussion . . . 56
4.4.1. Swing phase . . . 58
4.4.2. Landing strategy . . . 59
4.4.3. Stability . . . 59
4.4.4. Robustness . . . 61
4.5. Conclusion . . . 61

5. General Conclusion **63**
5.1. Summary 63
5.2. Extensions to the spring mass model 64
5.3. Outlook 67

Appendix **71**
A. Stability and robustness 71
B. General description of limit cycle stability analysis 73
C. Calculation of the normalized maximum drop (NMD) 74

Bibliography **75**

CV and List of Publications **87**

Ehrenwörtliche Erklärung **89**

List of Symbols, Terms and Definitions

Nomenclature

CoM	center of mass
CoP	center of pressure
GSM	ground speed matching
TD	touch down
TDc	touch down of the contralateral leg
TO	take off
TOc	take off of the contralateral leg

Dimensional variables

α	leg angle [deg]
α_{TD}	angle of attack [deg]
$\dot{\alpha}$	changing rate of the leg angle [deg/s]
BW	body weight [N]
Δh_{max}	maximum drop [m]
ΔL	leg compression [m]
Δy	vertical displacement of the CoM [m]
E	system energy [J]
E_{Ref}	reference energy [J]
F_{max}	maximum leg force [BW]
g	gravitational acceleration [m/s^2]
γ	angle of approach [deg]
GRF	ground reaction force [BW]
k_{Leg}	leg stiffness [BW/L_0]
k_{TD}	spring stiffness at TD [BW/L_0]
$\dot{k}$	changing rate of the leg stiffness [k_{TD}/s]
L_0	resting leg length [m]
$\dot{L}$	changing rate of the leg length [L_0/s]
m	body mass [kg]
NMD	normalized maximum drop [L_0]

t_{C}	contact time [s]
t_{F}	flight time [s]
t_{Fall}	falling time from apex to TD [s]
T	gait cycle [s]
v_{x}	horizontal velocity of the CoM [m/s]
v_{y}	vertical velocity of the CoM [m/s]
$v_{\mathrm{x,Ref}}$	reference velocity [m/s]
y_{A}	apex height [m]
$y_{\mathrm{i}}, y_{\mathrm{i+1}}$	apex heights of two subsequent apices [m]

Non-dimensional variables

DF	$=$	$\dfrac{t_{\mathrm{C}}}{2\,(t_{\mathrm{C}} + t_{\mathrm{F}})}$	duty factor
Fr	$=$	$\dfrac{v_{\mathrm{x}}^2}{g\,L_0}$	Froude number

1. General Introduction

1.1. Legged locomotion

Terrestrial locomotion has evolved as animals adapted from aquatic to terrestrial environments and yielded a diverse range of animals that share the common challenge of movement and support against gravity. There are two basic forms of locomotion found among terrestrial animals: Legged locomotion and limbless locomotion, which means moving forward without legs, primarily using the body itself as a propulsive structure (Gans, 1962; Gray, 1946).

Movement on legs is the most common form of terrestrial locomotion and it is found within two major groups with many terrestrial members, the vertebrates (Grillner, 1975; Alexander, 1989b) and the arthropods (Ritzmann et al., 2004). In this section, the following aspects of legged locomotion are introduced: (i) the leg posture, (ii) the number of legs with the resulting gaits and (iii) the functional structure of the leg.

1.1.1. Leg posture

The evolution of terrestrial locomotion is generally understood as a transition from a sprawling posture, with the limbs sweeping laterally to the body, to an erect posture with the limbs located underneath the body. Therefore, among living vertebrates three major classes of postural mechanics exist: Sprawling (e.g. salamanders and lizards), semi-erect (e.g. crocodilians and chameleons) and fully erect (e.g. birds and mammals) (Bakker, 1971). However, some animals may use different postures in different circumstances, depending on the posture's mechanical advantages.

The sprawling posture is the most primitive, and it is the original limb posture from which the others evolved. The upper leg segments (humerus and femur) are held almost horizontally and the body can be lifted off the ground only with much work from the ventral shoulder and hip muscles. The sprawling

limb posture is sufficient for most reptiles and amphibians, as they are usually passive and only get active for short time periods to hunt, defend their territory or escape predators (Bakker, 1971). This posture is typically associated with trotting gaits, and the body flexes from side-to-side during movement to increase step length (Reilly and Delancey, 1997; Farley and Ko, 1997). Among the invertebrates, most arthropods, which includes the most diverse group of animals, the insects, also exhibit a sprawling posture (Schmitt et al., 2002).

The semi-erect posture is more accurately interpreted as an extremely elevated sprawling posture. This kind of locomotion is typically found in large lizards such as monitor lizards (Jenkins, 1983) and crocodilians (Parrish, 1987). However, evidence suggests that crocodilians 'regressed' their posture as a result of adapting to a mostly aquatic lifestyle, and evolved their semi-erect stance from ancestors that already had a fully erect stance (Reilly and Elias, 1998).

Birds and nearly all mammals exhibit a fully erect posture, although they evolved it independently. In these groups the legs are placed underneath the body and the proximal limb segments operate in a nearly vertical, sagittal plane. The body weight can be supported with less muscle power, as the leg forces are transmitted more directly through bones and joints than in the sprawling posture (Bakker, 1971). This allows for a high level of activity and enduring locomotion.

1.1.2. Leg number and gaits

The number of locomotory appendages varies much between animals and an exemplary overview is given in this section. A definition of gait was given by Alexander (1989b): *"A gait is a pattern of locomotion characteristic of a limited range of speeds, described by quantities of which one or more change discontinuously at transitions to other gaits."* Naturally, gaits depend on the number of available legs and sometimes the same animal may use different numbers of its legs in different circumstances.

A number of species move and stand on two legs. Although the great majority of living terrestrial vertebrates are quadrupeds, bipedalism can be found within mammals, reptiles and birds. The group of animals that is exclusively bipedal are the birds, which have either an alternating or a hopping gait. Typically, smaller birds use hopping gaits, while heavier, ground-living birds such as the galliforms use striding gaits. Among mammals, various groups of primates

(Schmitt, 2003), macropods (Windsor and Dagg, 1971) and a few groups of heteromyd rodents (Djawdan, 1993) locomote bipedally. Most of these species move by hopping on both legs simultaneously, such as the macropods and many heteromyd rodents. Crows and jerboas, however, use a skipping gait when moving fast. Only a few mammals such as humans and other primates show an alternating, striding bipedal gait, namely walking and running. Within reptiles, some families of lizards are also capable of bipedal locomotion (Aerts et al., 2003), especially when running at high speeds (Irschick and Jayne, 1999). The basilisk lizard *Basiliscus basiliscus*, also known as Jesus Christ lizard, is even capable of running short distances on water (Glasheen and McMahon, 1996). Cockroaches have also been observed running bipedally at their highest running speeds (Full and Tu, 1991). Typical bipedal gaits are walking, running, skipping, hopping and jumping.

Macropods, such as kangaroos and wallabies, are the only mammals that naturally show tripedal movements. During slow progression, they use their thick and muscular tail and alternate between resting their weight on their tail and their two hind legs (Windsor and Dagg, 1971).

With the exception of birds, all terrestrial vertebrate groups with legs are mostly quadrupedal. Mammals, reptiles, and amphibians usually move on four legs and many quadrupedal gaits can be observed. Generally, quadrupedal gaits can be classified into two categories: symmetrical and asymmetrical gaits. Symmetrical gaits have the footfalls of each pair of feet (fore and hind) evenly spaced in time. They can be further subdivided into walking and running gaits, such as trot or pace. In asymmetrical gaits, the two feet function as a pair in parallel. They either strike the ground at the same time or slightly shifted. Typical asymmetrical gaits are gallop (e.g. horses and dogs), half-bound (e.g. weasels), bound (e.g. mice) and pronk (e.g. gazelles) (Hildebrand, 1989).

Insects, the largest group of arthropods and the most diverse group of animals on earth, typically have three pairs of legs, one pair on each of the three thoracic segments. From this, the alternative name for insects, namely 'hexapods', is derived, although not all hexapods are now regarded as insects. Most of the hexapods are also hexapedal, which means they move and stand on six legs. However, some hexapods are quadrupedal with their front two legs modified for grasping (e.g. the praying mantis) or digging (e.g. the cicada larva) (Chapman, 1998). Insect locomotion was extensively studied in cockroaches, and they typically use an alternating tripod gait (Full et al., 1991). The first and the third

leg on one side of the body move more or less simultaneously with the second leg on the opposite side. Each leg moves 180° out of phase with its corresponding contralateral leg.

Spiders, scorpions and other arachnids move on eight legs. They typically walk by moving their legs reciprocally, similar to the tripod movement of their hexapedal relatives. The first and the third leg on one side of the body move simultaneously with the second and forth leg on the opposite side. Every step creates only one new 'footprint', namely that of the first leg on one side. The other legs follow the footsteps of the preceding legs (Dixon, 1892; Ehlers, 1939).

Crustaceans have a fair number of legs that varies among species. Crabs and crayfishes for example move on either eight or ten legs. Crabs typically walk and run sideways (Burrows and Hoyle, 1973; Blickhan and Full, 1987), while other crustaceans such as crayfishes move forward.

However, some creatures have even more legs. Some insect larvae such as caterpillars and sawfly larvae have up to five (caterpillars) or nine (sawflies) additional fleshy pro-legs in addition to the six legs normal for insects. Caterpillars normally locomote by running a wave of contraction followed by relaxation along the body from tail to head, producing the characteristic traveling 'hump' on the caterpillar's back. As the wave passes, each segment is raised from the ground, telescoped forwards and then lowered back to the ground (Brackenbury, 1999).

Some species, the myriapods, move on many more legs. Centipedes have one pair of legs per body segment, which sums up to about 50 legs. However, some species may have more than 200 legs. The terrestrial animals with the most legs are the millipedes. They have two pairs of legs per body segment, with common species having between 80 and 400 legs overall. The rare species *Illacme plenipes* may have up to 750 legs (Marek and Bond, 2006). Animals with that many legs typically move by waves of motion traveling along their legs.

1.1.3. Leg structure

Legged locomotion requires that internal forces are effectively transmitted to the external environment. This is achieved by muscles attached to a rigid skeleton, which is either an endoskeleton (vertebrates), an exoskeleton (arthropods) or a hydrostatic skeleton (insect larvae).

The legs of terrestrial vertebrates have internal bones, with the skeletal muscles attached externally by tendons. The bone is a composite material, consisting

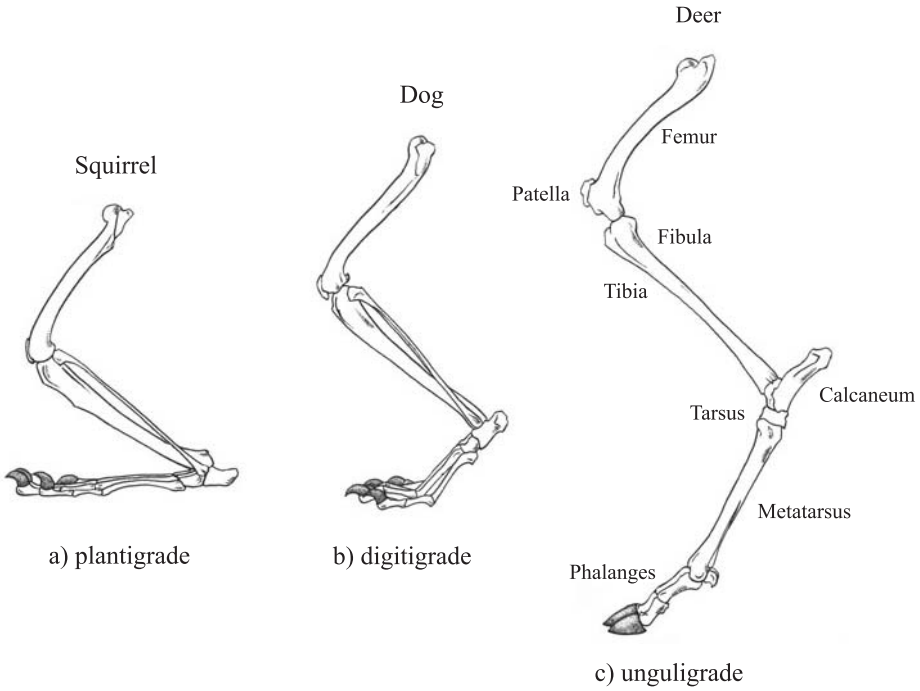

Figure 1.1.: Schematic drawings of three mammalian legs, representing a) plantigrade, b) digitigrade and c) unguligrade arrangement of leg and foot bones (© BioKIDS, University of Michigan, http://www.biokids.umich.edu/).

of collagen fibers and minerals, which allows for a light-weight and rigid, yet flexible, structure (Biewener, 2003).

The basic form of the vertebrate hind limb consists of the hip joint, the thigh (femur), the knee joint, the shank (tibia and fibula), the ankle joint, the heel (calcaneum) and the foot, consisting of tarsus, metatarsus and the toes (phalanges) (figure 1.1). Within this scheme there is much variation in form and function.

Typically, the vertebrate foot has five toes, however some animals have evolved fewer than this, and some early tetrapods had even more (Acanthostega, for example, had eight toes (Carroll et al., 2005)). Feet have evolved in many forms, depending on the animal's needs. Most amphibians, reptiles, and some mammals such as humans and bears are plantigrade, walking on the soles of their feet (figure 1.1(a)). Birds and many mammals, such as cats and dogs are digitigrade, walking on their toes, which allows for a the greater stride length (figure 1.1(b)). Some animals such as horses and deers are unguligrade, walking on the tips of their toes (figure 1.1(c)). This even further increases their stride length and thus their speed. A few mammals such as great apes are also known

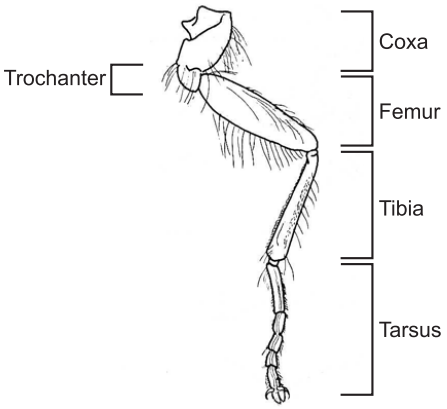

Figure 1.2.: Schematic drawing of an insect leg (© D.G. Mackean, http://www.biology-resources.com/).

to walk on their knuckles, at least with their front legs. Knuckle-walking allows the foot (hand) to specialize in fine motor skills.

The muscles of arthropods, which possess an exoskeleton, are attached to the inside of the skeleton. By containing the soft tissue inside, exoskeletons have the advantage of providing good protection and resistance to desiccation. On the other hand, the rigid exoskeleton limits the animal's growth and the cuticle must be shed at regular intervals. The cuticle of arthropod exoskeletons, like bone, is also a composite material. Nearly all arthropod exoskeletons contain approximately 15-20 % stiff chitin fibres, embedded in a protein matrix (Biewener, 2003).

The arthropod leg typically consists of five basic segments articulated by condylar joints: coxa, trochanter, femur, tibia and tarsus (Chapman, 1998). Although each joint hinges in only one direction, the end of the limb can be moved in any direction (figure 1.2).

1.2. Human and avian locomotion

The biological aspect of this work is the description and characterization of bipedal running. As humans and birds are species that are exclusively bipedal, I want to elucidate some similarities and differences of human and avian locomotion.

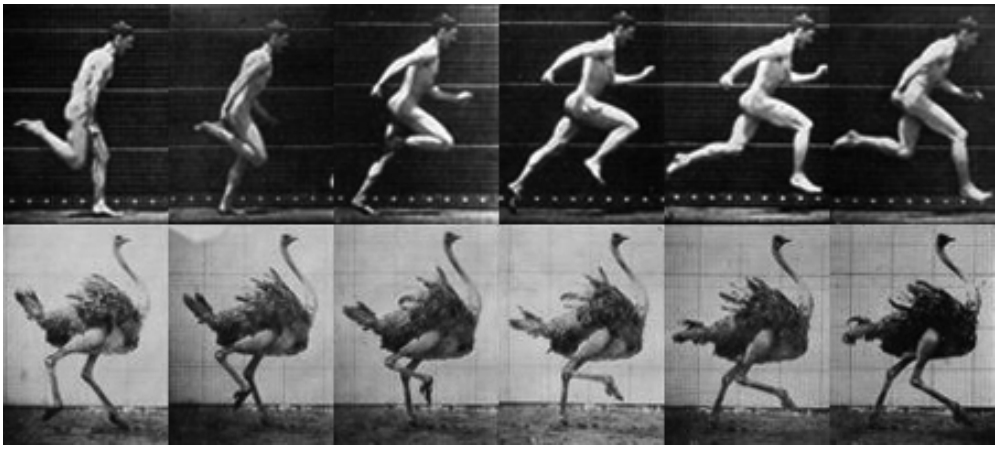

Figure 1.3.: Photographies of a running man (top) and a running ostrich (bottom). Adapted from Muybridge (2000, 1967).

1.2.1. Dynamic similarity

Similar animals of different sizes that locomote at equal Froude numbers tend to move in a dynamically similar manner (Alexander, 2003). However, strict dynamic similarity is impossible, because animals of different sizes are generally not geometrically similar. Therefore, the dynamic similarity depends on the appropriate choice of the characteristic quantities, speed v_x and length L_0, used to calculate the Froude number (Alexander, 2004). For our characteristic speed, we use the horizontal speed v_x at the instant of apex. For our characteristic length, we use the 'rest length' L_0, which is defined as the vertical hip position with respect to the ground during upright standing.

1.2.2. Stride length and duty factor

Further characteristic quantities are the relative stride length and the duty factor. The relative stride length is the distance traveled in a complete cycle of leg movement (i.e. between successive footfalls of the same foot) divided by the chosen characteristic length, and the duty factor is the fraction of the duration of a stride for which a particular foot has ground contact. Two animals that move dynamically similar would have equal relative stride lengths and equal duty factors (Alexander, 2004). Gatesy and Biewener (1991) showed that the relative stride lengths of humans and several grounded birds are of comparable size during both walking and running. Due to the leg posture, larger birds with rather extended legs such as ostriches have shorter stride lengths than smaller

and more crouched birds (figure 1.4(a)). In general, galliform birds take relatively long steps, as the total length of their leg bones is much greater than the hip height. The duty factors of birds are similar to those of humans at walking speeds, but larger than those of humans in running (figure 1.4(b)). According to Alexander et al. (1979), the lowest recorded avian duty factor is about 0.3 for a fast running ostrich.

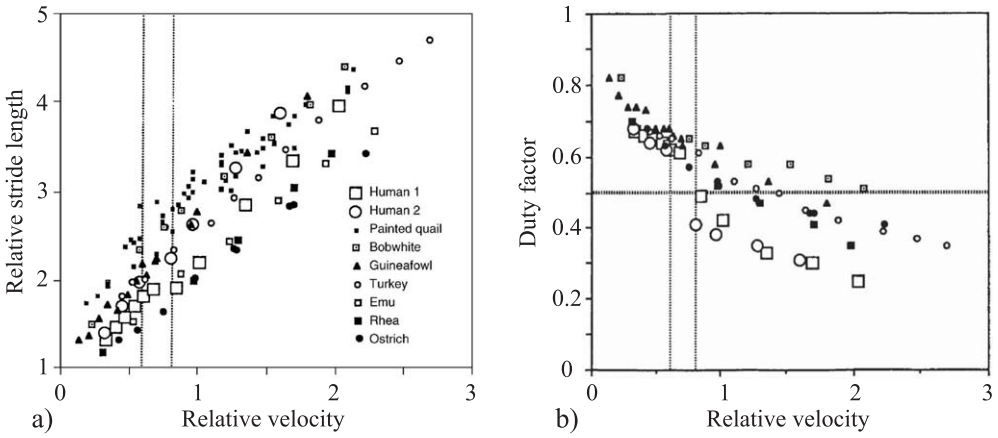

Figure 1.4.: Relative stride length (a) and duty factor (b) in relation to the relative velocity for humans and seven different birds. The vertical dashed lines indicate the walk-run transition. From Gatesy and Biewener (1991).

1.2.3. Posture

A main difference from humans is that birds are digitigrade (figure 1.1). Their long tarsometatarsals keep the foot well clear of the ground. In human running, ground clearance is only achieved by bending the knee. While humans walk and run with an upright trunk, birds (except for penguins) keep it much more horizontal. Gatesy (1999a) showed that the pelvic pitch angle (i.e. the angle of the pelvis with respect to the horizontal) of a guinea fowl tilts from about 25° in slow walking to about 11° in fast running. During locomotion, the avian center of mass is in front of the hip, and the knee remains forward of the hip throughout the entire stance phase (Gatesy, 1999a).

1.2.4. Ground reaction force

The forces a body exerts on the ground balance its weight, but these forces are not constant during locomotion, and the vertical component of the ground reaction force fluctuates about a mean value equal to the body weight (figure

1.5). The pattern of the vertical force F_y that the foot exerts during ground contact t_C can be represented by a sum of cosines and sines (Fourier series)

$$F_y(t) = a_1 \cos(\pi t/t_C) + b_2 \sin(2\pi t/t_C) + a_3 \cos(3\pi t/t_C) + ..., \quad (1.1)$$

with a_n and b_n being constants (Alexander and Jayes, 1980). Assuming symmetric force patterns, which means neglecting the sine terms, and ignoring high-frequency components, equation 1.1 reduces to

$$F_y(t) = a_1 (\cos(\pi t/t_C) - q \cos(3\pi t/t_C)). \quad (1.2)$$

The coefficient $q = -a_3/a_1$ is called shape factor, as it describes the shape of the force curve (Alexander and Jayes, 1978). As feet can not exert negative vertical forces, the shape factor lies within the range $q = [-0.33, 1]$. Negative shape factors describe bell-shaped force curves. When the shape factor is zero, the force curve becomes the single-peaked half cycle of a cosine (figure 1.5 (c) and (d)). As the shape factor increases, the force curve becomes flatter and eventually, for values above 0.15, double-humped (figure 1.5 (a) and (b)). In human walking, the shape factor generally increases from about $q = 0.2$ in very slow walking to about $q = 0.7$ at the fastest walking speeds. In running it typically lies between $q = [-0.2, 0]$ (Alexander, 1989b). Like humans, birds exert two-peaked vertical forces on the ground when walking, and single-peaked forces when running (Muir et al., 1996; Cavagna et al., 1977).

1.3. Spring mass running

In the previous chapters we have seen that the leg structure is very complex and therefore, it is difficult to identify its function. However, despite leg segmentation and different leg geometries, despite the interplay of muscles, tendons and tissues and despite the influence of neuronal control and reflexes, humans and animals exhibit a spring-like leg behavior during locomotion (Alexander, 2002). The simplest model that describes spring-like leg behavior is the spring mass model (Blickhan, 1989; McMahon and Cheng, 1990). Such simplified models are often called templates. But why are we using templates, although we know that they do not correspond to the complexity of real biological systems?

I would like to answer this question with a quote from Full and Koditschek (1999): *"A template is a pattern that describes and predicts the behavior of the body in pursuit of a goal. It is a model created by 'trimming away' all the*

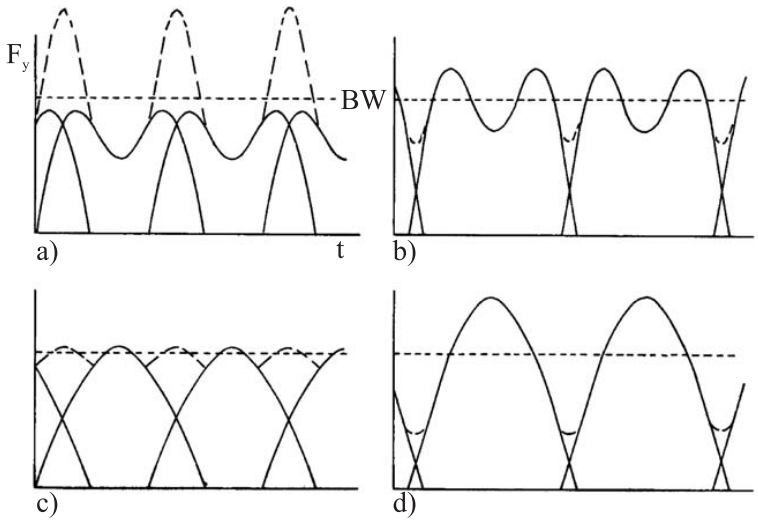

Figure 1.5.: Schematic graphs of the vertical ground reaction force F_y against time t during walking. The dotted line indicates the body weight (BW). Each graph shows the individual forces exerted by the left and right foot (solid line) and the total force when both feet are on the ground (dashed line). Shape factors are $q = 0.4$ in (a) and (b), and $q = 0$ in (c) and (d). Duty factors are DF = 0.75 in (a) and (c), and DF = 0.55 in (b) and (d). From Alexander and Jayes (1978).

incidental complexity of joints, muscles and neurons. A template is not only a simple model but also serves as a guide or target for the control of locomotion."

Biological systems show redundancy concerning kinematics, actuation and neuronal innervation, as they allow for many possible solutions to a desired movement task. Therefore, Full and Koditschek state that a *template* should be the simplest model (i) that contains the least number of variables and parameters, and (ii) that exhibits a target behavior. More realistic models that have the behavior of their templates embedded within shall then be called *anchors*.

This means, as we are investigating human and avian locomotion with respect to leg stiffness (chapter 2) and swing leg control (chapters 3 and 4), that the target behavior of the template is (i) to reproduce the dynamics of the center of mass and (ii) to be capable of adjusting the model parameters in order to stabilize the investigated running pattern. It has been shown that the planar spring mass model fulfills both conditions (Blickhan, 1989; McMahon and Cheng, 1990; Seyfarth et al., 2003; Geyer et al., 2006).

In the planar spring mass model (table 1.1) the axis of the leg runs within the sagittal plane defined by the body's center of mass (CoM) and the foot's contact point at the ground (center of pressure (CoP)). The position of the

Table 1.1.: Core assumptions of the spring mass model

Leg	massless represented by a compressible spring force acts along leg axis, no torques are generated
Body	CoM represented by a point mass no moments of inertia exist
Foot	represented by a foot point position is fixed during ground contact
Energy	total system energy is constant
Direction of motion	within the sagittal plane

CoP is assumed to be fixed, which means that (i) the extension of the foot is neglected and (ii) the foot point does not slide on the ground. As the leg force acts along the axis of the leg (i.e. directing from CoP to CoM), no torques are generated. Therefore, the whole body can be reduced to a point mass located at the position of the CoM. Additionally, the assumption of a point-mass body and massless legs, is supported by the observation that the upper body is much more massive then the legs. In humans, the relative mass of one leg is about 17% of the body mass (Braune and Fischer, 1893; Clauser et al., 1969), the avian leg (guinea fowl *Numida meleagris*) totals at least 10% of the body mass (Ellerby et al., 2005).

The legs of the spring mass model are assumed to be massless, and therefore, there exists no energy expenditure to swing the leg forward or backward. Also impacts a real leg would experience when it hits the ground can not be represented with the model. However, the foot point velocity at landing, which is a indirect measure for impacts, can be quantified (section 3.2.5). In the simple spring mass model the leg force only depends on the leg compression, which means that no dissipation or energy input is assumed. The system itself (i.e. without additional modifications) is energy conserving and the leg function is described by a compressible spring. Therefore, the system is completely described by four parameters: the system energy, the leg spring's angle of attack, the spring stiffness and its rest length (figure 2.1).

1.4. Thesis outline

In the following chapters we will gain a more profound insight into the characteristics of spring mass running. At first, we will learn about different approaches to extract parameters from experimental data in order to use them for model based predictions. While in spring mass running the touch down (TD) and take off (TO) angles are equal and the whole contact phase is symmetric, this is not true for experimentally observed leg angles. In human running the leg angles during contact are tilted towards steeper angles at TD and flatter angles at TO. However, as in spring mass running symmetric contact phases are assumed, a symmetric leg angle has to be determined that matches the experimental data with model based assumptions. Another key assumption of the model is the compressible leg spring. Biological limbs are much more complex as compared to simple mechanical springs and therefore, a method has to be established that converts experimentally observable parameters into a corresponding spring stiffness (chapter 2). Secondly, I will present a conceptual method that, while keeping the system energy constant, stabilizes the running pattern (chapter 3). This is realized by a swing leg control strategy that implies a linear adaptation of the leg parameters during late swing phase. Furthermore, in order to evaluate this swing leg control strategy concerning impacts a real leg with masses would experience, two quantities that describe the magnitude and the direction of the foot's velocity vector, *ground speed matching* and *angle of approach*, are introduced. Stability, measured as the system's ability to cope with small perturbations of the initial conditions, is evaluated using limit cycle stability analysis. At last, the findings of the presented methods are used to compare human with avian running, concerning stability and robustness (chapter 4). Here, the robustness is approximated using a simple kinematic estimation of the *normalized maximum drop*, which can be tolerated during spring mass running.

2. Effective Leg Stiffness in Running*

2.1. Introduction

Leg stiffness is a key parameter of data analysis and modeling of legged locomotion. In the scientific literature different methods of estimating leg stiffness can be found. Many approaches assume that leg stiffness k_{Leg} is given by the ratio of maximum vertical ground reaction force (GRF) and leg compression ΔL. But the approximation of the leg compression is not unique and several methods are used.

Leg compression can be expressed as a function of the vertical displacement of the center of mass (CoM), the leg length and the angle of attack. Assuming symmetric contact phases, the angle of attack can be substituted by horizontal velocity and contact time (McMahon and Cheng, 1990). This method (method A) is well established and frequently used (Farley and Gonzalez, 1996; Ferris et al., 1998; He et al., 1991).

Another way of calculating leg compression ΔL is the measurement of the CoM-center of pressure (CoP) displacement (Arampatzis et al., 1999). But this method poses other challenges: How should the displacement be quantified? Should it be the maximum displacement during contact phase, the displacement from TD to midstance (De Wit et al., 2000), or an adjusted value that accounts for the TD-TO-asymmetry (Cavagna, 2006) (method B)?

To estimate leg stiffness during hopping a completely different approach was proposed by Dalleau et al. (2004). The GRF is approximated by a sine-shaped force curve and the corresponding leg compression is calculated. This method is adopted to estimate an effective leg stiffness in running (method C) and extended by introducing an additional correction factor (method D). In this

*Blum Y., Lipfert S.W., Seyfarth A., *J. Biomech.,* 42: 2400-2405, 2009

paper, a last method only relying on temporal parameters, body mass, resting leg length and touch down angle is presented (method E).

These five different methods are compared with predictions of the spring mass model for running (Seyfarth et al., 2002).

2.2. Methods

Leg length is defined between CoM-CoP in accordance to the spring mass model (figure 2.1). Other definitions of leg length (e.g. derived from kinematic landmarks) may also be used, however, differences of stiffness estimations are marginal.

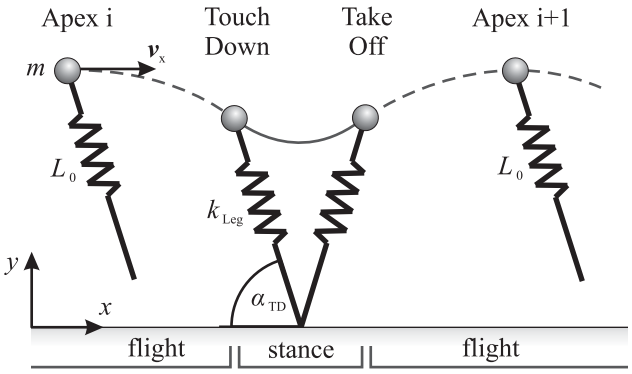

Figure 2.1.: Spring mass model for running. Point mass m supported by a compressible spring with rest length L_0, spring stiffness k_{Leg} and angle of attack α_{TD} running at horizontal speed v_x.

2.2.1. Sinusoidal force curve

Leg stiffness is defined as

$$k_{\text{Leg}} = -\frac{\partial F}{\partial L}, \tag{2.1}$$

with F being the vertical GRF and L the leg length during stance phase (figure 2.2(a)). Assuming a linear force-length relationship the leg stiffness reduces to

$$k_{\text{Leg}} = \frac{F_{\text{max}}}{\Delta L}, \tag{2.2}$$

where F_{max} is the maximum value of the GRF and ΔL the absolute value of the leg compression.

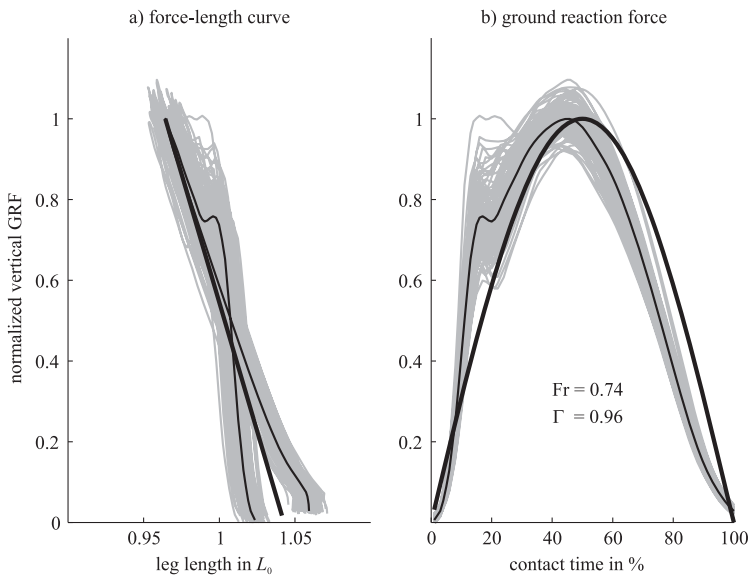

Figure 2.2.: Force-length curve of the effective leg length (CoM-CoP) (a) and ground reaction force (GRF) (b) of one representative subject (Fr = 0.74). a) Thin gray lines: force-length curves of individual contacts. Thin black line: mean force-length curve. Thick black line: linear approximation. b) Thin gray lines: GRF of individual contacts. Thin black line: mean GRF. Thick black line: sine-shaped curve. The ratio between the enclosed areas of mean curve (thin) and sine curve (thick) is $\Gamma = 0.96$.

To compare the experimental data with predictions of the spring mass model, the vertical GRF can be approximated by a sine-function with amplitude $F_{\max}$ and half of the periodic time t_C (Alexander, 1989a; Dalleau et al., 2004) (figure 2.2(b))

$$F_y(t) = F_{\max} \sin\left(t \frac{\pi}{t_C}\right). \tag{2.3}$$

Twice integrating the vertical acceleration $a(t) = \frac{F_y(t)}{m} - g$ results in

$$y(t) = -\frac{F_{\max}}{m} \left(\frac{t_C}{\pi}\right)^2 \sin\left(t \frac{\pi}{t_C}\right) - \frac{g}{2} t^2 + C\,t + y_0. \tag{2.4}$$

Taking the CoM's vertical velocity at midstance $\dot{y}\left(\frac{t_C}{2}\right) = -g\,\frac{t_C}{2} + C = 0$ and the initial condition $y_0 = L_0 \sin\alpha_{TD}$ into account, this leads to the vertical position of the CoM at midstance

$$y\left(\frac{t_C}{2}\right) = -\frac{F_{\max}}{m} \left(\frac{t_C}{\pi}\right)^2 + \frac{g}{8} t_C^2 + L_0 \sin\alpha_{TD}. \tag{2.5}$$

Thus, with calculation of the leg compression $\Delta L = L_0 - y\left(\frac{t_C}{2}\right)$, the leg stiffness

(equation (2.2)) is a function of the experimental parameters maximum vertical GRF , body mass , leg length , contact time and leg angle at TD (table 2.1).

2.2.2. Corrected force curve

By assuming a simple sinusoidal force pattern (equation 2.3), the area underneath the theoretical sine-curve $F_{\mathrm{y,sine}}$ is slightly larger than the area underneath the force curve of the experimental data $F_{\mathrm{y,exp}}$ (figure 2.2(b)). In order to equalize the impulses I_{exp} and I_{sine}, generated by the experimentally observed and the sine-shaped force curves, a correction factor

$$\Gamma = \frac{I_{\mathrm{exp}}}{I_{\mathrm{sine}}}, \tag{2.6}$$

with

$$I_{\mathrm{exp}} = \int_0^{t_{\mathrm{C}}} F_{\mathrm{y,exp}} \qquad \text{and} \qquad I_{\mathrm{sine}} = \frac{2}{\pi} F_{\mathrm{max}} t_{\mathrm{C}}, \tag{2.7}$$

is introduced that decreases the amplitude of the sine to $F'_{\mathrm{max}} = \Gamma \cdot F_{\mathrm{max}}$ and thereby the approximated force curve (equation 2.3) to

$$F'_{\mathrm{y}}(t) = \Gamma \cdot F_{\mathrm{max}} \sin\left(t \frac{\pi}{t_{\mathrm{C}}}\right). \tag{2.8}$$

This lower peak vertical GRF accords with predictions of the point of force translation (POFT) model in running (Bullimore and Burn, 2006).

In accordance to equation (2.5), the CoM's vertical position at midstance is identified as

$$y'\left(\frac{t_{\mathrm{C}}}{2}\right) = -\Gamma \frac{F_{\mathrm{max}}}{m} \left(\frac{t_{\mathrm{C}}}{\pi}\right)^2 + \frac{g}{8} t_{\mathrm{C}}^2 + L_0 \sin\alpha_{\mathrm{TD}} \tag{2.9}$$

and the leg stiffness k'_{Leg} is determined as a function of Γ and the variables of k_{Leg} (table 2.1).

2.2.3. Force - duty factor - relation

To compare the corrected with the uncorrected sinusoidal GRF approximation, the relationship between the maximum GRF F_{max} and the duty factor DF is derived. Considering the integration of the Γ-corrected sine-shaped force curve (equation 2.8), the velocity of the CoM at TD

$$\dot{y}'(0) \quad = \quad -\frac{F'_{\mathrm{max}}}{m} \frac{t_{\mathrm{C}}}{\pi} + C = -g \frac{t_{\mathrm{F}}}{2} \tag{2.10}$$

and the velocity of the CoM at midstance

$$\dot{y}'\left(\frac{t_C}{2}\right) = -g\,\frac{t_C}{2} + C = 0 \tag{2.11}$$

lead, by eliminating C, to the relationship (figure 2.3)

$$F'_{max} = m\,g\,\frac{\pi}{2}\left(\frac{t_F}{t_C} + 1\right) = m\,g\,\frac{\pi}{4}\left(\frac{1}{DF}\right). \tag{2.12}$$

Hence, the corrected maximum leg force $F'_{max} = \Gamma \cdot F_{max}$ (section 2.2.2) can be calculated based on temporal parameters, without estimating the Γ-factor.

2.2.4. Experiments

Experimental data of i) 21 human subjects (11 females, 10 males, $m = 71 \pm 12\,\mathrm{kg}$, $L_0 = 0.96 \pm 0.08\,\mathrm{m}$) running at five different speeds between 0.5 and 2.7 m/s and ii) 7 subjects (1 female, 6 males, $m = 77 \pm 9\,\mathrm{kg}$, $L_0 = 1.02 \pm 0.07\,\mathrm{m}$) running at 2, 3 and 4 m/s were collected and analyzed (Lipfert, 2010). The initial vertical position of the CoM, which corresponds to the leg's rest length L_0, was approximated by the vertical position of the greater trochanter multiplied with a gender specific factor A ($A = 1.05$ for women and $A = 1.10$ for men) (Lipfert, 2010). This factor had previously been determined by force recordings of five female and five male subjects lying on a force plate (Winter, 2005). A total of 9393 single-support running steps at speeds between 0.55 m/s ($\mathrm{Fr} = 0.03$) and 4.08 m/s ($\mathrm{Fr} = 1.65$) were analyzed. CoM movements are calculated by twice integrating the accelerations obtained from GRF data (figure 2.2(b)) and the effective leg is defined as the distance between CoM and CoP. The horizontal velocity v_x of the CoM is determined at the instance of apex. F_{max} is the maximum vertical GRF. Contact time t_C is measured from TD to TO and flight time t_F is calculated by subtracting contact time from step time (half of the gait cycle). In order to determine the leg angle, a hybrid leg is defined between the foot point (located half way between heel and toe) and the CoM. Leg angle α is measured with respect to the horizontal and increases with leg retraction. At the instance of TD the leg's angle of attack is α_{TD}.

2.2.5. Stiffness estimation

In this work, five different methods to estimate leg stiffness (equation 2.2), denoted in non-dimensional units as body weight per leg length (BW/L_0) (Geyer et al., 2006), are applied and compared (table 2.1):

A) Symmetric trajectories are assumed and resulting leg compression is calculated, using Δy which is the vertical displacement of the CoM from TD to midstance (McMahon and Cheng, 1990).

B) Leg compression is defined as the difference of adjusted leg length (the rest length is adjusted to match both, initial and final leg length at TD and TO, respectively) and minimum CoM-CoP distance.

C) Leg compression is estimated assuming a sinusoidal GRF (equation 2.3).

D) Leg compression is estimated assuming a Γ-corrected sinusoidal GRF (equation 2.8).

E) Maximum vertical leg force $F'_{\max}$ is derived from the duty factor (equation 2.12) and represents the amplitude of the sinusoidal GRF. Leg compression is estimated as in method C.

2.2.6. Modeling

To compare the results with predictions of the spring mass model (figure 2.1), the periodic k-α-region is calculated using a steps to fall method (Seyfarth et al., 2002). Model parameters leg length L_0, body mass m and initial conditions $(x_0, y_0) = (0, L_0)$ and $(v_{x0}, v_{y0}) = (v_x, 0)$ are taken from the experimental data. The running spring mass model is implemented in the Simulink tool of Matlab R2007b (The MathWorks, Inc.). For numerical integration a variable time-step integrator (ode113) is used with an absolute and relative error tolerance of 10^{-9}.

2.3. Results

The experimentally derived correction factors Γ are smaller than 1 and increase moderately with speed (table 2.2 and 2.3).

The five different methods A - E to estimate leg stiffness lead to different k-α distributions. Mean values and standard deviations of the different methods are listed for all 21 subjects (table 2.2) and for all 7 subjects (table 2.3). As the data have been taken from two different groups of subjects, stiffness values between the groups differ, but the tendency is consistent.

Figure (2.3) shows the predicted relationship between maximum GRF and duty factor (equation 2.12), compared to the experimentally observed distribution. A

Table 2.1.: Input parameters, equation of leg stiffness and required additional calculations for methods A - E.

	parameters	calculations	
A	$F_{max}, L_0, \Delta y,$ v_x, t_C	$k_A = \frac{F_{max}}{\Delta L_{Sym}}$	$\Delta L_{Sym} = \Delta y + L_0 - \sqrt{L_0^2 - \left(\frac{v_x\, t_C}{2}\right)^2}$
B	$F_{max}, L(t), t_C$	$k_B = \frac{F_{max}}{\Delta L_{Adj}}$	$\Delta L_{Adj} = L_{0,Adj} - L_{min}$ $L_{0,Adj} = L_{TD} + \frac{L_{TO} - L_{TD}}{t_C} \cdot t'$ $L(t') = L_{min}$
C	$F_{max}, m, L_0,$ α_{TD}, t_C	$k_C = \frac{F_{max}}{\Delta L}$	$\Delta L = L_0 + \frac{F_{max}}{m}\left(\frac{t_C}{\pi}\right)^2 - \frac{g}{8}t_C^2$ $-L_0 \sin\alpha_{TD}$
D	$F(t), m, L_0,$ α_{TD}, t_C	$k_D = \frac{\Gamma \cdot F_{max}}{\Delta L}$	$\Delta L = L_0 + \Gamma\frac{F_{max}}{m}\left(\frac{t_C}{\pi}\right)^2 - \frac{g}{8}t_C^2$ $-L_0 \sin\alpha_{TD}$ $\Gamma = \frac{\pi}{2\,F_{max}\,t_C}\int_0^{t_C} F(t)$
E	m, L_0, α_{TD} t_C, t_F	$k_E = \frac{F'_{max}}{\Delta L}$	$\Delta L = L_0 + \frac{F'_{max}}{m}\left(\frac{t_C}{\pi}\right)^2 - \frac{g}{8}t_C^2$ $-L_0 \sin\alpha_{TD}$ $F'_{max} = m\,g\,\frac{\pi}{4}\left(\frac{1}{DF}\right)$ $DF = \frac{t_C}{2\,(t_C + t_F)}$

comparison of the Γ-corrected (black line) with the uncorrected (gray line) force curve shows that the correction provides a better accordance with experimental data.

In figure (2.4) the k-α pairs of each step, whose Froude number Fr lies within the range of the first standard deviation $\mathrm{Fr} = 0.76 \pm 0.11$ are shown. (Assuming a normal distribution, the σ_1-interval ($\mu \pm \sigma$) includes 68.3% of the values.) Method A results in the lowest stiffness values ($k = 15.5 \pm 2.7\,\mathrm{BW/L_0}$). Method B leads to the highest and most distributed values of leg stiffness ($k = 24.3 \pm 3.7\,\mathrm{BW/L_0}$). Method C, D and E differ slightly, are much more focused compared to method A and B and result all in moderate stiffness values

Table 2.2.: Mean value and standard deviation of horizontal velocity v_x, Froude number Fr, correction factor Γ, duty factor DF, maximum vertical GRF F_{max}, derived maximum vertical GRF $F'_{max}(\mathrm{DF})$ and leg stiffness k_{Leg} estimated by methods A - E for 21 subjects (11 females, 10 males, age 25 ± 3 yrs, body mass $m = 71 \pm 12$ kg, resting leg length $L_0 = 0.96 \pm 0.08$ m) at five different speeds.

v_x [m/s]	0.55 ± 0.06	1.08 ± 0.09	1.62 ± 0.11	2.15 ± 0.14	2.66 ± 0.18
Fr	0.03 ± 0.01	0.13 ± 0.02	0.29 ± 0.04	0.49 ± 0.07	0.76 ± 0.11
Γ	0.87 ± 0.04	0.87 ± 0.05	0.88 ± 0.04	0.89 ± 0.04	0.91 ± 0.04
DF	0.40 ± 0.04	0.39 ± 0.04	0.40 ± 0.04	0.39 ± 0.04	0.37 ± 0.03
F_{max} [BW]	2.23 ± 0.19	2.26 ± 0.19	2.25 ± 0.18	2.29 ± 0.19	2.33 ± 0.22
$F'_{max}(\mathrm{DF})$ [BW]	1.97 ± 0.19	2.01 ± 0.21	1.99 ± 0.20	2.04 ± 0.21	2.12 ± 0.20
k_A [BW/L_0]	22.3 ± 3.9	20.6 ± 3.2	18.6 ± 3.4	17.1 ± 3.2	16.1 ± 2.9
k_B [BW/L_0]	22.3 ± 3.6	22.0 ± 2.9	22.4 ± 3.6	23.6 ± 3.7	24.1 ± 3.7
k_C [BW/L_0]	18.6 ± 3.2	17.9 ± 3.2	16.9 ± 3.0	16.6 ± 2.7	16.7 ± 2.4
k_D [BW/L_0]	22.5 ± 3.5	20.8 ± 3.1	19.2 ± 3.3	18.0 ± 2.8	17.4 ± 2.6
k_E [BW/L_0]	22.4 ± 3.3	20.8 ± 2.8	19.2 ± 3.1	18.0 ± 2.7	17.4 ± 2.6

($k = 17.0 \pm 2.4\,\mathrm{BW/L_0}$, $k = 17.5 \pm 2.4\,\mathrm{BW/L_0}$ and $k = 17.5 \pm 2.4\,\mathrm{BW/L_0}$, respectively). The methods D and E provide a slightly more stretched k-α distribution than method C.

2.4. Discussion

Stiffness approximation based on sine-shaped GRF is an appropriate approach for hopping (Dalleau et al., 2004) and running. For higher speeds ($\mathrm{Fr} \geq 0.7$) only F_{max} needs to be determined and the influence of Γ is negligible ($\Gamma > 0.9$). Since all $\Gamma \leq 1$ and $\Gamma = 1$ denotes the equality of the areas underneath the experimentally observed GRF and the approximated sinusoidal force pattern (figure 2.2(b)), increasing Γ stands for improving accordance of the impulses. In this case, method C is sufficient.

For lower speeds, both, F_{max} and Γ are required to estimate appropriate leg stiffness (method D).

Table 2.3.: Mean value and standard deviation of horizontal velocity v_x, Froude number Fr, correction factor Γ, duty factor DF, maximum vertical GRF F_{max}, derived maximum vertical GRF $F'_{max}(\mathrm{DF})$ and leg stiffness k_{Leg} estimated by methods A - E for 7 subjects (1 females, 6 males, age 24 ± 1 yrs body mass $m = 77 \pm 9$ kg, resting leg length $L_0 = 1.02 \pm 0.07$ m) at three different speeds.

v_x [m/s]	2.06 ± 0.03	3.07 ± 0.03	4.08 ± 0.03
Fr	0.42 ± 0.03	0.94 ± 0.06	1.65 ± 0.10
Γ	0.87 ± 0.01	0.91 ± 0.01	0.93 ± 0.02
DF	0.42 ± 0.03	0.36 ± 0.03	0.33 ± 0.03
F_{max} [BW]	2.18 ± 0.15	2.40 ± 0.20	2.55 ± 0.26
$F'_{max}(\mathrm{DF})$ [BW]	1.89 ± 0.13	2.20 ± 0.16	2.39 ± 0.20
k_A [BW/L_0]	17.4 ± 2.7	15.7 ± 2.6	14.8 ± 3.0
k_B [BW/L_0]	25.1 ± 3.4	24.9 ± 3.5	25.7 ± 4.2
k_C [BW/L_0]	18.6 ± 2.8	20.3 ± 3.5	21.2 ± 4.5
k_D [BW/L_0]	21.4 ± 3.4	20.4 ± 3.1	20.1 ± 3.4
k_E [BW/L_0]	21.6 ± 2.6	21.0 ± 3.4	21.3 ± 4.5

In order to estimate the maximum leg force based on the duty factor F'_{max} the Γ-factor needs to be considered. Otherwise the maximum forces are underestimated (figure 2.3). However, for stiffness estimation, the need of calculating the correction factor Γ can be avoided by deriving the corresponding maximum GRF F'_{max} from the duty factor (method E) as this underestimation of the maximum GRF corresponds to the desired reduction of the sine amplitude (method D). By estimating F'_{max} based on DF, the correction factor Γ becomes obsolete, as the vertical impulses generated i) by the sine of amplitude F'_{max} and ii) by the experimental force pattern are equal.

In conclusion, independent of running speed, the method which was presented here (method E) is a very good and simple approach to derive an effective leg stiffness corresponding to the spring mass model.

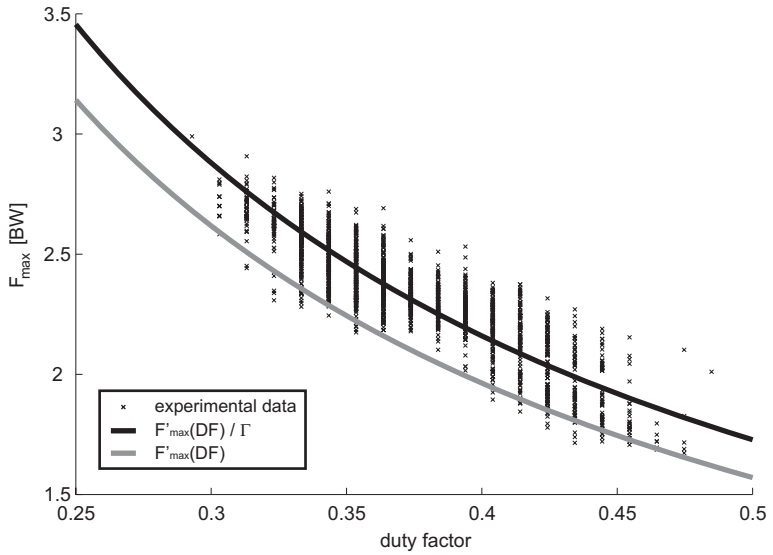

Figure 2.3.: Relationship between maximum ground reaction force $F_{\max}$ and duty factor DF for 21 subjects at Fr $= 0.76 \pm 0.11$. Black crosses: experimental data (discrete DF values are due to the sampling frequency of 240 Hz). Black line: relationship predicted for sinusoidal GRF with amplitude $F'_{\max}(\mathrm{DF})/\Gamma$ ($\Gamma = 0.91$). Gray line: predicted for sinusoidal GRF with amplitude $F'_{\max}(\mathrm{DF})$.

Acknowledgments

I would like to thank Juergen Rummel for so much help and support, Daniel Haeufle for proofreading and recalculating and Michael Günther for inspiring discussions. This study was supported by the grant SE 1042/1 provided by the German Research Foundation (DFG).

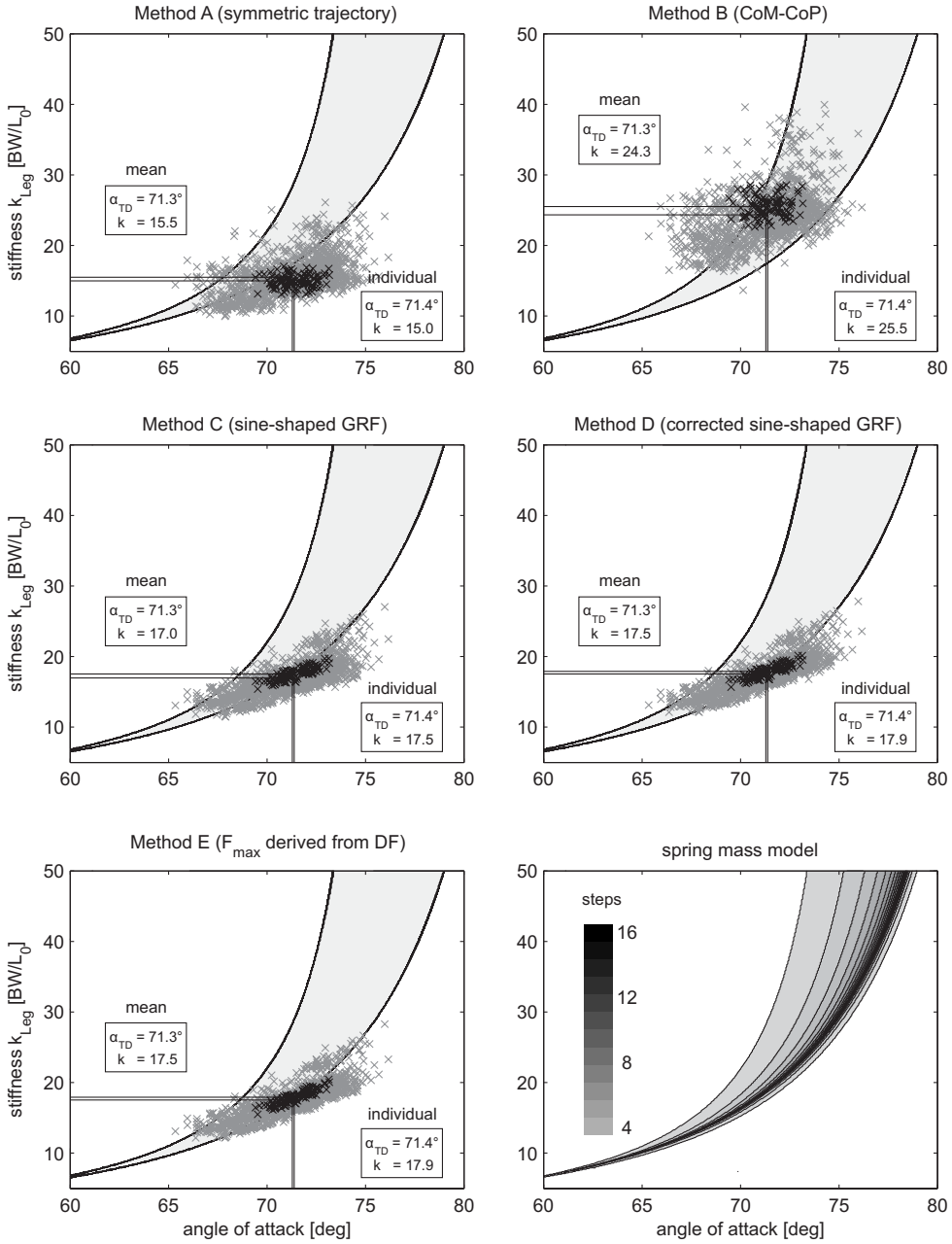

Figure 2.4.: k-α distributions of 21 subjects for all steps with Froude numbers within σ_1-interval of $\mathrm{Fr} = 0.76 \pm 0.11$ (gray crosses) and one representative individual subject ($\mathrm{Fr} = 0.74$) (black crosses). Leg stiffness k_{Leg} is estimated using methods A - E. Predictions of reachable steps using the steps to fall method for the spring mass model in running (last diagram).

3. Swing Leg Control in Human Running[†]

3.1. Introduction

Despite different gaits, speeds, and morphologies, human and legged animal locomotion can be described by spring-like leg behavior (Alexander, 2002), which originates in the elastic properties of muscles (Hill, 1938) and tendons spanning the joints. These elastic structures are located in the passive (tendon, ligament and aponeurosis) and active (titin and cross bridges) components of the muscle-tendon complex (Fung, 1967; Rode, Siebert, Herzog and Blickhan, 2009; Bressler and Clinch, 1974; Rode, Siebert and Blickhan, 2009). But why should a leg act like a spring? Elastic systems possess several crucial characteristics: (i) An elastic leg benefits from energy transfer by storage and release of spring energy (Cavagna et al., 1964; Alexander, 1991). (ii) Elasticities prevent the leg from damage by reducing the impact forces (Alexander, 1990). (iii) An elastic system moves with a predetermined natural oscillation and therefore acts as a pattern generator (Seyfarth et al., 2002). Due to the coupling of springs (i.e. tendons) with muscles in biological systems, the advantage of elasticity can be exploited by imitation of spring-like leg behavior (Geyer et al., 2003). A springy leg can be simulated by the interaction of energy loss and supply during stance (Kalveram et al., 2008). In a segmented leg, spring-like leg behavior arises from quasi-elastic operations of joints (Seyfarth et al., 2001; Günther and Blickhan, 2002; Rummel and Seyfarth, 2008).

In this paper, the leg function is represented by the planar spring mass model, which is a well-established template to describe human running (Blickhan, 1989; McMahon and Cheng, 1990) and walking (Geyer et al., 2006). It is known that the spring mass model is self-stabilizing for adequate leg parameter adjustments (angle of attack, leg stiffness and leg length) and sufficient speeds (e.g.

[†]Blum Y., Lipfert S.W., Rummel J., Seyfarth A., *Bioinspir. Biomim.,* 5: 026006, 2010

$v_x > 3\,\mathrm{m/s}$ for human-like dimensions) (Seyfarth et al., 2002). In other words, there exists a set of potential running solutions, but only a very small subset is attractive and can be used without control strategies. Therefore, to explore the whole solution space, or at least increase the amount of usable running solutions, the implementation of control mechanisms is essential. In previous studies it has been shown that swing leg retraction is one possible strategy that enhances stability in locomotion for both quadrupedal galloping (Herr and McMahon, 2001) and bipedal running (Seyfarth et al., 2003). This control strategy, namely the adaptation of the leg angle during swing phase, is now extended to all three leg parameters in a straightforward manner. In human running, the influence of running speed on leg retraction (in combination with leg length change) can be observed in the adaptation of the foot's landing velocity (De Wit et al., 2000). Adaptation of the leg stiffness during swing phase was found in a study on running on uneven ground (Grimmer et al., 2008). Experiments on running birds have also demonstrated that retraction and lengthening of the leg during swing phase are applied to prevent the birds from falling (Daley et al., 2007). The first step to investigate swing leg control strategies is the application of first order approximations (i.e. linear variations of the leg parameters), disregarding, for the moment, that natural adaptation rates of the leg parameters might be more complex.

Biological systems continuously encounter variations in both internal properties (e.g. leg parameters) and external conditions (e.g. roughness of the ground). Such variations can be considered as perturbations of the initial conditions and, depending on the system behavior, the resulting deviation from the original trajectory will increase or decrease from step to step. In this paper, swing leg control strategies are identified that stabilize running patterns derived from experimental data on human running, using the spring mass model. Within the framework of the model the leg function is determined by three parameters (leg angle, leg stiffness and leg length). From a biological point of view, these parameters are time-dependent, anticipating the ground contact and stabilizing the running pattern: Starting with undisturbed initial conditions, the parameter adaptations do not change the trajectory of the center of mass (CoM). However, in case of a disturbed initial height, the parameter adaptations are supposed to reduce the resulting deviation from the undisturbed CoM trajectory.

According to their biological archetype, humanoid robots have segmented legs but they are rigid and mostly fully actuated. These robots copy the kinematics but not the dynamics of human locomotion. Therefore, their legs are

non-compliant as the chosen control strategies (e.g. zero-moment point (Vukobratovic and Borovac, 2004)) tolerate no elasticities. So far, robots without compliant leg structures have not been capable of running, e.g. Johnnie (Löffler et al., 2003), Reem-B (Tellez et al., 2008), HUBO (Park et al., 2008), or run with extremely short flight phases, e.g. ASIMO (Hirose and Ogawa, 2007), HRP-2LR (Kajita et al., 2007). Currently, the fastest and most maneuverable legged robots have compliant legs. Spring-like leg behavior can be achieved with pogo sticks, as it was demonstrated by the robots of Raibert (1986). The cockroach inspired hexapedal robot iSprawl (Kim et al., 2006), one of the fastest running robots at present (up to 15 body lengths per second), shows the impressive capability of compliant legs, providing robust locomotion. In contrast to legs with actuation around the hip and along the leg axis, leg structure can also be purely passive like those of the spring mass model. This passive leg compliance has been successfully implemented in the hexapedal robot RHex (Saranli et al., 2001; Neville, 2005) and the quadrupedal robot ScoutII (Poulakakis et al., 2005). Thus, even with simple and unsegmented structures, compliant legs have great technical relevance.

The purpose of this work is to derive a conceptual method to identify potential swing leg control strategies for stable spring mass running. The space of control parameters (control space) is defined by the changing rates of the three leg parameters (leg rotation, stiffness adaptation and leg length adaptation). Here, the control strategies are assumed as linear adaptations of the leg parameters during swing phase. We hypothesize that periodic but unstable solutions in spring mass running can be stabilized by application of these simplified swing leg control strategies, and that such control strategies can be identified in human running. The method is implemented as follows: (i) The entire space of periodic running solutions (solution space) is explored and one solution that is unstable without control is selected. (ii) In order to stabilize this unstable solution the mentioned control strategies are applied. Depending on the selected control strategy, the initial conditions of the leg parameters are calculated such that when the system starts with the undisturbed initial height, the previously selected solution is achieved. If, however, the initial height is disturbed, the leg parameter adjustment at the instant of touch down is changed and therefore, a different solution is achieved. (iii) The entire control space for the selected solution is explored and compared with human running data.

3.2. Methods

3.2.1. Model

The planar spring mass model (Blickhan, 1989; McMahon and Cheng, 1990) is characterized by alternating flight and stance phases. The body is represented by a point mass m supported by a linear spring of stiffness k_{TD} and rest length L_0, touching the ground with the angle of attack α_{TD} (figure 3.1). During flight phase the center of mass (CoM) describes a ballistic curve, determined by the gravitational force. The transition from flight to stance occurs when the landing condition $y = L_0 \sin(\alpha_{\mathrm{TD}})$ is fulfilled. During stance phase the equation of motion is

$$m\ddot{\mathbf{r}} = k_{\mathrm{TD}} \left(\frac{L_0}{r} - 1 \right) \mathbf{r} - m\mathbf{g}, \tag{3.1}$$

where $\mathbf{r} = (x, y)$ is the position of the point mass with respect to the foot point, r its absolute value and $\mathbf{g} = (0, g)$ the gravitational acceleration, with $g = 9.81\,\mathrm{m/s^2}$. Since the system is conservative and assuming that the ground is even, the system's state is fully described by the apex condition, characterized by the state vector $(y_{\mathrm{A}},\ v_{\mathrm{x}})$. The apex is the highest point of the trajectory with zero vertical velocity v_{y}. Therefore, the system energy

$$E = \frac{1}{2} m v_{\mathrm{x}}^2 + m g y_{\mathrm{A}} \tag{3.2}$$

is determined by the horizontal velocity v_{x} and the apex height y_{A}. In order to give this energy an intuitive meaning, a reference speed

$$v_{\mathrm{x,Ref}} = \sqrt{2 \left(\frac{E}{m} - g L_0 \right)} \tag{3.3}$$

is introduced. The reference speed is that speed which corresponds to a given energy E, assuming that the apex height y_{A} equals the resting leg length L_0.

3.2.2. Stability analysis

The stability of spring mass running is analyzed using a one-dimensional return map $y_{\mathrm{i+1}}(y_{\mathrm{i}})$ of two subsequent apex heights y_{i} and $y_{\mathrm{i+1}}$ (figure 3.2) (Seyfarth et al., 2003). In this apex-return map, periodic movements are represented by fixed points y^* which satisfy (i) the identity $y_{\mathrm{i}} = y_{\mathrm{i+1}} = y^*$, while (ii) maintaining positive horizontal velocity $v_{\mathrm{x,i}} = v_{\mathrm{x,i+1}} > 0$. For stable running, these conditions

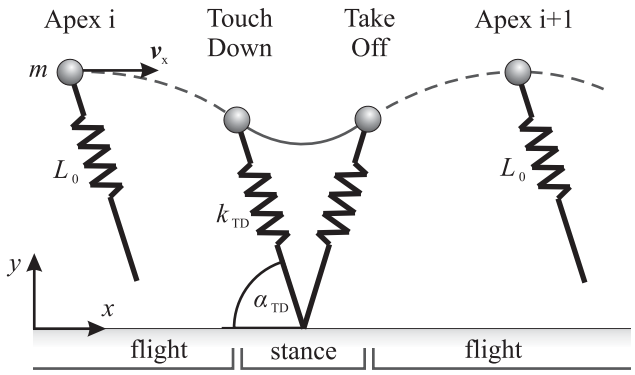

Figure 3.1.: One step cycle in spring mass running between two subsequent apices: point mass m (representing the body mass) supported by a translational spring with rest length L_0, stiffness k_{TD} and angle of attack α_{TD}.

need to be complemented by the requirement that the absolute value of the slope s of the return map $y_{\mathrm{i+1}}(y_{\mathrm{i}})$ has to be smaller than one in the neighborhood of the fixed point $y*$. The slope

$$s = \left.\frac{dy_{\mathrm{i+1}}}{dy_{\mathrm{i}}}\right|_{y^*} \tag{3.4}$$

characterizes the strength of the attraction (Strogatz, 1994):

$$s = \begin{cases} (0,1) & : \text{ stable} \\ 0 & : \text{ super-stable} \\ (-1,0) & : \text{ stable, oscillating} \end{cases} \tag{3.5}$$

Numerically, the slope s at a fixed point y^* is approximated by the difference quotient $s = (y_{\mathrm{i+1}} - y^*)/y_{\mathrm{P}}$, which analyzes the effect of a perturbed apex height $y_{\mathrm{i}} = y^* + y_{\mathrm{P}}$ on the subsequent apex $y_{\mathrm{i+1}}$. Here, a perturbation of $y_{\mathrm{P}} = 10^{-7}$ m is considered. The horizontal velocity v_{x} is adapted such that the system energy remains constant. For example, $s = 0.5$ means that small perturbations y_{P} affecting the apex height are reduced by half after each step, whereas zero slope ($s = 0$) indicates a super-stable running pattern, where perturbations are completely compensated within one step.

3.2.3. Periodic solutions

For the stability analysis, periodic solutions (fixed points in the apex-return map (figure 3.2)) matching the experimental data are considered. Steady state running patterns predicted by the spring mass model are defined by three parameters: angle of attack α_{TD}, reference velocity $v_{\mathrm{x,Ref}}$ (which corresponds to the

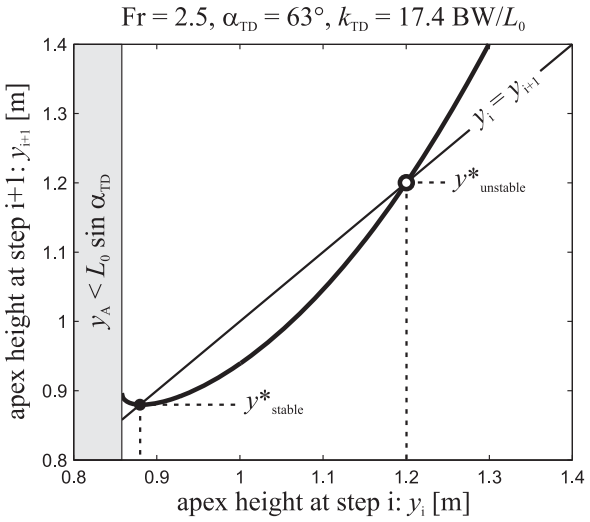

Figure 3.2.: Return map of the apex height $y_{i+1}(y_i)$ for one periodic solution. Intersections with the diagonal $y_i = y_{i+1}$ denote the fixed points y^*. In this example, the lower fixed point is stable ($s = -0.03$), the upper is unstable ($s = 1.79$).

system energy E) and leg stiffness k_{TD} (figure 3.5). The reference velocity $v_{x,Ref}$ can be expressed in terms of the non-dimensional Froude number $\mathrm{Fr} = \frac{v_{x,Ref}^2}{g L_0}$ (Alexander, 2003).

In contrast to the model, the experimentally observed leg angles at touch down (TD) and take off (TO) are asymmetric with respect to the vertical axis, as in human running the lower limb is more extended at TO than at TD (Cavagna, 2006). Therefore, to match experimental data with the spring mass model, a symmetric angle of attack is calculated from experimental parameters. As speed (in terms of Froude number Fr), angle of attack α_{TD}, leg stiffness at TD k_{TD} and falling time t_{Fall} are dependent parameters of the spring mass model (figure 3.5b), the angle of attack can be expressed as a function of the other three parameters. This symmetric (model based) angle of attack is flatter than experimentally observed (table 3.1), but the resulting angle swept during contact is about the same as for the asymmetric case. The Froude number Fr which corresponds to the forward velocity v_x, and the flight time t_F are determined using experimental data (section 3.2.7). The stiffness of the leg spring k_{TD} corresponds to the estimated effective leg stiffness k_{Leg} (section 3.2.8).

3.2.4. Control strategy

The spring mass model is able to run under fixed landing conditions: with appropriate leg parameters (α_{TD}, k_{TD} and $L_{\mathrm{TD}} = L_0$) and sufficient running speeds ($v_{\mathrm{x,Ref}} > 3\,\mathrm{m/s}$), the system shows self-stabilizing behaviour (i.e. small perturbations will be compensated passively without changing the model parameters) (Seyfarth et al., 2002). By adjusting the leg parameters during swing phase (e.g. swing leg retraction (Seyfarth et al., 2003)), it is possible to stabilize other periodic solutions. This concept will be extended to the following leg parameter adaptations

$$\begin{aligned} \alpha(t) &= \alpha_{\mathrm{A}} + \dot{\alpha} \cdot (t - t_{\mathrm{A}}) \\ k(t) &= k_{\mathrm{A}} + \dot{k} \cdot (t - t_{\mathrm{A}}) \\ L(t) &= L_{\mathrm{A}} + \dot{L} \cdot (t - t_{\mathrm{A}}). \end{aligned} \tag{3.6}$$

Beginning at the instant of apex t_{A}, constant changing rates $\dot{\alpha}$, $\dot{k}$ and $\dot{L}$ are assumed during the second half of the flight phase (figure 3.3). To guarantee the exploration of one previously determined periodic solution, the TD values α_{TD}, k_{TD} and L_{TD} have to be maintained tor every set of changing rates, if the system is not disturbed. Therefore, the apex conditions α_{A}, k_{A} and L_{A} are calculated, depending on changing rate and predicted falling time t_{Fall}

$$\begin{aligned} \alpha_{\mathrm{A}} &= \alpha_{\mathrm{TD}} - \dot{\alpha} \cdot t_{\mathrm{Fall}} \\ k_{\mathrm{A}} &= k_{\mathrm{TD}} - \dot{k} \cdot t_{\mathrm{Fall}} \\ L_{\mathrm{A}} &= L_{\mathrm{TD}} - \dot{L} \cdot t_{\mathrm{Fall}}, \end{aligned} \tag{3.7}$$

where t_{Fall} is the expected flight time from apex to TD for a given (undisturbed) apex height y_{A}. Within the framework of the spring mass model, the contact phases are symmetric with respect to the vertical axis (section 3.2.3) and the falling time t_{Fall} corresponds to the half of the flight time $t_{\mathrm{F}}/2 = \sqrt{\frac{2}{g}\left(y_{\mathrm{A}} - l_0 \sin(\alpha_{\mathrm{TD}})\right)}$. Swing leg control continues until TD and during stance the leg stiffness remains constant.

3.2.5. Landing strategy

For a given periodic solution, we expect different combinations of $\dot{\alpha}$, $\dot{k}$, $\dot{L}$ leading to stable running. To characterize appropriate swing leg control strategies, the region with $|s| \leq 0.5$ is identified (section 3.2.2). As a secondary criterion describing the pattern, the landing behavior is analyzed. Depending on the

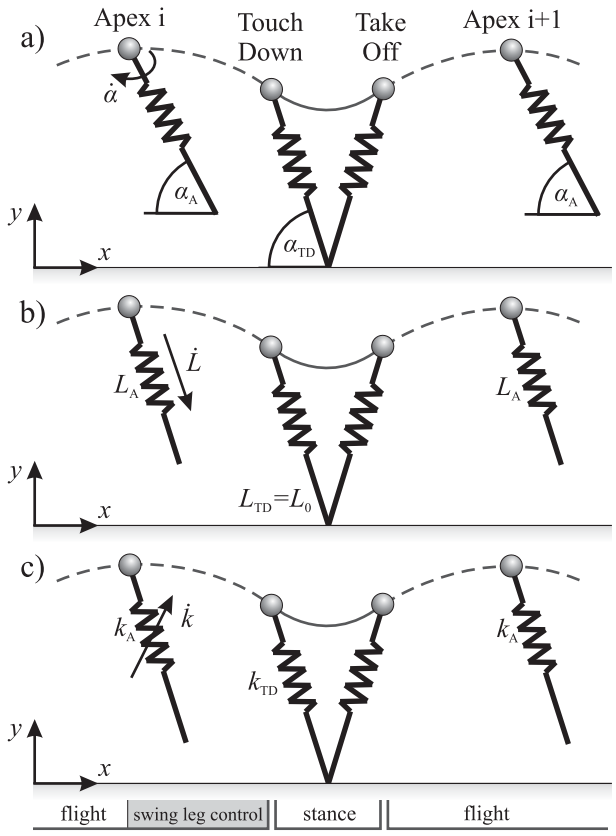

Figure 3.3.: Swing leg control strategies: a) leg rotation $\dot{\alpha}$, b) leg length change $\dot{L}$ and c) stiffness adaptation of the leg spring $\dot{k}$.

selected swing leg control strategy, different foot landing velocities and directions are possible.

Although the leg of the spring mass model is considered massless, the size of impacts a real leg would experience at TD can be approximated: With higher landing velocities of the foot with respect to the ground, larger impacts at TD are expected. The speed of the foot point with respect to the CoM defines the ground speed matching (GSM)

$$\mathrm{GSM} = \left(1 - \frac{v_{\mathrm{Foot}}}{v_{\mathrm{CoM}}}\right), \tag{3.8}$$

where $v_{\mathrm{Foot}} = \sqrt{v_{\mathrm{x,Foot}}^2 + v_{\mathrm{y,Foot}}^2}$ is the speed of the foot point and $v_{\mathrm{CoM}} = \sqrt{v_{\mathrm{x}}^2 + v_{\mathrm{y}}^2}$ the speed of the CoM at TD. 100% GSM indicates an absolutely smooth (impact-free) landing with $v_{\mathrm{Foot}} = 0$, whereas 0% GSM means that the foot point reaches the ground with the same speed as the CoM. The foot's

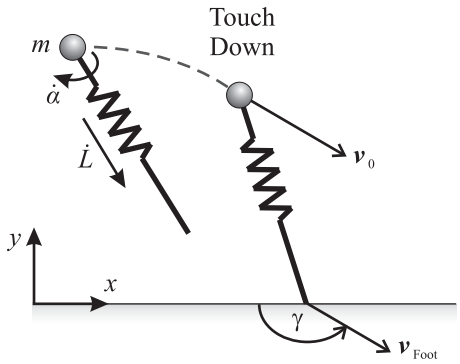

Figure 3.4.: Landing strategy: The adaptation rates $\dot{\alpha}$ and $\dot{L}$ of the kinematic parameters leg angle and leg length influence the magnitude v_{Foot} and the direction (indicated by the angle of approach γ) of the foot's landing velocity vector $\mathbf{v}_{\text{Foot}}$.

landing direction defines the angle of approach

$$\gamma = \tan^{-1}\left(\frac{v_{\text{x,Foot}}}{v_{\text{y,Foot}}}\right) + 180\,^\circ, \tag{3.9}$$

which is the angle between the foot velocity vector $\mathbf{v}_{\text{Foot}}$ and the ground (figure 3.4). In these terms, an approaching angle $\gamma = 180\,^\circ$ indicates completely flat landing (parallel to the ground) in forward direction, whereas $\gamma = 180\,^\circ\,^\circ$ indicates flat landing in backward direction. Foot landing perpendicular to the ground is described by $\gamma = 90\,^\circ$.

3.2.6. Simulation tools

The running spring mass model is implemented in Matlab/Simulink R2007b (The MathWorks, Inc.). For numerical integration a built-in variable time-step integrator (ode113) is used with an absolute and relative error tolerance of 10^{-9}.

3.2.7. Experiments

Experimental data were collected by Lipfert (2010), who had 21 human subjects (11 females, 10 males, body mass $m = 71 \pm 12\,\text{kg}$, leg length $L_0 = 0.96 \pm 0.08\,\text{m}$) running on an instrumented treadmill at different speeds. The initial vertical position of the CoM, which corresponds to the leg's rest length L_0, was approximated by the vertical position of the greater trochanter multiplied with a gender specific factor A (A = 1.05 for women and A = 1.10 for men). This factor had previously been determined by force recordings of five female and five male subject lying on a force plate (Winter, 2005). A total of 5110 running gait

cycles at speeds between 1.09 m/s ($\mathrm{Fr} = 0.13$) and 2.66 m/s ($\mathrm{Fr} = 0.76$) were analyzed. CoM movements are calculated by twice integrating the accelerations obtained from the ground reaction forces (GRF) and the effective leg is defined as distance between CoM and center of pressure (CoP). The horizontal velocity v_{x} of the CoM is determined at the instant of apex. Contact time t_{C} is measured from TD to TO, flight time t_{F} is calculated by subtracting contact time from step time (half of the gait cycle) and falling time t_{Fall} is measured from apex to TD. In order to determine the leg angle, a hybrid leg is defined between the foot point (located half way between heel and toe) and the CoM. Leg angle α is measured with respect to the horizontal and increases with leg retraction. The grand means (mean values of the subject's means) and standard deviations of the parameters are listed in table 3.1.

Table 3.1.: Grand means and standard deviations of experimental parameters (upper section) and derived model parameters (lower section) for 21 subjects (11 females, 10 males, body mass $m = 71 \pm 12\,\mathrm{kg}$, leg length $L_0 = 0.96 \pm 0.08\,\mathrm{m}$) at four different speeds.

Fr		0.13 ± 0.02	0.28 ± 0.04	0.49 ± 0.07	0.76 ± 0.12
v_{x}	[m/s]	1.09 ± 0.08	1.62 ± 0.10	2.14 ± 0.15	2.66 ± 0.18
t_{C}	[s]	0.348 ± 0.040	0.335 ± 0.038	0.309 ± 0.035	0.280 ± 0.028
t_{F}	[s]	0.069 ± 0.036	0.070 ± 0.033	0.080 ± 0.034	0.095 ± 0.027
t_{Fall}	[s]	0.039 ± 0.018	0.046 ± 0.012	0.048 ± 0.012	0.052 ± 0.011
$\alpha_{\mathrm{TD,exp}}$	[deg]	82.1 ± 1.8	77.4 ± 1.9	73.8 ± 2.3	71.2 ± 2.5
$\dot{\alpha}$	[deg/s]	33.6 ± 15.8	41.7 ± 17.4	45.6 ± 23.3	54.8 ± 26.4
$\dot{L}$	[L_0/s]	-0.27 ± 0.11	-0.30 ± 0.10	-0.33 ± 0.10	-0.37 ± 0.10
$\alpha_{\mathrm{TD,sym}}$	[deg]	79.3 ± 1.9	75.1 ± 1.8	71.6 ± 2.2	$69,0 \pm 2.2$
k_{TD}	[BW/L_0]	21.4 ± 2.9	19.5 ± 2.8	18.1 ± 2.7	17.4 ± 2.5
$\dot{k}$	[k_{TD}/s]	-7.6 ± 5.7	-2.8 ± 1.9	-0.3 ± 1.7	1.8 ± 1.9

3.2.8. Leg stiffness

Stiffness of a leg spring, assuming a linear force-length relationship, is defined as

$$k_{\mathrm{Leg}} = \frac{F_{\max}}{\Delta L} \tag{3.10}$$

with $F_{\max}$ being the maximum value of the GRF and ΔL the maximum leg compression during stance.

Assuming an elastic leg function the GRF can be approximated by a sine-function (Alexander, 1989a; Dalleau et al., 2004). Following this assumption, $F_{\max}$ and ΔL reduce to functions of body mass m, resting leg length L_0, contact time t_{C}, flight time t_{F} and angle of attack α_{TD}

$$F_{\max} = m\,g\,\frac{\pi}{4}\left(\frac{1}{\mathrm{DF}}\right), \quad \mathrm{DF} = \frac{t_{\mathrm{C}}}{2(t_{\mathrm{C}} + t_{\mathrm{F}})} \tag{3.11}$$

$$\Delta L = L_0 + \frac{F_{\max}}{m}\left(\frac{t_{\mathrm{C}}}{\pi}\right)^2 - \frac{g}{8}\,t_{\mathrm{C}}^2 - L_0\,\sin\alpha_{\mathrm{TD}}. \tag{3.12}$$

With this the effective leg stiffness (equation 3.10) is estimated (chapter 2) (table 3.1).

3.3. Results

3.3.1. Periodic solutions based on experimental data

In figure 3.5(a) periodic solutions of the spring mass model are shown for selected Froude numbers Fr and one leg stiffness $k_{\mathrm{TD}} = 17.4\,\mathrm{BW/L_0}$, which is the mean value of the effective leg stiffness corresponding to $Fr = 0.76$ (see table 3.1). With increasing running speed, in terms of Fr, the predicted angle of attack α_{TD}, aiming at one apex height y_{A}, becomes flatter and the overall range of possible leg angles enlarges. The maximum apex height, which is reached for vertical hopping (i.e. $\alpha_{\mathrm{TD}} = 90\,^\circ$), is given by $y_{\mathrm{A,max}} = \frac{E}{m\,g}$, whereas the minimum apex height is constrained by the landing condition $y_{\mathrm{A,min}} = L_0\,\sin(\alpha_{\mathrm{TD}})$. For $\mathrm{Fr} \geq 1$ stable solutions exist (thick gray lines), the other periodic solutions are unstable (black lines).

In figure 3.5(b) periodic solutions corresponding to selected leg stiffness are shown for one system energy equivalent to $\mathrm{Fr} = 0.76$. With increasing leg

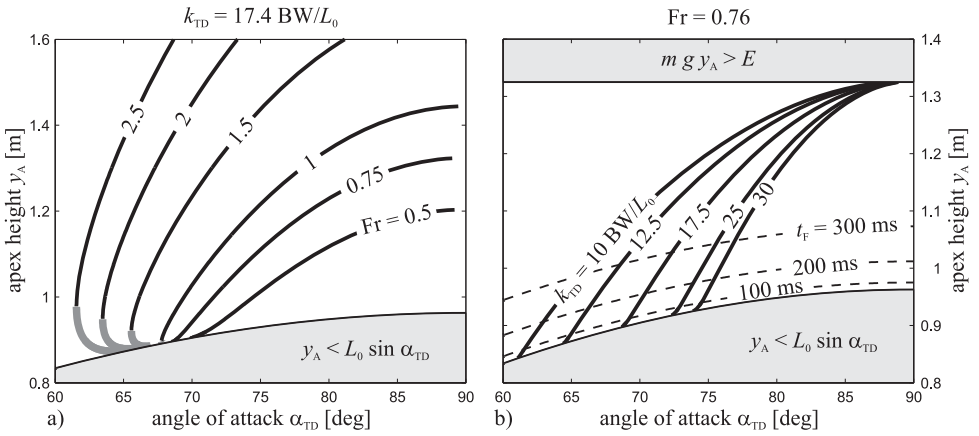

Figure 3.5.: Periodic solutions of spring mass running: apex heights $y_A = y^*$ (fixed points of the apex-return map) depending on the angle of attack α_{TD} a) for constant leg stiffness k_{TD} and selected system energies (represented by the corresponding Froude numbers Fr), and b) for constant energy E and selected spring stiffnesses k_{TD}. Thick grey lines in a) indicate stable solutions. The other illustrated solutions (black lines) are unstable. Dashed lines in b) indicate selected flight times t_F. During the time remaining from apex to TD $t_F/2$ (since symmetric contact phases are assumed), swing leg control is applied.

stiffness k_{TD}, compared at one apex height y_A, the angle of attack α_{TD} gets steeper and the flight time t_F shorter.

On average, the selected human running data correspond to a periodic solution with Fr = 0.76, $k_{TD} = 17.4\,\mathrm{BW/L_0}$ and $t_F = 0.095\,\mathrm{s}$. As symmetric contact phases are assumed, the corresponding model based angle of attack $\alpha_{TD,sym} = 69.0°$ is flatter than the experimentally observed angle $\alpha_{TD,exp} = 71.2°$ (table 3.1, section 3.2.3). With the slope $s = 1.69$ being larger than one, this solution is unstable (section 3.2.2).

3.3.2. Stability of the model

In figure 3.6(a) alternative control strategies leading to stable ($|s| < 0.5$) and super-stable ($s = 0$) running are shown for a perturbation $y_P = 10^{-7}\,\mathrm{m}$ and one selected periodic solution (Fr = 0.76, $\alpha_{TD} = 69.0°$ and $k_{TD} = 17.4\,\mathrm{BW}/L_0$). This figure is representative for all speeds, as for every set of model parameters (Froude number, angle of attack, leg stiffness and leg length), the identified stable areas describe similar wedges, whose inclinations and positions within the $(\dot{\alpha}, \dot{L})$ space vary slightly. Within the three-dimensional parameter space spanned by $\dot{\alpha}$, $\dot{k}$ and $\dot{L}$, four slices with $\dot{k} = [-5, 0, 5, 10]\,\mathrm{k_{TD}/s}$ (leg softening,

constant leg stiffness and two levels of leg stiffening, respectively) are selected. For each condition of $\dot{k}$, there exists a wedge-shaped stable area with $|s| \leq 0.5$, shifting parallel with $\dot{k}$ and enlarging with increasing $\dot{\alpha}$, $\dot{L}$. The vertices of the wedges have their origin in the intersection of the lines with $s = 0$ and $s = \pm 0.5$. Below these focus points (vertices) corresponding to different stiffness changing rates, there exists an area, where no combination of $\dot{\alpha}$ and $\dot{L}$ fulfill the landing condition $y > L_0 \sin(\alpha_{\mathrm{TD}})$ before TD. As the foot point would be below the ground during the entire flight phase, this area can not be exploited.

To characterize the foot landing, isolines of the relative foot point velocity (in percentage of GSM) and the foot's angle of approach γ are mapped in figure 3.6(b). Both are kinematic parameters, exclusively depending on the changing rates of leg length $\dot{L}$ and leg rotation $\dot{\alpha}$, but not on stiffness adaptation $\dot{k}$. The isolines of constant approaching angles γ intersect at the point of 100% GSM within the two-dimensional $(\dot{\alpha}, \dot{L})$ space independently of $\dot{k}$. The 0% GSM line, which contains $\dot{L} = 0$ and $\dot{\alpha} = 0$, describes locomotion patterns where the foot point moves relative to the ground with the same velocity as the CoM. The straight line of completely flat approaching angles ($\gamma = 0\,^\circ$ and $\gamma = 180\,^\circ$ respectively) defines the border between the accessible and inaccessible area.

3.3.3. Comparison between model and experimental data

In figure 3.6(c) the observed changing rates of leg angles and leg lengths of 21 subjects are shown (black dots) for one selected running speed ($v_{\mathrm{x,Ref}} = 2.66\,\mathrm{m/s}$). The average changing rate of the subjects are $\dot{L} = -0.37\,\mathrm{L_0/s}$ and $\dot{\alpha} = 54.8\,\mathrm{deg/s}$ (white circle). To obtain super-stable behavior ($s = 0$) in spring mass running with these experimental changing rates, a stiffness adaptation rate of $\dot{k} = 1.8\,\mathrm{k_{TD}/s}$ is required. This corresponds to a foot-to-ground velocity of 33% GSM with an approaching angle of $\gamma = 165\,^\circ$.

The experimental data are distributed over a large range of $\dot{\alpha}$ ($-50...130\,\mathrm{deg/s}$), located within the area of leg shortening ($\dot{L} < 0$), but with noticeable distance to the borderline of the accessible region ($\gamma = 180\,^\circ$). The cluster of experimental data is mainly arranged between 0% GSM and 60% GSM and with approaching angles $\gamma > 120\,^\circ$. However, individual subjects do not exploit the whole kinematic control space that is shown in figure 3.6(c), but rather they prefer kinematic control strategies which are clustered as well (figure 3.7).

Figure 3.7 shows the individual falling times t_{Fall} (in ascending order) and swing leg control strategies $\dot{\alpha}$, $\dot{L}$, $\dot{k}$ of all 21 subjects. The symbols represent the mean

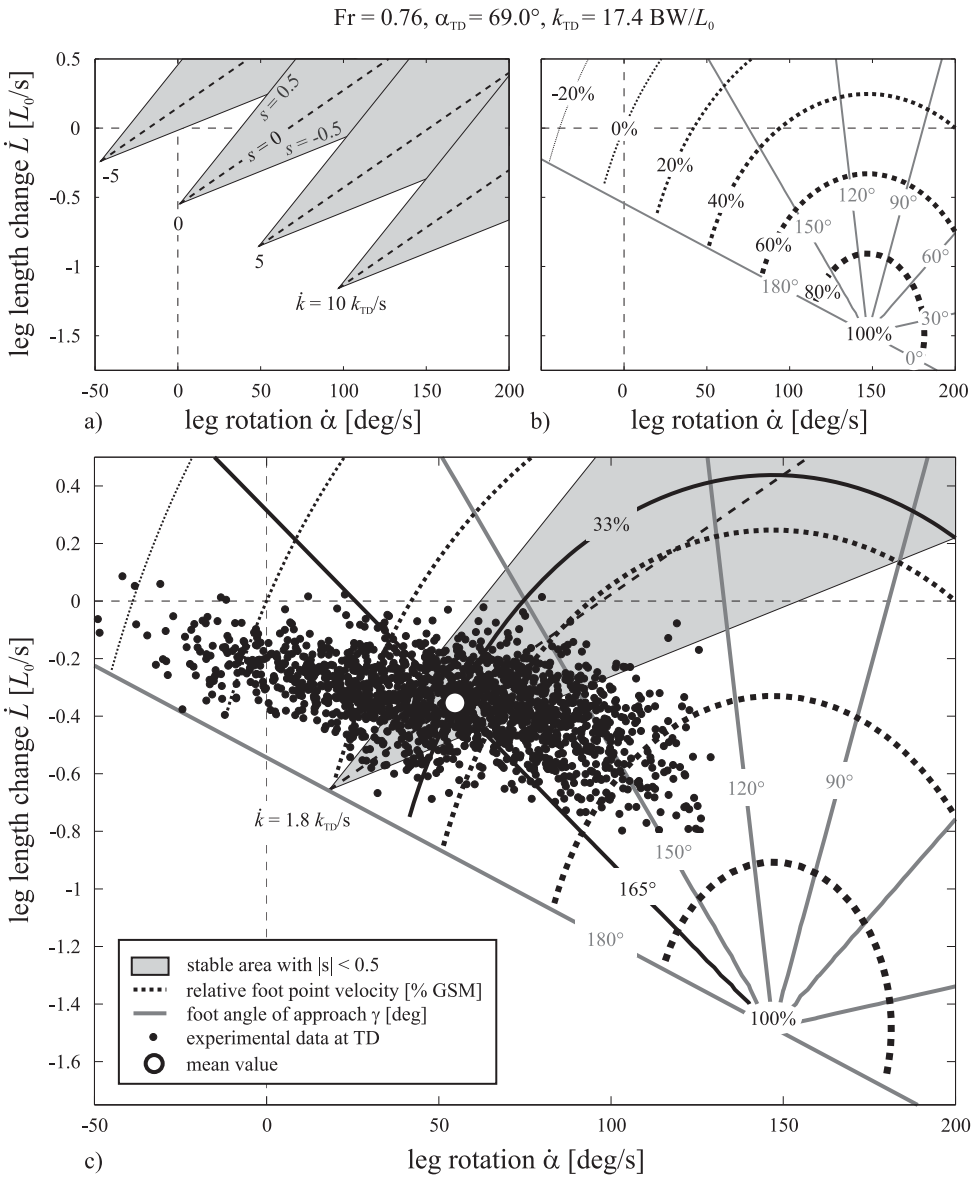

Figure 3.6.: Swing leg control and foot landing strategy in spring mass running with adaptation of leg angle $\dot{\alpha}$, leg length $\dot{L}$ and leg stiffness $\dot{k}$. ($\dot{\alpha} < 0$: leg protraction, $\dot{\alpha} > 0$: leg retraction, $\dot{L} < 0$: leg shortening, $\dot{L} > 0$: leg lengthening, $\dot{k} < 0$: leg softening, $\dot{k} > 0$: leg stiffening.) a) Stable areas ($|s| < 0.5$) of the spring mass model for selected stiffness adaptation rates $\dot{k}$. b) Relative foot point velocity (% GSM) and the approach angle of the foot. c) Individual (black dots) and mean (white circle) swing leg characteristics. Foot landing strategy and stable area matching the mean swing leg characteristics (circle), assuming super-stable behavior ($s = 0$) are shown.

values of all data points (black dots), and the mean values of the lower (gray squares) and upper (gray triangles) 10 % of t_{Fall} and the corresponding $\dot{\alpha}$, $\dot{L}$, $\dot{k}$. While $\dot{\alpha}$ and $\dot{L}$ are measured directly from experimental data, $\dot{k}$ is derived based

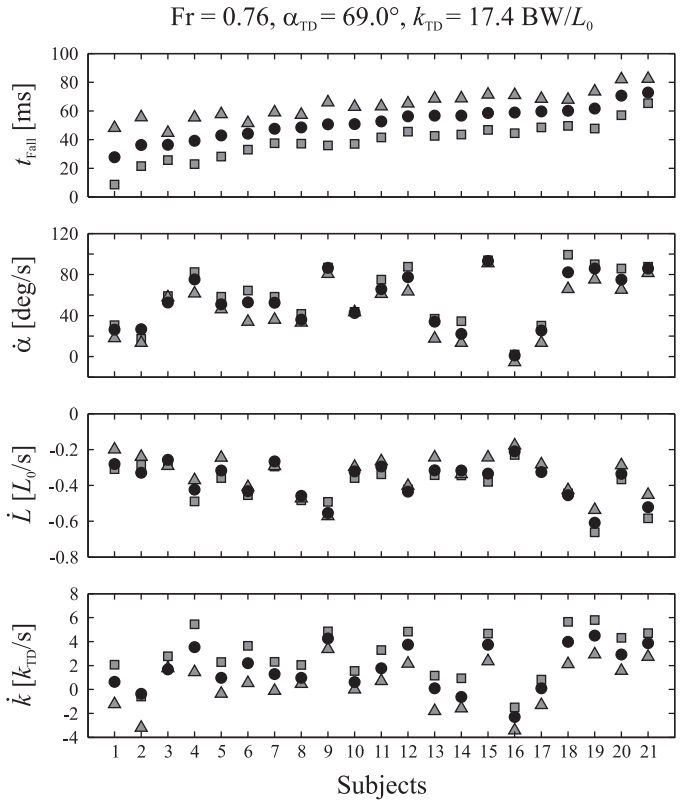

Figure 3.7.: Falling times t_{Fall} (in ascending order) and swing leg control strategies $\dot{\alpha}$, $\dot{L}$, $\dot{k}$ of all 21 subjects. The symbols represent the mean values of all data points (black dots), and the mean values of the lower (gray squares) and upper (gray triangles) 10 % of t_{Fall} and the corresponding $\dot{\alpha}$, $\dot{L}$, $\dot{k}$.

on model predictions assuming super-stable behavior. There exists no absolute correlation between falling time and control strategies, but within each subject following tendencies can be found: (i) Whereas $\dot{L}$ correlates proportionally with t_{Fall}, $\dot{\alpha}$ and $\dot{k}$ are inversely proportional to t_{Fall}. (ii) Whereas the intervals of t_{Fall} and $\dot{k}$ are comparatively large, $\dot{\alpha}$ and $\dot{L}$ lie within much smaller intervals which indicates that the kinematic control strategies are more clustered and the influence of t_{Fall} on $\dot{\alpha}$ and $\dot{L}$ is less significant. This means, short falling times (squares) result in higher stiffness adaptation rates $\dot{k}$ and longer falling times (triangles) result in lower $\dot{k}$, respectively.

3.4. Discussion

In this paper swing leg control strategies to stabilize running were derived based on the spring mass model. Within this model the gait pattern is influenced by

three leg parameters (angle of attack α, leg length L and leg stiffness k), which need to be adjusted before ground contact. However, only a very small subset of these periodic solutions is attractive and can be used without control (indicated by the thick gray lines in figure 3.5(a)). For lower speeds, corresponding to lower Froude numbers, periodic gaits are not stable for any apex height, angle of attack or leg stiffness. The model predicts alternative adaptation strategies during swing phase with constant changing rates $\dot{\alpha}$, $\dot{L}$ and $\dot{k}$ of these three leg parameters for given periodic running patterns. Swing leg control for stable running is not unique but consists of redundant implementations of $\dot{\alpha}$, $\dot{L}$ and $\dot{k}$. Thus, the kinematic control strategies $\dot{\alpha}$ and $\dot{L}$ can be adapted to additional constraints (e.g. ground speed matching) by adjusting $\dot{k}$.

As mentioned above, independent of the applied adaptation rates, the previously determined periodic solution is maintained, if the system is not disturbed. This is an important difference between the swing leg control strategy presented here and the swing leg retraction of Seyfarth et al. (2003), as they used fixed apex conditions (α_{A}, k_{A}, L_{A}). As a result, the TD conditions (α_{TD}, k_{TD}, L_{TD}) changed with leg retraction speed and therefore different periodic solutions were investigated and compared.

3.4.1. Strategies to stabilize running

The control space is spanned by two kinematic swing leg adaptation strategies $\dot{\alpha}, \dot{L}$ and the adaptation of leg stiffness $\dot{k}$. For a given running pattern this control space can be fully explored within the framework of the spring mass model. All kinematic strategies $(\dot{\alpha}, \dot{L})$ that provide negative vertical landing velocities of the foot ($v_{\mathrm{Foot,y}} < 0$) can be used to guarantee stable running (figure 3.6(a)). Within the $(\dot{\alpha}, \dot{L})$ space, there also exists a region where the foot would hit the ground from below ($v_{\mathrm{Foot,y}} > 0$), which can not be realized on flat ground. The separating line ($v_{\mathrm{y}} = 0$ which corresponds to $\gamma = 180\,^{\circ}$) can be closely approached without stability loss, but the robustness with respect to the control parameter adaptations $\dot{\alpha}$, $\dot{k}$, and $\dot{L}$ decreases noticeably. With that, even small perturbations of $\dot{\alpha}$, $\dot{L}$ and $\dot{k}$, as well as inaccuracies within the initial conditions (Blum et al., 2007) can not be compensated anymore, which consequently leads to instability (Appendix A). For any combination of $(\dot{\alpha}, \dot{L})$ providing $v_{\mathrm{Foot,y}} < 0$, one $\dot{k}$ exists which optimally stabilizes the system ($s = 0$). This means that the swing leg kinematics before TD (e.g. landing velocity of the foot) can be chosen arbitrarily without threatening stability, as

long as leg stiffness is properly adjusted. Hence, swing leg kinematics alone are not sufficient to reveal running stability.

We could identify these kinematic control strategies ($\dot{\alpha}$,$\dot{L}$) in human running and, based on model predictions, estimate corresponding stiffness adaptations rates $\dot{k}$. It is noticeable that humans apparently use variable $\dot{k}$ to explore a wide range of $\dot{\alpha}$ and $\dot{L}$ (figure 3.6 (c)). This is feasible as the identified range of $\dot{\alpha}$ and $\dot{L}$ provides sufficient robustness with respect to variations within the adaptation rates during swing phase (figure 3.6(a)). Thus, it appears that humans seem to compromise between vertical impacts and robustness.

3.4.2. Biological relevance

In human running swing leg retraction and leg shortening are observed simultaneously (figure 3.6(c)). This coupling is achieved by a combination of hip extension and knee flexion within the segmented leg, which is facilitated by the biarticular hamstring muscles (Gazendam and Hof, 2007).

However, from the model results presented here, leg lengthening seems to be a much better strategy to improve the range of stable running within the control space (figure 3.6(a)). Exactly this strategy, namely leg lengthening during swing phase, can be observed in running birds (Daley et al., 2007). Here, the configuration of leg segments, the bent posture and the lightweight architecture of the bird's leg allow this adaptability: As birds run on their toes, the backward-pointing ankle joint and the TMP (tarsometatarsal-phalangeal) joint, both connect the elongated distal leg segments. While the proximal leg joints, hip and knee, primarily control leg protraction and retraction, the distal joints, ankle and TMP, control leg compression and extension (Gatesy, 1999b). By contrast, as mentioned above, retraction of the human leg is coupled with knee flexion, which shortens the leg. Most birds (especially smaller ones) run with a more bent (crouched) leg posture than humans (Gatesy and Biewener, 1991), which gives them greater adaptability for leg lengthening. The straight and relatively heavy human leg is not suitable to lengthen before TD, as this would increase the impact force and risk of overextending the knee joint.

While leg angle and leg length, and therefore their changing rates as well, can be experimentally determined throughout the entire gait cycle, the leg stiffness is a model parameter, which can only be estimated during stance. Because of this, the direct measurement of the stiffness adaptation rate during swing phase

is impossible. However, Grimmer et al. (2008) showed that when humans run up a step ($v_x > 3.5\,\mathrm{m/s}$), their leg stiffness on the step is reduced: the higher the step, the lower the leg stiffness. This means, taking into account that a step-up reduces the flight time, that with decreasing flight time, the leg stiffness decreases as well. To put it another way, increasing flight time results in leg stiffening ($\dot{k} > 0$), which coincides with our results ($\mathrm{Fr} = 0.76$, figure 3.6(c)). Furthermore, the model predicts the stiffness adaptation rate being coupled with speed and that with decreasing speed the stiffness adjustment changes from stiffening to softening (table 3.1).

In contrast to the model, the parameter adaptation rates in biological limbs are most likely not controlled separately: Muscle activities enabling the kinematic control ($\dot{\alpha}, \dot{L}$) can also effect leg stiffness $\dot{k}$. In this case, the desired leg parameters at TD are altered. The dependency and redundancy of kinematic and dynamic control is represented in the shape of the stable area predicted by the spring mass model (figure 3.6(a)). For example, increasing retraction speed $\dot{\alpha}$ at a constant changing rate of leg length $\dot{L}$, or decreasing $\dot{L}$ at a constant $\dot{\alpha}$, require both an increasing changing rate of leg stiffness $\dot{k}$.

As aforementioned, parameter adaptations require muscle activities. To adjust the adaptation rate of a leg parameter (e.g. the retraction speed), sensory feedback is needed. These mechanisms were not addressed in this study. But even without feedback control, swing leg parameters can be adapted before TD. For instance, feedforward muscle activities in the hip extensors could lead to accelerations in the leg angle. Such changing leg retraction speeds have been previously identified to optimize running stability even for large perturbations in the initial apex height (Seyfarth et al., 2003). As the linear adaptations of leg parameters might not be found in human or animal locomotion, further studies will incorporate higher order time derivatives. Furthermore, the concept can also be extended to energy based control mechanisms, or applied to more complex models (e.g. by considering leg segmentation, momentum effects, muscle reflexes).

3.4.3. Technical relevance

So far, swing leg control strategies concerning human and animal running were discussed. Bipedal locomotion is also performed in technical systems where stabilizing strategies, like those presented here, could be implemented. Fully actuated legs (section 3.1) with non-compliant joints and rigid segments allow

a wide variety of motions but running robustness is limited, as higher impacts cannot be tolerated. However, as predicted in this paper, vertical impacts may be essential for stable and robust running with compliant legs (figure 3.6 (a)).

Robots with passive compliant legs already tolerate impacts, but their motion is restricted and leg parameters are usually not adjustable during motion. Recently, new concepts of joints and structures with adaptable stiffness have been developed. Translational stiffness adaptation can be implemented by using Jack Springs^{TM} (Hollander et al., 2005). Rotational stiffness adaptation was demonstrated by mechanically adjustable compliance and controllable equilibrium position actuators (MACCEPA) (Van Ham, 2006) and a by a new variable joint stiffness design presented by Wolf and Hirzinger (2008). Another approach to achieve variable leg stiffness in a passive manner is segmentation of the leg combined with implementation of rotational springs at the joint (Rummel et al., 2008). By this leg design, stiffness adaptation is coupled with leg length change (i.e. bending of the leg results in leg softening and vice versa) and improves stability in running and hopping.

The results of this study may guide the development of new leg designs which compromise between passive compliance and actuation for robust and fast legged robots or leg prostheses. Prospectively, the identified strategies of biological systems should be made technically serviceable, as it was demonstrated successfully by implementing swing leg retraction into a robotic testbed of a monopedal pogo hopper (Dittrich et al., 2006).

3.4.4. Passive stability and energy control

In this paper running stability was achieved based on an energy conserving control mechanism (swing leg control). This approach merely exploits the passive dynamics offered by spring-like leg behavior, which allows for energy efficient running based on compliant energy-saving structures. The low dimensional model allows to explore the entire space of conservative swing leg control strategies. An alternative approach is to consider energy based control mechanisms. For example, leg function during stance phase can be represented more realistically by taking the properties of the muscles and reflex mechanisms into account (Geyer et al., 2003). Based on a proprioceptive feedback applied to a leg extensor muscle, spring-like leg function can also be energetically stable. In fact, spring-like leg function should be only partially provided by passively compliant structures (such as tendons, ligaments or connective tissues) and needs to be

complemented by active control as demonstrated with the muscle-reflex simulations. The composition of passive versus actively controlled spring-like leg behavior is an important design issue which depends on the required movement repertoire of humans, animals and novel legged robots.

Acknowledgments

I would like to thank Monica Daley for helpful comments on the manuscript. This work was supported by the German Research Foundation (DFG) grants SE 1042/1 and SE 1042/7.

4. Does A Crouched Leg Posture Enhance Running Stability and Robustness?[‡]

4.1. Introduction

The great majority of living terrestrial vertebrates are quadrupeds. However, bipedalism can be found within a few families of mammals, reptiles and within all birds. Among mammals, various groups of primates (Schmitt, 2003), the macropods (Windsor and Dagg, 1971) and a few groups of heteromyd rodents (Djawdan, 1993) locomote bipedally. Within reptiles, some families of lizards are also capable of bipedal locomotion (Aerts et al., 2003), especially when running at high speeds (Irschick and Jayne, 1999). While macropods, some smaller birds and heteromyd rodents move by hopping on both legs simultaneously, primates, lizards and larger birds use striding gaits. In this paper, we concentrate on bipedal running and compare two types of leg architecture: The straight leg posture, represented by the human leg, and the crouched leg posture, represented by the avian leg. Associated with these differences in leg architecture, the movement strategies of these two species differ fundamentally from each other. While humans are plantigrade, birds are digitigrade, whereby their elongated tarsometatarsals keep their ankles clearly off the ground during walking and running (Alexander, 2004). This avian leg geometry in combination with the crouched leg posture allows for leg lengthening before touching the ground and thereby coping with large ground disturbances, as it was impressively demonstrated by experiments on running guinea fowl (*Numida meleagris*) (Daley and Biewener, 2006; Daley et al., 2007).

In general, legged locomotion can be described by spring-like leg behavior (Alexander, 2002) and here, the leg function is represented by the planar spring mass

[‡]Blum Y., Birn-Jeffery A., Daley M.A., Seyfarth A., *J. Theor. Biol.,* (in press)

model, which is a well-established template to describe running (Blickhan, 1989; McMahon and Cheng, 1990) and walking (Geyer et al., 2006). For adequate leg parameter adjustments (angle of attack, leg stiffness and leg length) and sufficient speeds (e.g. $v_x > 3\,\mathrm{m/s}$ for human-like dimensions), the spring mass model shows self-stabilizing behavior (Seyfarth et al., 2002). However, periodic running solutions that are unstable without control can also be stabilized. It has been shown that swing leg retraction is one elegant approach to enhance stability in locomotion for both quadrupedal galloping (Herr and McMahon, 2001) and bipedal running (Seyfarth et al., 2003). This control strategy, namely the adaptation of the leg angle during the swing phase, can be extended to all three leg parameters: leg angle, leg length and leg stiffness (section 3).

This work investigates human and avian running by assuming such a swing leg control strategy, namely the linear adaptation of the three leg parameters during late swing phase, in anticipation of the ground contact. Previous work observed adaptation of the foot's landing velocity to running speed (De Wit et al., 2000), indicating a speed-dependent leg retraction and leg length change in preparation for ground contact. The adaptation of the leg stiffness during swing phase was suggested in a recent study on running on uneven ground (Grimmer et al., 2008). Furthermore, experiments on running birds have demonstrated that retraction and lengthening of the leg during swing phase prevent the birds from falling (Daley et al., 2007).

Stability is the system's ability to reduce a deviation in the center of mass trajectory caused by a onetime perturbation. To evaluate the stability of a running pattern, limit cycle stability analysis (Dingwell and Kang, 2007; McGeer, 1993) is used. The robustness, in terms of the maximum perturbation the system can cope with, can be determined by estimating the size of the basin of attraction (Rummel et al., 2010). However, this analysis requires the assumptions that (i) the system is energy conserving and (ii) returns to the same limit cycle trajectory after the perturbation. This makes the analysis difficult to compare to experimental data on which those assumption might be violated. As an alternative, the normalized maximum drop (NMD) is calculated, which defines the maximum perturbation before stance is missed completely (Daley and Usherwood, 2010). This boundary condition measure is intuitive and easy to calculate, can be compared to experimental data, and makes no explicit assumptions about how the system deals with the energy associated with the perturbation.

The purpose of this work is to evaluate the stability and robustness charac-

teristics of running with a straight versus a crouched leg posture, using both experimental data and predictions of the spring mass model. Previous experimental observations on human and avian running suggest that birds, compared to humans, are able to negotiate much larger perturbations when running on uneven terrain. Therefore, we hypothesize that the crouched leg posture of the avian leg provide greater running stability and robustness than the straight leg posture of humans.

4.2. Methods

4.2.1. Model

The simplest template to describe the dynamics of bouncing gaits like human and avian running is the planar spring mass model (Blickhan, 1989; McMahon and Cheng, 1990). In this model, the center of mass (CoM) is represented by a point mass m, which is supported by a linear spring representing the leg. Assuming that the system is energy conserving, the system is fully described by three leg parameters at the instant of touch down (TD): angle of attack α_{TD}, leg stiffness k_{TD} and resting length of the leg spring L_0. The CoM undergoes alternating flight and stance phases, with the transition from flight to stance occurring when the landing condition $y = L_0 \sin\alpha_{\mathrm{TD}}$ is fulfilled. Since the system is conservative and with the assumption that the ground is even, the system's state is fully described by the apex condition $(y_{\mathrm{A}}, v_{\mathrm{x}})$. The apex is the highest point of the CoM-trajectory with zero vertical velocity. Therefore, the system energy

$$E = \frac{1}{2} m v_{\mathrm{x}}^2 + m g y_{\mathrm{A}} \tag{4.1}$$

is determined by the horizontal velocity v_{x} and the apex height y_{A}. To give this energy a more intuitive meaning, we define the reference speed

$$v_{\mathrm{x,Ref}} = \sqrt{2\left(\frac{E}{m} - g L_0\right)}, \tag{4.2}$$

assuming that the apex height y_{A} equals the resting leg length L_0.

The spring mass model is capable of running with fixed landing conditions: for adequate leg parameters and sufficiently high running speeds, the system shows self-stabilizing behavior (Seyfarth et al., 2002). However, by adjusting the leg parameters during swing phase (e.g. swing leg retraction (Seyfarth et al., 2003)),

it is possible to stabilize running patterns which are unstable without control. Here we assume linear adaptations of the leg parameters (section 3)

$$\begin{aligned} \alpha(t) &= \alpha_{\mathrm{A}} + \dot{\alpha}\,(t - t_{\mathrm{A}}) \\ k(t) &= k_{\mathrm{A}} + \dot{k}\,(t - t_{\mathrm{A}}) \\ L(t) &= L_{\mathrm{A}} + \dot{L}\,(t - t_{\mathrm{A}}), \end{aligned} \tag{4.3}$$

beginning at the instant of apex t_{A} and continuing during the second half of the flight phase (figure 3.3). The apex conditions α_{A}, k_{A} and L_{A} are calculated such that, if the system is not disturbed, the landing conditions α_{TD}, k_{TD} and L_{TD} remain the same for every parameter adaptation rate $\dot{\alpha}$, $\dot{k}$ and $\dot{L}$.

To characterize the running patterns, we analyze the direction and the magnitude of the foot landing velocity (section 3). Although the leg of the spring mass model is massless, this analysis approximates the size of the impact a real leg would experience. With increasing landing velocity of the foot, the landing impact would increase as well. The relative speed of the foot point defines the *ground speed matching* (GSM)

$$\mathrm{GSM} = 1 - \frac{v_{\mathrm{Foot}}}{v_{\mathrm{CoM}}}, \tag{4.4}$$

where v_{Foot} is the speed of the foot point and v_{CoM} the speed of the CoM at TD. The foot's landing direction defines the *angle of approach*

$$\gamma = \tan^{-1}\left(\frac{v_{\mathrm{x,Foot}}}{v_{\mathrm{y,Foot}}}\right) + 180°, \tag{4.5}$$

which is the angle between the foot velocity vector $\mathbf{v}_{\mathrm{Foot}}$ and the ground (figure 3.4).

4.2.2. Stability analysis

We estimate the stability of a running pattern based on the spring mass model. The vertical movement of the CoM describes an oscillation, which can be analyzed using a Poincaré map. We define the Poincaré section at the instant of apex and therefore, the corresponding map $y_{\mathrm{i+1}}(y_{\mathrm{i}})$ is the apex-return map of two subsequent apices y_{i} and $y_{\mathrm{i+1}}$ (figure 3.2). In this Poincaré map, periodic running solutions (also known as limit cycle trajectories (Dingwell and Kang, 2007; McGeer, 1993)) are identified by fixed points y^*, which satisfy (i) the identity $y_{\mathrm{i}} = y_{\mathrm{i+1}}$, while (ii) maintaining positive horizontal velocity $v_{\mathrm{x,i}} = v_{\mathrm{x,i+1}} > 0$. The stability of such a periodic running solution is estimated by analyzing the

slope s of the apex-return map $y_{i+1}(y_i)$ in the neighborhood of the fixed point y^* (Geyer et al., 2005) (Appendix B). If the absolute value of the derivative

$$s = \left.\frac{dy_{i+1}}{dy_i}\right|_{y^*} \tag{4.6}$$

is smaller than one ($|s| < 1$), the fixed point and therefore the corresponding periodic running pattern is stable (Strogatz, 1994).

4.2.3. Gait robustness

The robustness of a stable running solution is defined as the maximum perturbation the system can cope with, and its upper bound can be approximated by the *normalized maximum drop* (NMD)

$$\text{NMD} = \frac{\Delta h_{max}}{L_0}, \tag{4.7}$$

which defines the maximum perturbation before stance is missed completely (Daley and Usherwood, 2010). The extended NMD (hereinafter referred to as NMD) indicates the maximum drop Δh_{max} relative to the leg length L_0, the runner could negotiate, assuming (i) the leg continues retracting with constant leg retraction speed, (ii) the leg length continues lengthening or shortening with constant changing rate, and (iii) Δh_{max} is reached when the leg is vertically oriented ($\alpha = 90°$). Under these assumptions, Δh_{max} is a function of the kinematic parameters angle of attack α_{TD}, leg retraction speed $\dot{\alpha}$ and leg length change $\dot{L}$ (Appendix C).

4.2.4. Experiments

Experimental data on human running were collected by Lipfert (2010). Seven human subjects (one female, six males, body mass $m = 77 \pm 9\,\text{kg}$, leg length $L_0 = 1.02 \pm 0.07\,\text{m}$) were running on an instrumented treadmill at three different speeds, namely $2\,\text{m/s}$ ($\text{Fr} = 0.42$), $3\,\text{m/s}$ ($\text{Fr} = 0.94$) and $4\,\text{m/s}$ ($\text{Fr} = 1.66$) and a total of 2867 running gait cycles were analyzed. The initial vertical position of the CoM, which corresponds to the leg's rest length L_0, was approximated by the vertical position of the greater trochanter multiplied with a gender specific factor A ($A = 1.05$ for women and $A = 1.10$ for men) (Lipfert, 2010). CoM movements were calculated by twice integrating the accelerations obtained from the ground reaction forces (GRF) and the effective leg was defined as the distance between

CoM and center of pressure (CoP). The horizontal velocity v_x of the CoM was determined at the instant of apex. The contact time t_C was measured from TD to take off (TO), the flight time t_F was calculated by subtracting contact time from step time (half of the gait cycle T). To determine the leg angle during flight, a hybrid leg was defined between the foot point (located half way between heel and toe) and the CoM, and the leg angle was measured with respect to the horizontal, which increases with leg retraction. The time derivatives of the experimentally observable leg parameters ($\dot{\alpha}$, $\ddot{\alpha}$, $\dot{L}$ and $\ddot{L}$) were estimated at the instant before TD.

Avian running trials were conducted on a $0.6 \times 4.5\,\mathrm{m}$ runway. Five $0.6 \times 0.9\,\mathrm{m}$ force plates (model 9287B, Kistler, Winterthur, Switzerland) were arranged in a row to record the GRF, and a camera system (Qualisys, Gothenburg, Sweden), consisting of eight high speed infrared cameras, was used to capture body kinematics. To approximate the CoM position and the foot point, two markers were attached to the birds' back (cranial and caudal), one at digit III and one at the tarsometatarsophalangeal joint. Five male pheasants (*Phasianus colchicus*, body mass $m = 1.2 \pm 0.1\,\mathrm{kg}$, standing hip height $L_0 = 0.21 \pm 0.01\,\mathrm{m}$) were encouraged to run from one end of the runway to the other, and a total of 62 running steps at speeds between $\mathrm{Fr} = 2.32$ and $\mathrm{Fr} = 3.68$ were analyzed. Since we could not control the birds' running speeds, we analyzed the speed in post-processing. The horizontal velocity v_x of the CoM was determined at the instant of apex and the corresponding steps were divided into Froude number categories of $\mathrm{Fr} = 2$, 3 and 4 (meaning, for instance, that Froude numbers within the interval $\mathrm{Fr} = [1.5, 2.5)$ are assigned to category $\mathrm{Fr} = 2$). The initial vertical position of the CoM was defined by the average of the cranial and caudal marker position, and the initial velocity condition was estimated corresponding to Daley and Biewener (2006). CoM movements, contact time t_C, flight time t_F and time derivatives of the leg parameters were estimated as mentioned above, with the hybrid leg being defined between foot point (located half way between digit III and tarsometatarsophalangeal joint) and CoM.

Human running data were measured on a treadmill, while avian data were collected using an overground runway. The comparison of treadmill and overground running can be somewhat problematic, as joint angle kinematics may differ slightly, even though the cause of these discrepancies is not completely understood (Nelson et al., 1972; Nigg et al., 1995). Nonetheless, as long as the speed of the treadmill belt is constant, and dynamics and kinematics are not measured during belt acceleration, there exists no fundamental mechanical dif-

ference between treadmill and overground running (Van Ingen Schenau, 1980). Therefore, for the purposes of our comparison to the spring mass model, this difference between the two datasets is unlikely to substantially alter the findings.

The stiffness of a leg spring, assuming a linear force-length relationship, is defined as $k_{\mathrm{Leg}} = \frac{F_{\max}}{\Delta L}$, with $F_{\max}$ being the maximum value of the GRF and ΔL the maximum leg compression during stance. Assuming an elastic leg function, the GRF can be approximated by a sine function (Alexander, 1989b; Dalleau et al., 2004). With this, k_{Leg} reduces to a function of body mass m, resting leg length L_0, duty factor DF and angle of attack α_{TD} (section 2).

To estimate the stability of spring mass running, periodic solutions (section 4.2.2) have to be found based on experimental data. Within the spring mass model, a periodic solution is uniquely determined by four parameters (Energy E, angle of attack α_{TD}, leg stiffness k_{TD} and leg length L_0 (section 4.2.1)). However, the angle of attack α_{TD} is the parameter that matches the least with the model. On the one hand, the CoP is shifted during stance due to the roll-over characteristic of the foot (Bullimore and Burn, 2006), and on the other hand, the human leg angles at TD and TO are asymmetric with respect to the vertical axis (Cavagna, 2006). Both effects are not considered in the simple spring mass model. Therefore, to estimate periodic solutions, symmetric angles of attack $\alpha_{\mathrm{TD,sym}}$ were estimated based on the observed flight time after apex (falling time t_{fall}), assuming simulated contact phases, which are symmetric with respect to the vertical axis (section 3).

4.2.5. Data analysis and simulation

Experimental data analysis and numerical calculations were implemented in Matlab (version R2007b, The MathWorks™, Natick, MA, USA), the spring mass model in Matlab/Simulink. For numerical integration a built-in variable timestep integrator (ode113) was used with an absolute and relative error tolerance of 10^{-9}.

4.3. Results

The comparison of human (table 4.1) and avian (table 4.2) leg parameters reveals some fundamental differences in running strategies and applied control strategies (table 4.3 and figure 4.1). Compared to birds, humans touch the

ground with steeper angles of attack α_{TD}, which decrease with increasing running speed. By contrast, the avian angles of attack do not change significantly. While in human running the leg's angular acceleration $\ddot{\alpha}$ increases with increasing running speed, the avian $\ddot{\alpha}$ shows no significant trend. However, the most conspicuous difference is that humans shorten their legs before TD ($\dot{L} < 0$), while birds lengthen them ($\dot{L} > 0$). With increasing running speed the human leg shortening enhances slightly, whereas the avian leg lengthening does not change significantly. While the avian leg length acceleration $\ddot{L}$ increases with increasing running speed, the human $\ddot{L}$ decreases. Compared to birds, humans touch the ground with a flatter angle of approach ($\gamma > 150°$ for humans, $\gamma < 150°$ for birds). Furthermore, with increasing running speed the human angle of approach γ gets flatter, whereas the avian γ does not change significantly.

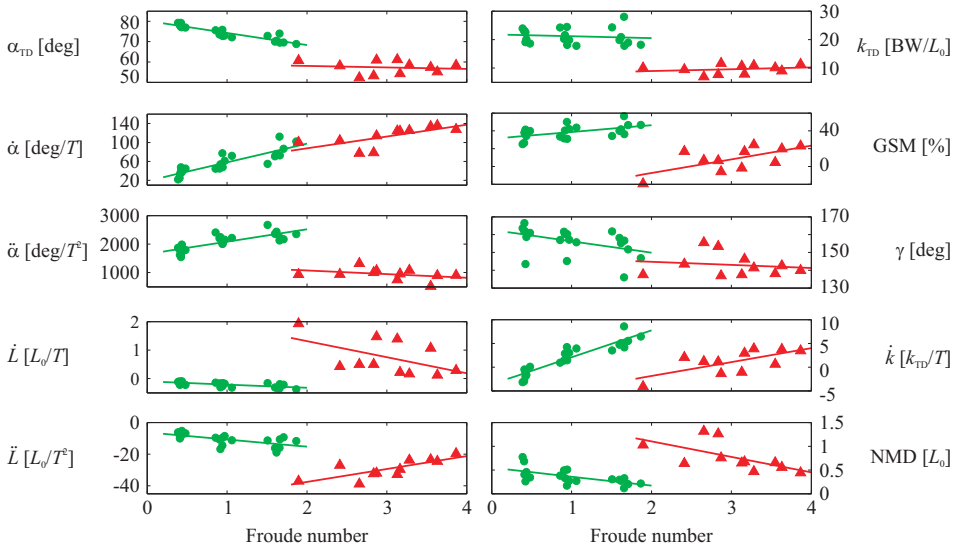

Figure 4.1.: Mean values of experimentally derived and model based parameters for human (green dots) and avian (red triangles) running are plotted over speed (indicated as Froude number).

Despite all differences, there also exist some similar tendencies in leg parameter adaptation for both humans and birds. For both, the angular velocity $\dot{\alpha}$ increases with increasing running speed. Although, compared to birds, humans run with stiffer legs, for both the leg stiffness k_{TD} does not change significantly with speed. For low speeds the model predicts the lowest stiffness adaptation rate $\dot{k}$ for the mean value of the kinematic control strategies ($\dot{k} = -1.6k_{\mathrm{TD}}/T$ at $\mathrm{Fr} = 0.42$ for humans, $\dot{k} = -0.2k_{\mathrm{TD}}/T$ at $\mathrm{Fr} = 2.36$) and with increasing speed $\dot{k}$ increases as well. However, humans might exploit a much bigger range

Table 4.1.: Human running: Grand means and standard deviations of experimentally derived (upper section) and model based parameters (lower section) are listed for 7 subjects (1 female, 6 males, age 24 ± 1 yrs, body mass $m = 77 \pm 9$ kg, leg length $L_0 = 1.02 \pm 0.07$ m) at three different speeds.

			Fr		
			0.42 ± 0.03	0.94 ± 0.06	1.66 ± 0.11
experimentally derived	v_x	[m/s]	2.06 ± 0.01	3.07 ± 0.01	4.07 ± 0.01
	T	[s]	0.78 ± 0.02	0.75 ± 0.02	0.70 ± 0.03
	$\alpha_{\mathrm{TD,exp}}$	[deg]	78.1 ± 1.0	73.8 ± 1.4	70.7 ± 1.9
	$\dot{\alpha}$	[deg/T]	35.6 ± 9.5	57.3 ± 13.2	82.2 ± 19.7
	$\ddot{\alpha}$	[deg/T^2]	1750 ± 160	2178 ± 139	2335 ± 186
	$\dot{L}$	[L_0/T]	-0.14 ± 0.06	-0.22 ± 0.07	-0.28 ± 0.08
	$\ddot{L}$	[L_0/T^2]	-7.4 ± 1.6	-11.6 ± 3.0	-13.4 ± 3.6
	k_{TD}	[BW/L_0]	21.5 ± 2.2	21.0 ± 3.4	21.3 ± 4.5
	GSM	[%]	34 ± 6	39 ± 7	43 ± 8
	γ	[deg]	160 ± 7	157 ± 6	152 ± 9
model based	$\alpha_{\mathrm{TD,sym}}$	[deg]	74.0 ± 1.4	70.1 ± 1.6	67.3 ± 2.0
	$\dot{k}$	[k_{TD}/T]	-1.6 ± 1.2	2.5 ± 1.3	5.4 ± 1.7
	NMD	[L_0]	0.48 ± 0.18	0.35 ± 0.12	0.25 ± 0.07

of stiffness adaptation rates than birds ($\Delta\,\mathrm{Fr} = 1.24$ and $\Delta\dot{k} = 3.2k_{\mathrm{TD}}/T$ for humans, $\Delta\,\mathrm{Fr} = 1.27$ and $\Delta\dot{k} = 0.7k_{\mathrm{TD}}/T$ for birds). For both humans and birds the GSM increases and the NMD decreases with increasing running speed.

Figure 4.2 shows the kinematic leg parameters, leg angle $\alpha(t)$ and leg length $L(t)$, for human (subfigures (a) and (b)) and avian (subfigures (c) and (d)) running mapped against each other. One orbit describes one stride cycle, beginning and ending with the TD of the same leg. For the averaged trajectories (indicated by the green, respectively red lines), the instants of TD and TO of the ipsi- and the contralateral leg are displayed. As the graphs contain no direct time information, it should be noted that the durations of the stance phases of the ipsilateral and the contralateral leg (i.e. the elapsing time between TD and TO, respectively TDc and TOc) within each graph are similar, as we were

Table 4.2.: Avian running: Grand means and standard deviations of experimentally derived (upper section) and model based parameters (lower section) are listed for 5 adult male pheasants (*Phasianus colchicus*, body mass $m = 1.2 \pm 0.1\,\mathrm{kg}$, leg length $L_0 = 0.21 \pm 0.01\,\mathrm{m}$) at three different speeds.

			Fr		
			2.32 ± 0.39	3.06 ± 0.19	3.68 ± 0.16
experimentally derived	v_x	[m/s]	2.22 ± 0.17	2.54 ± 0.08	2.77 ± 0.10
	T	[s]	0.35 ± 0.02	0.33 ± 0.02	0.31 ± 0.03
	$\alpha_{\mathrm{TD,exp}}$	[deg]	57.0 ± 4.3	57.6 ± 3.7	57.0 ± 1.6
	$\dot{\alpha}$	$[\mathrm{deg}/T]$	93.9 ± 14.4	113.2 ± 20.0	132.4 ± 4.3
	$\ddot{\alpha}$	$[\mathrm{deg}/T^2]$	1064 ± 223	971 ± 136	773 ± 222
	$\dot{L}$	$[L_0/T]$	0.95 ± 0.85	0.75 ± 0.64	0.49 ± 0.50
	$\ddot{L}$	$[L_0/T^2]$	-34.3 ± 6.3	-30.1 ± 3.8	-22.5 ± 2.6
	k_{TD}	$[\mathrm{BW}/L_0]$	8.8 ± 1.7	9.8 ± 1.8	10.1 ± 1.2
	GSM	[%]	2 ± 19	8 ± 13	16 ± 10
	γ	[deg]	145 ± 9	143 ± 7	140 ± 2
model based	$\alpha_{\mathrm{TD,sym}}$	[deg]	52.5 ± 5.1	51.9 ± 4.2	51.5 ± 2.8
	$\dot{k}$	$[k_{\mathrm{TD}}/T]$	0.3 ± 3.3	1.1 ± 2.3	2.6 ± 1.7
	NMD	$[L_0]$	0.99 ± 0.34	0.76 ± 0.30	0.55 ± 0.11

investigating symmetric running. Humans touch and leave the ground with a leg length that is comparable to the resting leg length L_0 of the hybrid leg (section 4.2.4) ($L_{\mathrm{TD}} = 1.01 \pm 0.01 L_0$ and $L_{\mathrm{TO}} = 0.99 \pm 0.06 L_0$ for $\mathrm{Fr} = 0.42$, $L_{\mathrm{TD}} = 1.01 \pm 0.01 L_0$ and $L_{\mathrm{TO}} = 1.00 \pm 0.06 L_0$ for $\mathrm{Fr} = 1.66$). Their phase plots are asymmetric (section 4.2.4: asymmetry of the human stance phase), whereas the avian phase plots are more symmetrical with respect to the leg angle in both phases stance and swing, and can be mirrored at $\alpha = 90°$. Compared to the resting leg length L_0, which is defined as the standing hip height, birds touch and leave the ground with more extended legs ($L_{\mathrm{TD}} = 1.25 \pm 0.04 L_0$ and $L_{\mathrm{TO}} = 1.18 \pm 0.06 L_0$ for $\mathrm{Fr} = 2.32$, $L_{\mathrm{TD}} = 1.23 \pm 0.05 L_0$ and $L_{\mathrm{TO}} = 1.18 \pm 0.04 L_0$ for $\mathrm{Fr} = 3.68$). Even during the entire stance phase, the avian leg does not compress below L_0.

Table 4.3.: Regression analysis with respect to the Froude number. Statistics (slope, R^2, p-value) of the linear regression displayed in figure 4.1 are listed for humans and pheasants. Significant relationships (p-value ≤ 0.05) are indicated by an asterisk.

			Humans				Pheasants			
			slope	R^2	p-value		slope	R^2	p-value	
experimental	α_{TD}	[deg]	−6.0	0.84	< 0.001	*	−0.7	0.02	0.700	
	$\dot{\alpha}$	[deg/T]	39.4	0.74	< 0.001	*	25.0	0.48	0.018	*
	$\ddot{\alpha}$	[deg/T^2]	434.9	0.59	< 0.001	*	−127.9	0.13	0.271	
	$\dot{L}$	[L_0/T]	−0.1	0.45	0.001	*	−0.6	0.27	0.100	
	$\ddot{L}$	[L_0/T^2]	−4.5	0.40	0.002	*	8.2	0.60	0.005	*
	k_{TD}	[BW/L_0]	−0.6	0.01	0.599		0.7	0.06	0.479	
	GSM	[%]	7.6	0.28	0.014	*	15.4	0.42	0.030	*
	γ	[deg]	−6.4	0.20	0.045	*	−1.7	0.02	0.646	
model	$\dot{k}$	[k_{TD}/T]	5.7	0.84	< 0.001	*	2.9	0.45	0.023	*
	NMD	[L_0]	−0.2	0.38	0.003	*	−0.3	0.39	0.041	*

In figure 4.3, control strategies ($\dot{\alpha}$, $\dot{k}$ and $\dot{L}$) leading to stable spring mass running are shown for four different periodic solutions (subfigures (a) and (b) for human, (c) and (d) for avian parameters) and compared with experimental data. The illustrated space is spanned by the kinematic control parameters $\dot{\alpha}$ and $\dot{L}$. Depending on these kinematic control parameters, the ground speed matching (GSM) and the angle of approach γ are calculated, and selected isolines of GSM and γ are mapped within the ($\dot{\alpha}$,$\dot{L}$)-space. The gray wedges indicate stable areas with $|s| < 0.5$ that correspond to the displayed stiffness adaptation rates $\dot{k}$. For humans, the distribution of ($\dot{\alpha}$,$\dot{L}$)-pairs is elongated and oriented parallel to the $\gamma = 180°$ line. With increasing speed this distribution expands and shifts away from $\gamma = 180°$. By contrast, the avian distribution of ($\dot{\alpha}$,$\dot{L}$)-pairs is circularly clustered and does not enlarge with speed. Furthermore the avian ($\dot{\alpha}$,$\dot{L}$)-cluster is largely covered by the wedge-shaped area of predicted stability.

Figure 4.4 shows the grand means of the normalized maximum drop (NMD) as a function of angle of attack α_{TD} (subfigure (a)), leg rotation $\dot{\alpha}$ (subfigure (b)) and leg length change $\dot{L}$ (subfigure (c)) for different speeds. Compared to humans (green dots), birds (red triangles) run with flatter angles of attack and

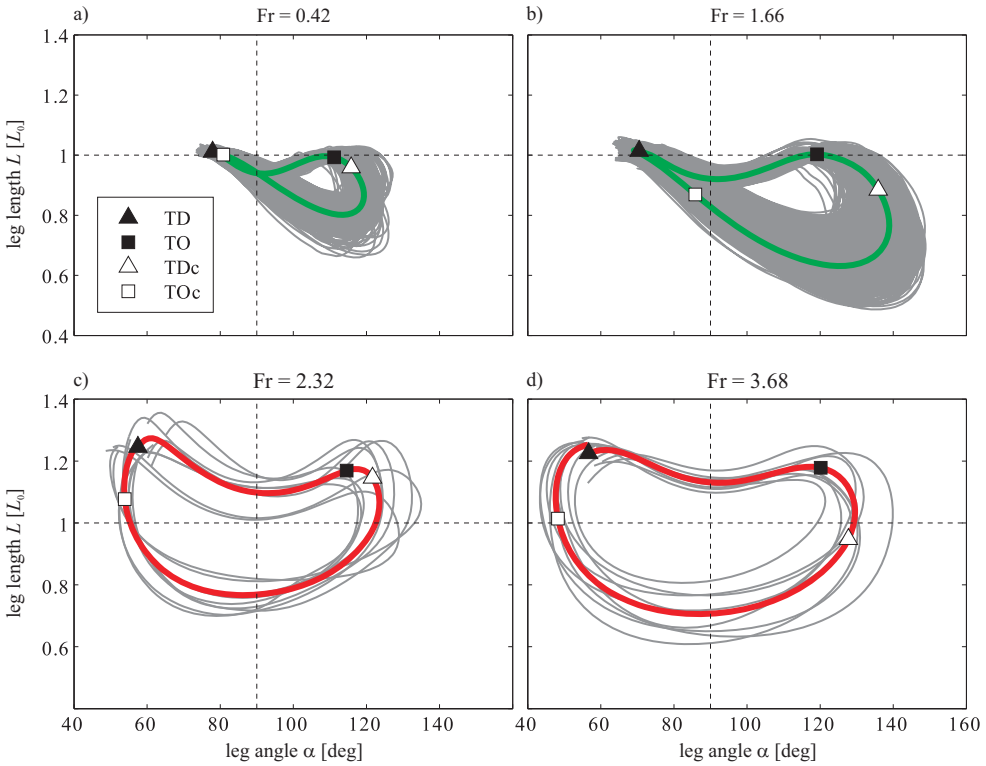

Figure 4.2.: Experimentally observed kinematic leg parameters, leg angle α and leg length L, for human (subfigure (a) and (b)) and avian (subfigure (c) and (d)) running cycles are plotted against each other. The grand means of the trajectories are highlighted in green (human) and red (avian), respectively. The markers indicate touch down (TD), take off (TO) and TD and TO of the contralateral leg (TDc and TOc).

higher retraction speeds. Additionally, birds lengthen their legs before touching the ground, while humans shorten them. This combination of strategies results in a higher avian NMD, compared to the human NMD.

4.4. Discussion

This study investigated differences in leg kinematics and implied swing leg control strategies between human and avian bipedal running. The analysis of these swing leg control strategies using a simple spring mass model allowed the comparison of stability and robustness characteristics for human-like and bird-like running. Model based findings were compared with experimental data from humans and pheasants, exemplifying straight-legged versus bent-legged running postures. Stability, which is the system's ability to reduce a deviation in the CoM trajectory caused by a onetime perturbation, was estimated using limit

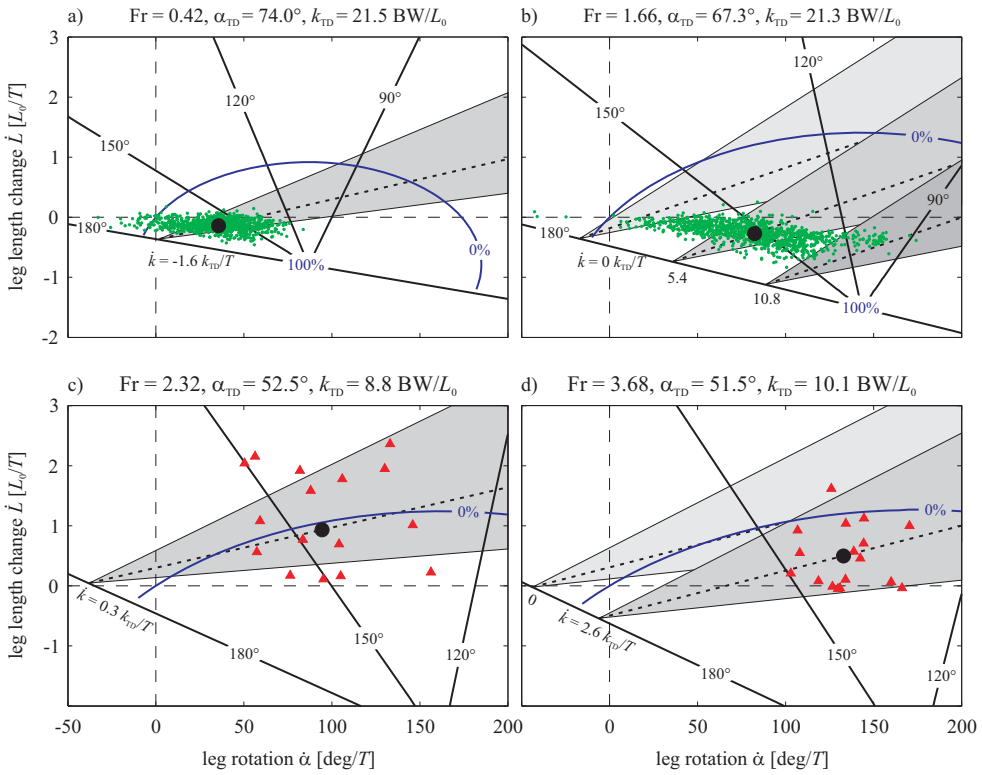

Figure 4.3.: Swing leg control, stability and foot landing strategy are shown for selected periodic solutions of spring mass running. Stable areas ($|s| < 0.5$) of the spring mass model, corresponding to selected stiffness adaptation rates $\dot{k}$, are indicated by the gray wedges. The relative foot point velocity (100% and 0% GSM are illustrated in blue) and the foot point's angle of approach γ (black lines) describe the foot landing strategy. The experimentally observed individual swing leg characteristics for human (green dots) and avian (red triangles) running at different speeds are shown, with the stable area matching the mean swing leg characteristics (black circle), assuming super-stable behavior ($s = 0.5$). ($\dot{\alpha} < 0$: leg protraction, $\dot{\alpha} > 0$: leg retraction, $\dot{L} < 0$: leg shortening, $\dot{L} > 0$: leg lengthening, $\dot{k} < 0$: leg softening, $\dot{k} > 0$: leg stiffening)

cycle stability analysis (section 4.2.2). To evaluate the robustness, which is determined by the maximum perturbation the system can cope with, a new intuitive and easily accessible parameter, the NMD (section 4.2.3), was applied.

The bent posture of the bird-like leg provides an important advantage for swing leg control strategies in running. It possesses an increased ability for leg parameter adaptation, as it can be both lengthened and shortened in preparation for the TD. However, running with bent legs is also expected to reduce leg stiffness, require increased muscle forces to support body weight, and result in increased energy consumption (McMahon et al., 1987). As tissue strengths and specific muscle forces (force/area) are similar in animals of different size, the inevitable

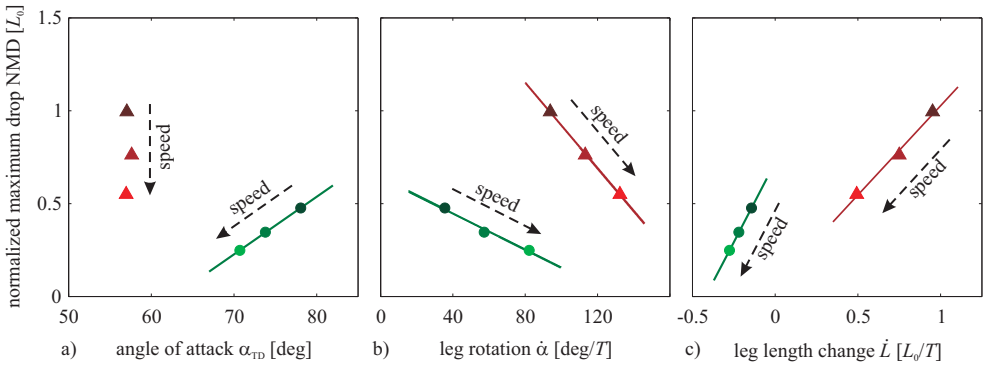

Figure 4.4.: The NMD's grand mean for human (green dots) and avian (red triangles) running is illustrated as a function of a) the angle of attack α_{TD}, (b) the leg rotation speed $\dot{\alpha}$ and c) the leg length change $\dot{L}$. The speeds correspond to the values listed in table 4.1 and 4.2.

size-dependent adaptations relate to changes in skeletal form and muscle mechanics (Pearson and Misiaszek, 2001; Biewener, 1990). Therefore, due to limits to muscle and bone strength in large animals, only smaller and more lightweight animals run with crouched postures, whereas larger species run more straight (Biewener, 1989). Taking birds as an example: small birds like the painted quail (*Excalfactoria*, $m \approx 0.05\,\text{kg}$, $L_0 \approx 0.05\,\text{m}$) walk and run very crouched, while tall birds such as the rhea (*Rhea*, $m \approx 20\,\text{kg}$, $L_0 \approx 0.8\,\text{m}$) have a rather straight leg posture (Gatesy and Biewener, 1991). In the following sections we want to further elucidate the advantages and disadvantages of crouched locomotion.

4.4.1. Swing phase

Leg kinematics of human and avian running differ significantly from each other and two distinct running strategies are observed (figure 4.2). Due to the straight posture of the human leg, most of the gait cycle the leg length is below $L = L_0$ (figure 4.2 (a) and (b)). As mentioned above, the contact phase of human running is slightly asymmetric, as the leg angle at TD is steeper than at TO. There also exists an asymmetry within the leg length (Cavagna, 2006). In heel-toe-running, the CoP moves during stance from heel to toe (Bullimore and Burn, 2006), and the lift of the heel causes a lengthening of the leg (Maykranz et al., 2009). However, to demonstrate leg kinematics during both phases stance and swing, we defined a hybrid leg between the CoM and the foot point, which neglects the effect of leg lengthening due to the influence of the foot.

The asymmetric shape of the human phase plots and the accentuated turning

point, at which leg retraction is initiated (shortly before TD), suggest that the preparation of the ground contact is crucial. This could be due to the fact that, as humans touch the ground with a very extended leg posture, they have to retract and bend their legs shortly before TD to reduce the landing impacts and prevent their knees from damage. In contrast, the smooth and symmetric phase plots of avian running (figure 4.2 (c) and (d)) appear as the movements of a clock-driven pendulum.

4.4.2. Landing strategy

Ground speed matching (GSM) and the angle of approach γ indicate the magnitude and the direction of the foot's landing velocity vector and qualitatively estimate the impact a real leg would experience (section 4.2.1). Touching the ground with 100% GSM stands for a smooth and absolutely impact-free landing, while 0% GSM means that the foot moves with the same speed as the CoM. GSM < 0 indicates that the foot is actively pushed towards the ground and the resulting impact is enforced. $\gamma = 90°$ means that the foot approaches the ground perpendicular (i.e. the foot's velocity vector has only a vertical component). Accordingly, $\gamma = 180°$ means that the foot approaches parallel to the ground (i.e. the foot's velocity vector has only a horizontal component).

As the human kinematic control parameters ($\dot{\alpha}$,$\dot{L}$) are distributed parallel and near to $\gamma = 180°$ (figure 4.3(a) and (b)), this suggests that humans avoid vertical impacts. They shorten their legs before TD (which is in accordance to the findings of Seyfarth et al. (2003)), and thus smooth their landing. In contrast, the avian ($\dot{\alpha}$,$\dot{L}$)-pairs are circularly clustered and more distributed (figure 4.3(c) and (d)). As birds lengthen their legs (which is in accordance to the findings of Daley et al. (2007)), they do not reduce the TD-impact so much and their feet hit the ground with almost the same speed as the CoM. However, with increasing running speed, both humans and birds reduce their landing-impacts by increasing the GSM (figure 4.1).

4.4.3. Stability

Within the kinematic control space ($\dot{\alpha}$,$\dot{L}$), figure 4.3 shows model predicted stable areas, which satisfy $|s| < 0.5$ (gray wedges), in comparison with experimental data (green dots and red triangles). When the stiffness adaptation rate

$\dot{k}$ gets smaller, the stable area (gray wedge) shifts to the left within the kinematic parameter space, while when $\dot{k}$ gets larger, the wedge shifts to the right (exemplarily displayed in subfigure(b)).

As humans run with rather straight leg posture, their leg architecture does not allow for larger leg extension. Leg retraction, which is a potential strategy to stabilize running patterns (Seyfarth et al., 2003), is also limited, as leg retraction speed is restricted due to physiological limitations. Doke et al. (2005) showed that the force and work, required to swing the leg back and forth, sharply increase with the frequency of the movement, which might explain the fourfold increase in metabolic cost they observed. Therefore, to achieve running stability, humans might take advantage of the control strategies' redundancy and adapt their leg stiffness in anticipation of the ground contact (figure 4.3 (a) and (b)). For low speeds (figure 4.3 (a)), the distribution of experimental ($\dot{\alpha}$,$\dot{L}$)-points is mostly covered by the predicted stable area that corresponds to one stiffness adaptation rate, namely leg softening ($\dot{k} = -1.6k_{\mathrm{TD}}/T$). This quality changes with increasing running speed. Whereas for low speeds, the predicted stiffness adaptation rate $\dot{k}$ remains almost constant, for higher speeds the model suggest a variation of $\dot{k}$ to explore the entire kinematic control area (figure 4.3 (b), $\dot{k} = [0, 10.8]k_{\mathrm{TD}}/T$). With increasing running speed the predicted control strategy changes from leg softening to leg stiffening (table 4.1). In contrast, for birds a constant $\dot{k}$ seems to be sufficient for properly selected kinematics control strategies ($\dot{\alpha}$,$\dot{L}$) (figure 4.3 (c) and (d)).

Previous studies on human running and hopping have shown that leg stiffness is not a constant parameter, but that it is adjusted when the properties of the surface change (Ferris et al., 1998; Moritz and Farley, 2006). Although the leg stiffness of humans and animals during level running does not even change much with speed (Farley et al., 1993), which is consistent to our findings (table 4.1 and 4.2, figure 4.1), our results predict that human leg stiffness is adjusted in anticipation of ground contact with a speed-dependent changing rate $\dot{k}$ (figure 4.1, table 4.3). However, this behavior would only be revealed experimentally through perturbations of the terrain height, and our findings might explain the results of recent studies: Grimmer et al. (2008) found that with increasing step height Δh the estimated leg stiffness of a human runner decreases ($k_{\mathrm{Leg}} = 32.5\,\mathrm{BW}/L_0$ for $\Delta h = 0$, $k_{\mathrm{Leg}} = 23.7\,\mathrm{BW}/L_0$ for $\Delta h = 15\,\mathrm{cm}$, $v_{\mathrm{x}} > 3.5\,\mathrm{m/s}$). As an increase in step height results in a decrease in the flight time, this suggests that the human leg is stiffened during late flight phase This characteristic, namely leg stiffening in anticipation of ground contact for higher running speeds, corresponds to

the results of our work (table 4.1). In contrast, Daley et al. (2007) could not find significant differences in avian leg stiffness when the birds (guinea fowl, *Numida meleagris*) ran over an unexpected perturbation (8.5 cm drop). This corresponds to our model prediction, suggesting that pheasants do not use a distinct stiffness adaptation as their predominant control strategy.

4.4.4. Robustness

The robustness of the simulated running solutions, in terms of the maximum drop height the system can cope with, was approximated by the NMD (figure 4.4), which is a function of the angle of attack α_{TD}, the leg rotation speed $\dot{\alpha}$ and the leg length change $\dot{L}$ (Appendix C). Compared to birds, the human combinations of steeper α_{TD}, lower $\dot{\alpha}$ and leg shortening ($\dot{L} < 0$) result in lower NMD values, whereas the influence of $\dot{L}$ predominates. Accordingly, the avian combinations of flatter α_{TD}, higher $\dot{\alpha}$ and leg lengthening ($\dot{L} < 0$) result in higher NMDs. However, compared to humans, birds retract their legs with much lower angular acceleration $\ddot{\alpha}$ (figure 4.1), and the actual drop height they can overcome might be even larger.

As Daley and Biewener (2006) showed by their drop down experiments, guinea fowls, (*Numida meleagris*) can easily negotiate drops of 8.5 cm, which corresponds to 40% of their standing hip height L_0. If we transfer this into human scaling, this would mean to run over a drop of approximately 40 cm, which is hardly feasible. So far, we could only find literature concerning human running on uneven terrain with downward steps of 10 cm (Müller and Blickhan, 2010) and upward steps of 15 cm (Grimmer et al., 2008). Further perturbation studies are required to explicitly test these predictions for differing robustness of human versus avian locomotion.

4.5. Conclusion

This paper compared swing and landing behavior of avian and human running. Based on experimental data and spring mass simulations, predictions about stability, robustness and stiffness adaptation during swing phase were made.

- Birds lengthen their legs before TD ($\dot{L} > 0$), whereas humans shorten them ($\dot{L} < 0$).

- While model predictions suggest that birds might be able to stabilize their running pattern by using one constant stiffness adaptation rate $\dot{k}$, humans may have to adjust $\dot{k}$ on a larger scale to exploit the experimentally observed kinematic control space. With increasing running speed, the range of the predicted human $\dot{k}$ increases as well.
- Compared to humans, birds are more robust in terms of the normalized maximum drop NMD. Additionally, because birds retract their legs with much lower angular acceleration $\ddot{\alpha}$, the actual drop height they can overcome could be even larger.

We have shown that the applied control strategies are redundant in stabilizing the spring mass model. Therefore, a crouched leg posture does not necessarily enhance running stability. Nonetheless a crouched leg offers more adaptation possibilities, as it is capable of both leg lengthening and shortening. The question of whether a crouched leg posture enhances robustness can not be answered satisfactorily by solely taking the NMD as a basis, because this measure only estimates the upper bound for a drop perturbation, and ignores other limitations (e.g. size of the basin of attraction, peak force). Additionally, further investigation is required to extend the NMD concept by taking angular acceleration $\ddot{\alpha}$ and leg length acceleration $\ddot{L}$ into account.

Further perturbation experiments on humans and animals in comparable conditions will be required to test many of the predictions resulting from our analysis here.

Acknowledgments

I would like to thank J. Rummel and D. Maykranz for fruitful discussion and S. W. Lipfert for collecting and sharing the experimental data on human running. This work was supported by grants SE1042/1 and SE1042/7 of the DFG (German Research Foundation) and a travel grant of the JEB (Journal of Experimental Biology).

5. General Conclusion

5.1. Summary

Based on the spring mass model, we have learned about the relevance of simplified models, so called *templates*. According to Full and Koditschek (1999), a template is the simplest model (least number of variables and parameters) that exhibits a targeted behavior. Here, this target behavior was (i) to reproduce the dynamics of the center of mass and (ii) to be capable of adjusting the model parameters in order to stabilize the investigated running pattern.

In **chapter 2**, a method to derive an effective leg stiffness based on temporal-spatial parameters was presented. This approach stands for a simple, but still meaningful manner of leg stiffness estimation when it comes to comparing experimental data with spring mass running.

In **chapter 3**, a conceptual method to evaluate the stability of a running spring mass model was established. The main result is that the applied swing leg control strategies are redundant and therefore, different combinations of these control strategies lead to similarly stable running patterns. Thus, the stabilizing leg parameter adaptations can be attuned to additional constraints or requirements, such as ground clearance or ground speed matching.

In **chapter 4**, the previously presented method was used to compare human with avian running, concerning stability and robustness. Main findings are that, due to differences in their leg geometry, humans and birds use different strategies to stabilize their movement pattern. Humans shorten their legs before TD, while birds are capable of leg lengthening, which positively influences the range of stable running. Because of the greater possibilities of kinematic leg parameter adaptations, birds do not necessarily have to adapt their leg stiffness in preparation of ground contact. In contrast, for human running the model predicts an adjustment of the stiffness adaptation rate on a larger scale to exploit the experimentally observed kinematic control space.

5.2. Extensions to the spring mass model

In this work, all simulations and predictions were made based on the simple, planar spring mass model. In order to stabilize the running pattern, the model was extended in terms of allowing for time varying leg parameters during swing phase describing the leg function. Due to its simplicity the model describes the fundamental characteristics of spring mass running, but it can not answer the questions of how - for example - leg segmentation or leg geometry influences the movement pattern. Furthermore, at fast walking speeds ($v_x > 1.04\,\mathrm{m/s}$) and slow running speeds ($v_x < 3\,\mathrm{m/s}$) experimentally observed locomotion can not satisfactorily be described by the spring mass model (Lipfert et al., submitted). However, a detailed understanding of all these interactions might help to invent and design new prostheses and legged robots. Depending on the particular task, the underlying spring mass model can be further extended. At the Lauflabor Locomotion Laboratory, different model assumptions to investigate and understand the principles of spring like walking, running and hopping are considered.

Leg segmentation

The spring mass model describes the global leg function, but it is no indicator for leg behavior at joint level. Taking leg segmentation into account, the simplest approach is to consider two massless leg segments (e.g. representing thigh and shank) connected by a linear torsional spring at the joint (e.g. representing the knee) (Rummel and Seyfarth, 2008). Thus, the adaptation of the leg length, which is caused by the adjustment of the inner leg angle (i.e. the angle included by the leg segments), affects both the resulting angle of attack and the effective leg stiffness. While the linear leg spring of the spring mass model limits the minimum speed required for self-stabilizing behavior to $v_x \approx 3.5\,\mathrm{m/s}$ (for human-like dimensions) (Seyfarth et al., 2002), the segmented leg is capable of reducing this minimum speed to $v_x \approx 1.5\,\mathrm{m/s}$, which is even below the preferred transition speed between human walking and running ($v_x \approx 2\,\mathrm{m/s}$). Furthermore, the region within the leg parameter space (k-α-space) where stable running occurs can be enlarged, depending on the adjustment of the inner leg angle. Here, a straighter leg reduces the minimum speed required for stable running. This is also found experimentally, where straighter leg configurations occur at lower running speeds.

It was shown in a robotic testbed (JenaHopper) that a two-segmented leg results in running speeds that are even slower than predicted by the corresponding two-segmented model (Rummel et al., 2008). The JenaHopper is actuated by a sinusoidal control pattern in the hip, which generates swing leg retraction because of the inherent system dynamics. The swing leg retraction, in turn, increases the ground speed matching and therefore, reduces the impacts the robot experiences. With this, not only perturbations due to impacts are reduced but also stability is increased due to swing leg retraction. This might explain the stability at even lower running speeds than predicted by the model. However, to describe the system's response to impacts, the legs of the model can not be regarded as massless and the underlying model has to be further anchored (e.g. by taking distal masses into account (Seyfarth et al., 1999)).

Foot function

In human locomotion, the GRF during contact phase do not intersect at ground level (as predicted by the spring mass model), but may intersect below the ground (Rose and Gamble, 2006). This can be explained by the shift of the CoP due to the rolling characteristic of the foot. In order to investigate the influence of the foot and describe heel-toe-running, the spring mass model was extended by a rigid foot segment (foot spring model) (Maykranz et al., 2009). Here, the foot element is attached to the distal end of the leg spring by a torsional spring with constant spring stiffness at the foot joint. While in the spring mass model the intersection point of the GRF (pivot point) during contact phase is fixed and equals the CoP, in the foot spring model there exists a moving pivot point below ground level. As the functional leg pivots about a point below the ground, the effective leg length is increased and the CoP is moving forward from heel to toe until the heel lifts off the ground. Due to the combination of a compressible spring (acting in leg axis) and a rotational spring (at the foot joint), a combination of leg softening and leg lengthening during contact phase is observed. With this, the model provides an explanation for both the translation of the point of force application (Bullimore and Burn, 2006), and the asymmetry of the contact phase concerning the shape of the GRF (with the maximum occurring before midstance) and the increase of the leg length (Cavagna, 2006).

Upper body

The challenge of walking upright and stabilizing an upper body was described by the virtual pendulum (VP) concept (Maus et al., 2010). Here, the point mass of the simple spring mass model is replaced by a rigid body and a hip torque is introduced to redirect the GRF to a point located at the the upper body (trunk). This point, aligned at the body axis defined by the CoM and the hip joint, defines a virtual pivot point (VPP). If the VPP is shifted backward or forward with respect to the body axis, the trunk is leaning forward or backward, respectively. As a result, the CoM velocity increases or decreases. With this, the functional role of the trunk lies in the possibility to adjust the speed during locomotion.

Three-dimensional locomotion

The previously presented models - the segmented spring like leg, the foot spring model and the VPP model - move solely in the sagittal plane, which is defined by the main direction of locomotion. However, this simplification becomes unsustainable when it comes to the investigation of lateral movement. Stable spring mass running in three dimensions was successfully simulated by Peuker and Seyfarth (2010). They found that stable running in three dimensions can be achieved by orienting the leg in preparation of ground contact with respect to a local reference system defined by the CoM velocity vector. This approach is different to previous models on three-dimensional running, where leg placement was realized with respect to the world reference system (global reference system) (Seipel and Holmes, 2005). In the three-dimensional spring mass model, stability might be increased by applying a lateral swing leg retraction or protraction, following the concept that was presented in this thesis.

Leg asymmetry

Usually, perfectly symmetric legs are assumed. But the question arises, in which way does asymmetric leg behavior (e.g. due to an injury or an uni-lateral prosthetic supply) affect the overall walking or running pattern. Asymmetric walking, concerning asymmetry in the angle of attack and the leg stiffness was investigated by Merker et al. (submitted). Interestingly, a small asymmetry in the angle of attack can even increase the range of stable walking. Taking this

into account, slightly asymmetric leg behavior does not necessarily have to be a disadvantage.

Energy-based control

In the presented thesis (chapters 3 and 4), a swing leg control strategy that does not affect the system energy was established and applied to stabilize bipedal running. An alternative approach to stabilize spring mass walking, running and hopping is to consider energy based control schemes. For example, leg length and leg stiffness can be adapted during contact, which was applied to vertical hopping (Riese and Seyfarth, submitted). Here, the interplay between leg length adaptation, stiffness adaptation and optional damping is adjusted such that the total energy balance remains constant. Without damping, leg lengthening in combination with leg softening results in stable hopping, while leg shortening in combination with leg stiffening becomes unstable. By taking velocity dependent damping into account, the region of stable hopping can be enlarged and even leg stiffening can be used.

So far, all presented models are based on the spring mass model. However, the leg function during stance phase can be represented more realistically by taking muscle properties and reflex mechanisms into account (Geyer et al., 2003). Based on a proprioceptive feedback (positive force feedback) applied to a leg extensor muscle, spring-like leg function can be approximated and energy fluctuations can be compensated.

In order to determine the level of detail of the physiological muscle that is required for stable locomotion, Haeufle et al. (2010) analyzed a one-dimensional hopping model with a Hill-type muscle (one contractile element, neither serial nor parallel elastic elements). They showed that both a linear and a Hill-shaped force-velocity relation result in stable hopping and that the characteristics of the force-length relation marginally influence hopping stability. This result indicates that the intrinsic properties of the contractile element could be responsible for the stabilization of periodic movements.

5.3. Outlook

In the work presented in this thesis, model predictions were compared to experimental data on human and avian running, and questions have been posed that

need to be addressed in future studies.

In the models presented here, perfectly periodic running patterns were assumed and used for stability analyses. It is questionable to what extend the locomotion of real biological systems can be assumed to be periodic (i.e. absolutely steady). In contrast to the model assumption of steady state running, in experimental data considerable variations in state and leg parameters can be observed. Therefore, it would be interesting and important to consider both system parameter and environmental parameter variations in the model and to investigate the influence of these variations. This might affect the shape of the predicted region for stable running and, for instance, landing strategies without or with low impacts might become unstable.

In this work, stability and control strategies to stabilize running were addressed. However, not only stability is an important feature to locomote successfully, but also robustness needs to be considered. A walking or running solution is only practicable when variations in the system properties and in the environment can be tolerated. Thus, stability and robustness of a system should be treated as entity. While stability can be determined by limit cycle analysis, practicable methods to estimate robustness are less established. One approach is to calculate the size of the basin of attraction (BoA) surrounding a stable solution, and define this value as a measure for robustness, as proposed by Rummel et al. (accepted). We found that swing leg control strategies affect not only the system's stability but also its robustness (size of the BoA) (Blum et al., 2007). This interplay needs to be systematically investigated.

In the presented work, robustness was described by the normalized maximum drop (NMD), which is defined by the kinematic leg parameters, angle of attack α_{TD} and retraction speed $\dot{\alpha}$. This method provides a simple approximation of the maximum drop the model can cope with, and might be a meaningful quantity for describing robustness. In order to extend the NMD concept, not only the angle of attack and its angular velocity should be considered, but the leg length and its adaptation rate should also be taken into account. Furthermore, based on the method proposed by Rummel et al. (accepted), the actual size of the BoA should be compared with the predicted NMD.

In human running swing leg retraction, which is coupled with leg shortening, is facilitated by the Gluteus maximus muscle and the biarticular hamstrings. However, a muscle generates a force, which, in turn, generates an accelerated movement. Therefore, the assumption of linear leg parameter adaptations might

be too simple to explain human control strategies. The data provided by Lipfert (2010) indicate that shortly before TD, the human leg is retracted with almost constant angular acceleration (figure 5.1), and further investigations should take higher orders of parameter adaptations into account.

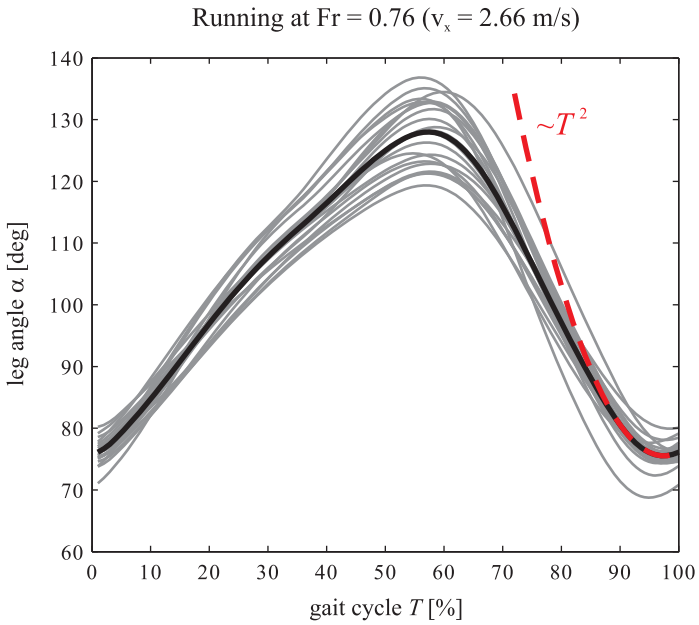

Figure 5.1.: Mean leg angles α of 21 human subjects (gray lines) and the corresponding grand mean (black line) are plotted against the normalized gait cycle T (beginning and ending with TD). For the last 10% of the gait cycle a quadratic dependency is assumed and illustrated by the dashed red line.

From a model based point of view, walking is more complex than running. In bipedal walking, necessarily two legs are needed to describe the system dynamics, while in running one leg is sufficient to alter between subsequent stance and flight phases. In the presented work, spring mass running was considered to establish a methodology that investigates swing leg control strategies regarding stability, landing behavior and robustness. So far, these strategies have not been implemented into walking models. However, the application of control strategies to spring mass walking might be important. Even though a large range of walking solutions predicted by the spring mass model is unstable, it might become accessible for human walking (Rummel et al., accepted) by applying control strategies as presented in this thesis. Here, the implementation of control strategies and the comparison with experimental data might give a more profound understanding of human walking and help to find new approaches for gait rehabilitation and prosthetics.

Appendix

A. Stability and robustness

A more detailed consideration of the system's behavior concerning stability and robustness reveals some interesting characteristics. Figure A.1 shows an enlarged section of the kinematic control space $(\dot{\alpha}, \dot{L})$ of figure 3.6, where the illustrated wedge shaped stable area ($|s| < 0.5$) corresponds to the identified stiffness adaptation rate $\dot{k} = 1.8 k_{\mathrm{TD}}/\,\mathrm{s}$. To elucidate the behavior of this periodic solution, six $(\dot{\alpha}, \dot{L})$-pairs are selected and the corresponding apex return maps are displayed (figure A.1(a)-(f)).

Drawing closer to the vertex of the stable area along the isolines $s = \text{const}$ (e.g. a $\rightarrow$ b at $s = 0.5$), the unstable fixed points converge to the stable ones. As all vertices identify the stumbling border (i.e. the separating line with $v_{\mathrm{y}} = 0$ and $\gamma = 180°$, respectively), the vertex itself can not be reached, but there exits a limit of the slope s as the unstable fixed point approaches the stable fixed point, which equals one (neither stable, nor instable). The stability of a fixed point is identified by the slope s of the apex return map (section 3.2.2). The robustness of such a stable fixed point can be quantified by the size of the basin of attraction, which is limited (i) by the landing condition $y = L_0 \sin(\alpha_{\mathrm{TD}})$, (ii) by the system energy $y = \frac{E}{m\,g}$ and, if existent, (iii) by another (unstable) fixed point. As the distance between the unstable and the stable fixed point decreases, the size of the basin of attraction decreases as well, and the robustness diminishes. With this, close to the vertex of the stable area, not only small variations of $\dot{\alpha}$, $\dot{L}$ and $\dot{k}$ lead to instability, but also small variations of the apex height can no longer be compensated.

The vertex of the wedge shaped stable area only exists for infinitesimal perturbations. In this work, a perturbation of $y_{\mathrm{P}} = 10^{-7}\,\mathrm{m}$ was considered, which is precise enough to develop a defined vertex. However, for real perturbations (which means being increased by orders of magnitude) the vertex shifts into an open funnel (Blum et al., 2007).

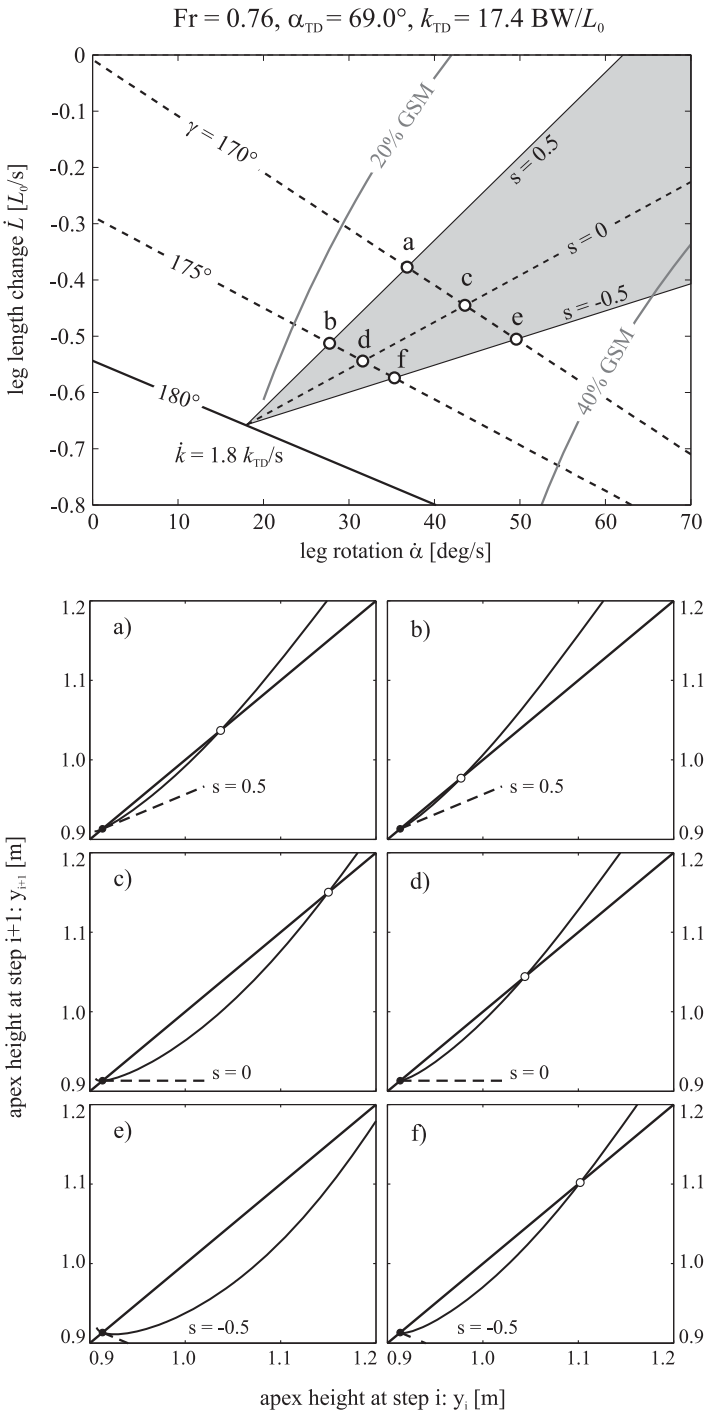

Figure A.1.: Apex return maps $y_{i+1}(y_i)$ for one periodic solution and selected kinematic control strategies $(\dot{\alpha}, \dot{L})$. The upper graph shows the stable area ($|s| < 0.5$) of the spring mass model for one stiffness adaptation rate $\dot{k} = 1.8 k_{TD}/\mathrm{s}$. The apex return maps (a)-(f) illustrate the system's behavior for the selected combinations of $(\dot{\alpha}, \dot{L})$, which are indicated by the intersections of the approaching angles $\gamma = 170°$ and 175°, respectively, and the isolines of the slope $s = 0.5$, 0 and -0.5, respectively.

B. General description of limit cycle stability analysis

The system's state at the instant of apex is described by the state vector

$$\mathbf{S}_{\mathrm{i}} = (y_{\mathrm{A,i}}, v_{\mathrm{x,i}}), \tag{1}$$

with the index i enumerating the individual steps, $y_{\mathrm{A,i}}$ being the apex height and $v_{\mathrm{x,i}}$ the corresponding horizontal velocity. The Poincaré map is defined by

$$\mathbf{S}_{\mathrm{i+1}} = \mathbf{F}(\mathbf{S}_{\mathrm{i}}) \tag{2}$$

and a limit cycle trajectory corresponds to fixed points in each Poincaré map

$$\mathbf{S}^* = \mathbf{F}(\mathbf{S}^*). \tag{3}$$

To analyze the stability of the system in the neighborhood of the fixed point, the Poincaré map is linearized

$$\left[\mathbf{S}_{\mathrm{i+1}} - \mathbf{S}^*\right] \approx \mathbf{J}(\mathbf{S}^*)\left[\mathbf{S}_{\mathrm{i}} - \mathbf{S}^*\right] \tag{4}$$

and the eigenvalues λ_{i} of the Jacobian matrix $\mathbf{J}(\mathbf{S}^*)$ are evaluated. If the magnitude of all complex-valued eigenvalues is smaller than one $\|\lambda_{\mathrm{i}}\| < 1$, the limit cycle is stable (Dingwell and Kang, 2007; Guckenheimer and Holmes, 1983).

Assuming the system to be energy conserving, the apex height y_{A} and the horizontal velocity v_{x} are coupled by the energy $E = \frac{1}{2}\, m\, v_{\mathrm{x}}^2 + m\, g\, y_{\mathrm{A}}$. With this, the state vector can be reduced to

$$\mathbf{S}_{\mathrm{i}} = y_{\mathrm{A,i}} \tag{5}$$

and the Poincaré map (equation 2) becomes a one dimensional apex-return map

$$y_{\mathrm{i+1}} = \mathbf{F}(y_{\mathrm{i}}). \tag{6}$$

In this case, the Jacobian matrix $\mathbf{J}(\mathbf{S}^*) = \mathbf{J}(y^*)$ of the linearized Poincaré map $\left[y_{\mathrm{i+1}} - y^*\right] \approx \mathbf{J}(y^*)\left[y_{\mathrm{i}} - y^*\right]$ reduces to the one dimensional derivative

$$\mathbf{J}(y^*) = \left.\frac{dy_{\mathrm{i+1}}}{dy_{\mathrm{i}}}\right|_{y^*}, \tag{7}$$

which actually is the slope of the apex-return map (figure 3.2) in the neighborhood of the fixed point y^*.

C. Calculation of the normalized maximum drop (NMD)

The normalized maximum drop (NMD) (Daley and Usherwood, 2010) is a simple kinematic measure of the runner's ability to negotiate uneven terrain, which indicates the maximum drop $\Delta h_{\max}$ relative to the leg length L_0, the runner could overcome until the leg is vertically oriented ($\alpha = 90°$):

$$\text{NMD} = \frac{\Delta h_{\max}}{L_0}. \tag{8}$$

Here, the concept of the NMD is extended by allowing not only for constant leg retraction $\dot{\alpha}$, but also for constant leg length change $\dot{L}$ (figure C.2).

Assuming the vertical position of the foot at the instant of nominal TD equals zero ($y_{\text{Foot,TD}} = 0$), the landing height of the CoM is

$$y_{\text{TD}} = L_{\text{TD}} \sin \alpha_{\text{TD}}. \tag{9}$$

Considering that the vertical component of the CoM velocity at apex equals zero ($\dot{y}_{\text{A}} = 0$), the vertical CoM speed at the instant of nominal TD results in

$$\dot{y}_{\text{TD}} = -g\, t_{\text{Fall}}. \tag{10}$$

The time Δt from the nominal TD until vertical leg orientation is reached is given by the remaining leg angle divided by leg retraction speed,

$$\Delta t = \frac{90° - \alpha_{\text{TD}}}{\dot{\alpha}}. \tag{11}$$

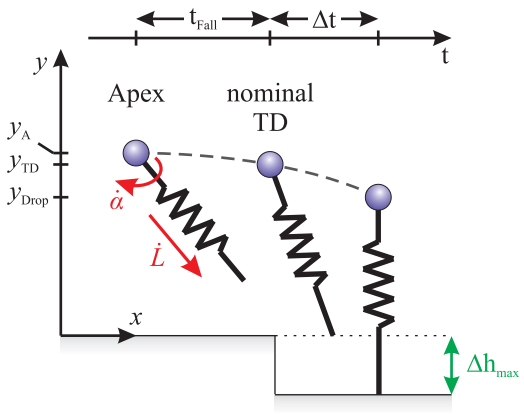

Figure C.2.: The NMD defines the maximum perturbation $\Delta h_{\max}$ before stance is missed completely, assuming both leg rotation $\dot{\alpha}$ and leg length change $\dot{L}$ continue with constant changing rates.

With this (equations 9 - 11), the CoM height of the maximum drop results in

$$y_{\mathrm{Drop}} \quad = \quad y_{\mathrm{TD}} + \dot{y}_{\mathrm{TD}}\,\Delta t - \frac{g}{2}\,(\Delta t)^2, \tag{12}$$

and the corresponding vertical position of the foot and therefore the maximum drop yields

$$\Delta h_{\mathrm{max}} = y_{\mathrm{Drop}} - \left(L_{\mathrm{TD}} + \dot{L}\,\Delta t\right). \tag{13}$$

Bibliography

Aerts, P., Van Damme, R., D'Aout, K. and Van Hooydonck, B. (2003). Bipedalism in lizards: Whole-body modelling reveals a possible spandrel, *Philosophical Transactions of the Royal Society London B* **358**: 1525–1533.

Alexander, R. M. (1989a). On the synchronization of breathing with running in wallabies (macropus spp.) and horses (equus caballus), *Journal of Zoology* **218**: 69–85.

Alexander, R. M. (1989b). Optimization and gaits in the locomotion of vertebrates, *Physiological Reviews* **69**: 1199–1227.

Alexander, R. M. (1990). Three uses for springs in legged locomotion, *International Journal of Robotics Research* **9**: 53–61.

Alexander, R. M. (1991). Energy-saving mechanisms in walking and running, *Journal of Experimental Biology* **160**: 55–69.

Alexander, R. M. (2002). Tendon elasticity and muscle function, *Comparative Biochemistry and Physiology A* **133**: 1001–1011.

Alexander, R. M. (2003). *Principles of Animal Locomotion*, Princeton University Press, Princeton.

Alexander, R. M. (2004). Bipedal animals, and their differences from humans, *Journal of Anatomy* **204**: 321–30.

Alexander, R. M. and Jayes, A. S. (1978). Vertical movements in walking and running, *Journal of Zoology* **185**: 27–40.

Alexander, R. M. and Jayes, A. S. (1980). Fourier analysis of forces exerted in walking and running, *Journal of Biomechanics* **13**: 383–390.

Alexander, R. M., Maloiy, G. M. O., Njau, R. and Jayes, A. S. (1979). Mechanics of running of the ostrich (struthio camelus), *Journal of Zoology* **187**: 169–178.

Arampatzis, A., Brüggemann, G.-P. and Metzler, V. (1999). The effect of speed on leg stiffness and joint kinetics in human running, *Journal of Biomechanics* **32**: 1349–1353.

Bakker, R. T. (1971). Dinosaur physiology and the origin of mammals, *Evolution* **25**: 636–658.

Biewener, A. A. (1989). Scaling body support in mammals: Limb posture and muscle mechanics, *Science* **245**: 45–48.

Biewener, A. A. (1990). Biomechanics of mammalian terrestrial locomotion, *Science* **250**: 1097–1103.

Biewener, A. A. (2003). *Animal Locomotion*, Oxford University Press, Oxford.

Blickhan, R. (1989). The spring-mass model for running and hopping, *Journal of Biomechanics* **22**: 1217–1227.

Blickhan, R. and Full, R. J. (1987). Locomotion energetics of the ghost crab: II. Mechanics of the centre of mass during walking and running, *Journal of Experimental Biology* **135**: 155–174.

Blum, Y., Rummel, J. and Seyfarth, A. (2007). Advanced swing leg control for stable locomotion, *Autonome Mobile Systeme*, Kaiserslautern, Germany, pp. 301–307.

Brackenbury, J. (1999). Fast locomotion in caterpillars, *Journal of Insect Physiology* **45**: 525–533.

Braune, W. and Fischer, O. (1893). Bestimmung der Trägheitsmomente des menschlichen Körpers und seiner Glieder, *Abhandlungen der Mathematisch-Physischen Classe der Königlich-Sächsischen Gesellschaft der Wissenschaften* **18**: 410–492.

Bressler, B. H. and Clinch, N. F. (1974). The compliance of contracting skeletal muscle, *Journal of Physiology* **237**: 477–493.

Bullimore, S. R. and Burn, J. F. (2006). Consequences of forward translation of the point of force application for the mechanics of running, *Journal of Theoretical Biology* **238**: 211–219.

Burrows, M. and Hoyle, G. (1973). The mechanism of rapid running in the ghost crab, ocypode ceratophthalma, *Journal of Experimental Biology* **58**: 327–349.

Carroll, R. L., Irwin, J. and Green, D. M. (2005). Thermal physiology and the origin of terrestriality in vertebrates, *Zoological Journal of the Linnean Society* **143**: 345–358.

Cavagna, G. A. (2006). The landing-take-off asymmetry in human running, *Journal of Experimental Biology* **209**: 4051–4060.

Cavagna, G. A., Heglund, N. C. and Taylor, C. R. (1977). Mechanical work in terrestrial locomotion: Two basic mechanisms for minimizing energy expenditure, *American Journal of Physiology* **233**: 243–261.

Cavagna, G. A., Saibene, F. P. and Margaria, R. (1964). Mechanical work in running, *Journal of Applied Physiology* **19**: 249–256.

Chapman, R. F. (1998). *The Insects: Structure and Function*, Cambridge University Press, Cambridge.

Clauser, C. E., McConville, J. T. and Young, J. W. (1969). Weight, volume, and center of mass of segments of the human body, *Aerospace Medical Research Laboratory Report AMRL-RT-69-70*, Wright-Patterson Air Force Base Ohio.

Daley, M. A. and Biewener, A. A. (2006). Running over rough terrain reveals limb control for intrinsic stability, *Proceedings of the National Academy of Sciences of the USA* **103**: 15681–15686.

Daley, M. A., Felix, G. and Biewener, A. A. (2007). Running stability is enhanced by a proximo-distal gradient in joint neuromechanical control, *Journal of Experimental Biology* **210**: 383–394.

Daley, M. A. and Usherwood, J. R. (2010). Two explanations for the compliant running paradox: Reduced work of bouncing viscera and increased stability in uneven terrain, *Biology Letters* **6**: 418–421.

Dalleau, G., Belli, A., Viale, F., Lacour, J.-R. and Bourdin, M. (2004). A simple method for field measurements of leg stiffness in hopping., *International Journal of Sports Medicine* **25**: 170–176.

De Wit, B., De Clercq, D. and Aerts, P. (2000). Biomechanical analysis of the stance phase during barefoot and shod running, *Journal of Biomechanics* **33**: 269–278.

Dingwell, J. B. and Kang, H. G. (2007). Differences between local and orbital dynamic stability during human walking, *Journal of Biomechanical Engineering* **129**: 586–593.

Dittrich, E., Geyer, H., Karguth, A. and Seyfarth, A. (2006). Obstacle avoidance in a simple hopping robot, *International Conference on Climbing and Walking Robots*, Brussels, Belgium.

Dixon, H. H. (1892). On the walking of arthropoda, *Nature* **47**: 56–58.

Djawdan, M. (1993). Locomotor performance of bipedal and quadrupedal heteromyid rodents, *Functional Ecology* **7**: 195–202.

Doke, J., Donelan, J. M. and Kuo, A. D. (2005). Mechanics and energetics of swinging the human leg, *Journal of Experimental Biology* **208**: 439–445.

Ehlers, M. (1939). Untersuchungen über Formen aktiver Lokomotion bei Spinnen, *Zoologische Jahrbücher (Systematik)* **72**: 373–499.

Ellerby, D. J., Henry, H. T., Carr, J. A., Buchanan, C. I. and Marsh, R. L. (2005). Blood flow in guinea fowl Numida meleagris as an indicator of energy expenditure by individual muscles during walking and running, *Journal of*

Physiology **564**: 631–648.

Farley, C. T., Glasheen, J. and McMahon, T. A. (1993). Running springs: speed and animal size, *Journal of Experimental Biology* **185**: 71–86.

Farley, C. T. and Gonzalez, O. (1996). Leg stiffness and stride frequency in human running, *Journal of Biomechanics* **29**: 181–186.

Farley, C. T. and Ko, T. C. (1997). Mechanics of locomotion in lizards, *Journal of Experimental Biology* **200**: 2177–2188.

Ferris, D. P., Louie, M. and Farley, C. T. (1998). Running in the real world: Adjusting leg stiffness for different surfaces, *Proceedings of the Royal Society B* **265**: 989–994.

Full, R. J., Blickhan, R. and Ting, L. H. (1991). Leg design in hexapedal runners, *Journal of Experimental Biology* **158**: 369–390.

Full, R. J. and Koditschek, D. E. (1999). Templates and anchors: Neuromechanical hypotheses of legged locomotion on land, *Journal of Experimental Biology* **202**: 3325–3332.

Full, R. J. and Tu, M. S. (1991). Mechanics of a rapid running insect: Two-, four- and six-legged locomotion, *Journal of Experimental Biology* **156**: 215–231.

Fung, Y. C. B. (1967). Elasticity of soft tissues in simple elongation, *American Journal of Physiology* **213**: 1532–1544.

Gans, C. (1962). Terrestrial locomotion without limbs, *American Zoologist* **2**: 167–182.

Gatesy, S. M. (1999a). Guineafowl hind limb function. I: Cineradiographic analysis and speed effects, *Journal of Morphology* **240**: 115–125.

Gatesy, S. M. (1999b). Guineafowl hind limb function. II: Electromyographic analysis and motor pattern evolution, *Journal of Morphology* **240**: 127–142.

Gatesy, S. M. and Biewener, A. A. (1991). Bipedal locomotion: Effects of speed, size and limb posture in birds and humans, *Journal of Zoology* **224**: 127–147.

Gazendam, M. G. J. and Hof, A. L. (2007). Averaged EMG profiles in jogging and running at different speeds, *Gait & Posture* **25**: 604–614.

Geyer, H., Seyfarth, A. and Blickhan, R. (2003). Positive force feedback in bouncing gaits?, *Proceedings of the Royal Society B* **270**: 2173–2183.

Geyer, H., Seyfarth, A. and Blickhan, R. (2005). Spring-mass running: Simple approximate solution and application to gait stability, *Journal of Theoretical Biology* **232**: 315–328.

Geyer, H., Seyfarth, A. and Blickhan, R. (2006). Compliant leg behaviour explains basic dynamics of walking and running, *Proceedings of the Royal Society B* **273**: 2861–2867.

Glasheen, J. W. and McMahon, T. A. (1996). Size-dependence of water-running ability in basilisk lizards (basiliscus basiliscus), *Journal of Experimental Biology* **199**: 2611–2618.

Gray, J. (1946). The mechanism of locomotion in snakes, *Journal of Experimental Biology* **23**: 101–120.

Grillner, S. (1975). Locomotion in vertebrates: Central mechanisms and reflex interaction, *Physiological Reviews* **55**: 247–304.

Grimmer, S., Ernst, M., Günther, M. and Blickhan, R. (2008). Running on uneven ground: Leg adjustment to vertical steps and self-stability., *Journal of Experimental Biology* **211**: 2989–3000.

Guckenheimer, J. and Holmes, P. (1983). *Nonlinear Oscillations, Dynamical Systems, and Bifurcations of Vector Fields*, Springer, New York.

Günther, M. and Blickhan, R. (2002). Joint stiffness of the ankle and the knee in running, *Journal of Biomechanics* **35**: 1459–74.

Haeufle, D., Grimmer, S. and Seyfarth, A. (2010). The role of intrinsic muscle properties for stable hopping-stability is achieved by the force-velocity relation, *Bioinspiration & Biomimetics* **5**: 016004.

He, J., Kram, R. and McMahon, T. A. (1991). Mechanics of running under simulated low gravity, *Journal of Applied Physiology* **71**: 863–870.

Herr, H. M. and McMahon, T. A. (2001). A galloping horse model, *International Journal of Robotics Research* **20**: 26–37.

Hildebrand, M. (1989). The quadrupedal gaits of vertebrates, *BioScience* **39**: 766–775.

Hill, A. V. (1938). The heat of shortening and the dynamic constants of muscle, *Proceedings of the Royal Society B* **126**: 136–195.

Hirose, M. and Ogawa, K. (2007). Honda humanoid robots development, *Philosophical Transactions of The Royal Society A* **375**: 11–19.

Hollander, K. W., Sugar, T. G. and Herring, D. E. (2005). Adjustable robotic tendon using a 'Jack Spring', *International Conference on Rehabilitation Robotics*, Chicago, USA, pp. 113–118.

Irschick, D. J. and Jayne, B. C. (1999). Comparative three-dimensional kinematics of the hindlimb for high-speed bipedal and quadrupedal locomotion of lizards, *Journal of Experimental Biology* **202**: 1047–1065.

Jenkins, F. A. (1983). The functional anatomy of the shoulder of the savannah monitor lizard (varanus exanthematicus), *Journal of Morphology* **175**: 195–216.

Kajita, S., Nagasaki, T., Kaneko, K. and Hirukawa, H. (2007). ZMP-based biped running control - the HRP-2LR humanoid biped robot, *IEEE Robotics & Automation Magazine* **14**: 63–72.

Kalveram, K. T., Häufle, D. and Seyfarth, A. (2008). From hopping to walking: How the biped jena-walker can learn from the single-leg marco-hopper, advances in mobile robotics, *International Conference on Climbing and Walking Robots*, Coimbra, Portugal, pp. 638–645.

Kim, S., Clark, J. E. and Cutkosky, M. R. (2006). iSprawl: Design and tuning for high-speed autonomous open-loop running, *International Journal of Robotics Research* **25**: 903–912.

Lipfert, S. W. (2010). *Kinematic and Dynamic Similarities between Walking and Running*, Verlag Dr. Kovac, Hamburg.

Lipfert, S. W., Günther, M., Renjewski, D., Grimmer, S. and Seyfarth, A. (submitted). A model-experiment comparison of system dynamics for human walking and running, *Journal of Theoretical Biology* .

Löffler, K., Gienger, M. and Pfeiffer, F. (2003). Sensors and control concept of walking 'Johnnie', *International Journal of Robotics Research* **22**: 229–239.

Marek, P. E. and Bond, J. E. (2006). Biodiversity hotspots: Rediscovery of the world's leggiest animal, *Nature* **441**: 707.

Maus, H.-M., Lipfert, S. W., Gross, M., Rummel, J. and Seyfarth, A. (2010). Upright human gait did not provide a major mechanical challenge for our ancestors, *Nature Communications* **1**: 70.

Maykranz, D., Grimmer, S., Lipfert, S. W. and Seyfarth, A. (2009). Foot function in spring mass running, *Autonome Mobile Systeme*, Karlsruhe, Germany, pp. 81–88.

McGeer, T. (1993). Dynamics and control of bipedal locomotion, *Journal of Theoretical Biology* **163**: 277–314.

McMahon, T. A. and Cheng, G. C. (1990). The mechanics of running: How does stiffness couple with speed?, *Journal of Biomechanics* **23**: 65–78.

McMahon, T. A., Valiant, G. and Frederick, E. C. (1987). Groucho running, *Journal of Applied Physiology* **62**: 2326–2337.

Merker, A., Rummel, J. and Seyfarth, A. (submitted). Stable walking with asymmetric legs, *IEEE International Conference on Robotics and Automation*,

Shanghai, China.

Moritz, C. T. and Farley, C. T. (2006). Human hoppers compensate for simultaneous changes in surface compression and damping, *Journal of Biomechanics* **39**(6): 1030–1038.

Muir, G. D., Gosline, J. M. and Steeves, J. D. (1996). Ontogeny of bipedal locomotion: Walking and running in the chick, *Journal of Physiology* **493**: 589–601.

Müller, R. and Blickhan, R. (2010). Running on uneven ground: Leg adjustments to altered ground level, *Human Movement Science* **29**: 578–589.

Muybridge, E. (1967). *Animals in Motion*, Dover Publications, Inc., New York.

Muybridge, E. (2000). *The Human Figure in Motion*, Dover Publications, Inc., New York.

Nelson, R. C., Dillman, C. J., Lagasse, P. and Bickett, P. (1972). Biomechanics of overground versus treadmill running, *Medicine and Science in Sports and Exercise* **4**: 233–240.

Neville, N. (2005). *Bipedal Running with One Actuator per Leg*, ME Thesis, McGill University, Montreal, Canada.

Nigg, B. M., De Boer, R. W. and Fisher, V. (1995). A kinematic comparison of overground and treadmill running, *Medicine and Science in Sports and Exercise* **27**: 98–105.

Park, I.-W., Kim, J.-Y. and Oh, J.-H. (2008). Online walking pattern generation and its application to a biped humanoid robot - KHR-3 (HUBO), *Advanced Robotics* **22**: 159–190.

Parrish, J. M. (1987). The origin of crocodilian locomotion, *Paleobiology* **13**: 396–414.

Pearson, K. G. and Misiaszek, J. E. (2001). Locomotion, *Encyclopedia of Life Sciences* . doi:10.1038/npg.els.0000163.

Peuker, F. and Seyfarth, A. (2010). Adjusting legs for stable running in three dimensions, *World Congress of Biomechanics*, Singapore, pp. 3–6.

Poulakakis, I., Smith, J. A. and Buehler, M. (2005). Modeling and experiments of untethered quadrupedal running with a bounding gait: The Scout II robot, *International Journal of Robotics Research* **24**: 239–256.

Raibert, M. H. (1986). *Legged Robots That Balance*, The MIT Press, Cambridge.

Reilly, S. M. and Delancey, M. J. (1997). Sprawling locomotion in the lizard sceloporus clarkii: Quantitative kinematics of a walking trot, *Journal of Experimental Biology* **200**: 753–765.

Reilly, S. M. and Elias, J. E. (1998). Locomotion in alligator mississippiensis: Kinematic effects of speed and posture and their relevance to the sprawling-to-erect paradigm, *Journal of Experimental Biology* **201**: 2559–2574.

Riese, S. and Seyfarth, A. (submitted). Decreasing leg stiffness supports stable hopping, *IEEE International Conference on Robotics and Automation*, Shanghai, China.

Ritzmann, R. E., Quinn, R. D. and Fischer, M. S. (2004). Convergent evolution and locomotion through complex terrain by insects, vertebrates and robots, *Arthropod Structure & Development* **33**: 361–379.

Rode, C., Siebert, T. and Blickhan, R. (2009). Titin-induced force enhancement and force depression: A 'sticky-spring' mechanism in muscle contractions?, *Journal of Theoretical Biology* **259**: 350–360.

Rode, C., Siebert, T., Herzog, W. and Blickhan, R. (2009). The effects of parallel and series elastic components on the active cat soleus force-length relationship, *Journal of Mechanics in Medicine and Biology* **9**: 105–122.

Rose, J. and Gamble, J. G. (2006). *Human Walking*, Lippincott Williams & Wilkins, Philadelphia.

Rummel, J., Blum, Y., Maus, H. M., Rode, C. and Seyfarth, A. (2010). Stable and robust walking with compliant legs, *IEEE International Conference on Robotics and Automation*, Anchorage, USA, pp. 5250–5255.

Rummel, J., Blum, Y. and Seyfarth, A. (accepted). Robust and efficient walking with spring-like legs, *Bioinspiration & Biomimetics* .

Rummel, J., Iida, F., Smith, J. A. and Seyfarth, A. (2008). Enlarging regions of stable running with segmented legs, *IEEE International Conference on Robotics and Automation*, Pasadena, USA, pp. 367–372.

Rummel, J. and Seyfarth, A. (2008). Stable running with segmented legs, *International Journal of Robotics Research* **27**: 919–934.

Saranli, U., Buehler, M. and Koditschek, D. E. (2001). RHex: A simple and highly mobile hexapod robot, *International Journal of Robotics Research* **20**: 616–631.

Schmitt, D. (2003). Insights into the evolution of human bipedalism from experimental studies of humans and other primates, *Journal of Experimental Biology* **206**: 1437–1448.

Schmitt, J., Garcia, M., Razo, R. C., Holmes, P. and Full, R. J. (2002). Dynamics and stability of legged locomotion in the horizontal plane: A test case using insects, *Biological Cybernetics* **86**: 343–353.

Seipel, J. E. and Holmes, P. (2005). Running in three dimensions: Analysis of a point-mass sprung-leg model, *International Journal of Robotics Research* **24**: 657–674.

Seyfarth, A., Friedrichs, A., Wank, V. and Blickhan, R. (1999). Dynamics of the long jump, *Journal of Biomechanics* **32**: 1259–1267.

Seyfarth, A., Geyer, H., Guenther, M. and Blickhan, R. (2002). A movement criterion for running, *Journal of Biomechanics* **35**: 649–655.

Seyfarth, A., Geyer, H. and Herr, H. (2003). Swing-leg retraction: A simple control model for stable running, *Journal of Experimental Biology* **206**: 2547–2555.

Seyfarth, A., Günther, M. and Blickhan, R. (2001). Stable operation of an elastic three-segment leg, *Biological Cybernetics* **84**: 365–382.

Strogatz, S. H. (1994). *Nonlinear dynamics and chaos: With applications to physics, biology, chemistry, and engineering*, Westview Press, Cambridge.

Tellez, R., Ferro, F., Garcia, S., Gomez, E., Jorge, E., Mora, D., Pinyol, D., Oliver, J., Torres, O., Velazquez, J. and Faconti, D. (2008). Reem-B: An autonomous lightweight human-size humanoid robot, *IEEE-RAS International Conference on Humanoid Robots*, Daejeon, South Korea, pp. 462–468.

Van Ham, R. (2006). *Compliant Actuation for Biological Inspired Bipedal Walking Robots*, PhD Thesis, Vrije Universiteit Brussel, Brussels, Belgium.

Van Ingen Schenau, G. J. (1980). Some fundamental aspects of the biomechanics of overground versus treadmill locomotion, *Medicine and Science in Sports and Exercise* **12**: 257–261.

Vukobratovic, M. and Borovac, B. (2004). Zero-moment point - thirty five years of it's life, *International Journal of Humanoid Robotics* **1**: 157–173.

Windsor, D. E. and Dagg, A. I. (1971). The gaits of the macropodinae (marsupialia), *Journal of Zoology* **163**: 165–175.

Winter, D. A. (2005). *Biomechanics and Motor Control of Human Movement*, Wiley, New York.

Wolf, S. and Hirzinger, G. (2008). A new variable stiffness design: Matching requirements of the next robot generation, *IEEE International Conference on Robotics and Automation*, Pasadena, USA, pp. 1741–1746.

Curriculum Vitae

Name:	Yvonne Nadine Blum
Date of birth:	January 25, 1980
Place of birth:	Delmenhorst
Nationality:	German

Education

2006 - 2010:	PhD student at the Locomotion Laboratory, University of Jena, Germany
2005:	Diplom in physics, University of Jena, Germany
1999:	Abitur, Gymnasium Ganderkesee, Germany

Publications in peer-reviewed journals

- Blum Y., Birn-Jeffery A., Daley M.A., Seyfarth A., Does a crouched leg posture enhance running stability and robustness?, *Journal of Theoretical Biology,* (in press)
- Rummel J., Blum Y., Seyfarth A., Robust and efficient walking with spring-like legs, *Bioinspiration & Biomimetics,* 5: 046004, 2010
- Blum Y., Lipfert S.W., Rummel J., Seyfarth A., Swing leg control in human running, *Bioinspiration & Biomimetics,* 5: 026006, 2010
- Blum Y., Lipfert S.W., Seyfarth A., Effective leg stiffness in running, *Journal of Biomechanics,* 42: 2400-2405, 2009

Publications in conference proceedings

- Rummel J., Blum Y., Maus H.M., Rode C., Seyfarth A., Stable and robust walking with compliant legs, *IEEE International Conference on Robotics and Automation,* Anchorage, AK, USA, 2010
- Rummel J., Blum Y., Seyfarth A., From walking to running, *Autonome Mobile Systeme,* Karlsruhe, Germany, 2009
- Blum Y., Rummel J., Seyfarth A., Advanced swing leg control for stable locomotion, *Autonome Mobile Systeme,* Kaiserslautern, Germany, 2007

Conference abstracts

- Blum Y., Birn-Jeffery A., Daley M.A., Seyfarth A., Does a crouched leg posture enhance running stability?, *US National Congress of Theoretical and Applied Mechanics,* State College, PA, USA, 2010
- Blum Y., Lipfert S.W., Seyfarth A., Stiffness estimation in human running, *Congres of the International Society of Biomechanics,* Cape Town, South Africa, 2009
- Blum Y., Lipfert S.W., Seyfarth A., Leg parameter adaptation for stable running, *Annual Main Meeting of the Society for Experimental Biology,* Glasgow, Scotland, 2009
- Blum Y., Lipfert S.W., Seyfarth A., Can impacts be avoided in stable running?, *Dynamic Walking,* Vancouver, BC, Canada, 2009
- Blum Y., Movement control by leg parameter adaptation, *Neuro-Robotics Symposium,* Freiburg, Germany, 2008
- Blum Y., Lipfert S.W., Rummel J., Seyfarth A., Advanced swing leg control, *Dynamic Walking,* Delft, Netherlands, 2008
- Lipfert S.W., Blum Y., Seyfarth A., Estimation of leg stiffness in human locomotion, *Dynamic Walking,* Ann Arbor, MI, USA, 2006

Ganderkesee, den 28.04.2011

Yvonne Blum

Ehrenwörtliche Erklärung

Hiermit erkläre ich, dass mir die geltende Promotionsordnung der Fakultät bekannt ist und dass ich die Dissertation selbst angefertigt habe, insbesondere die Hilfe eines Promotionsberaters nicht in Anspruch genommen und alle von mir benutzten Hilfsmittel und Quellen in meiner Arbeit angegeben habe.

Mit Ausnahme der allgemeinen Einleitung (Kapitel 1) und der Schlussfolgerung (Kapitel 5) sind die Kapitel der vorliegenden Dissertation in internationalen wissenschaftlichen Zeitschriften publiziert, bzw. zur Publikation eingereicht. An den publizierten, bzw. eingereichten Teilen (Kapitel 2*, 3† und 4‡) waren die Mitautoren in unterschiedlicher Weise beteiligt. Die experimentellen Daten wurden von Dr. Susanne W. Lipfert (Kapitel 2, 3 und 4) und Aleksandra Birn-Jeffery (Kapitel 4) erhoben. Zudem standen mir Dr. Susanne W. Lipfert (Kapitel 2 und 3) und Jürgen Rummel (Kapitel 3) beratend zur Seite. Von Dr. Andre Seyfarth (Kapitel 2, 3 und 4) und Dr. Monica A. Daley (Kapitel 4) habe ich konzeptionelle Unterstützung bei der Erstellung der Manuskripte erhalten. Alle Kapitel wurden federführend von mir ausgearbeitet. Weitere Personen haben mich bei der Erstellung der Manuskripte nicht unterstützt. Weiterhin erkläre ich, dass Dritte weder unmittelbar noch mittelbar geldwerte Leistungen von mir für Arbeiten erhalten haben, die im Zusammenhang mit dem Inhalt der vorgelegten Dissertation stehen. Die Dissertation wurde noch nicht als Prüfungsarbeit für eine staatliche oder andere wissenschaftliche Prüfung eingereicht und keine gleiche, in wesentlichen Teilen ähnliche oder andere Abhandlung liegt bei einer anderen Hochschule als Dissertation vor.

Ich versichere, nach bestem Wissen die reine Wahrheit gesagt und nichts verschwiegen zu haben.

Ganderkesee, den 28.04.2011

Yvonne Blum

*Blum Y., Lipfert S.W., Seyfarth A., *J. Biomech.,* 42: 2400-2405, 2009

†Blum Y., Lipfert S.W., Rummel J., Seyfarth A., *Bioinspir. Biomim.,* 5: 026006, 2010

‡Blum Y., Birn-Jeffery A., Daley M.A., Seyfarth A., *J. Theor. Biol.,* (in press)